INVESTIGATION OF THE FIELD PERFORMANCE FOR INDUSTRIAL REFRIGERATION SYSTEMS

By

Kyle A. Brownell

A thesis submitted in partial fulfillment of

The requirements for the degree of

MASTER OF SCIENCE

(MECHANICAL ENGINEERING)

at the

UNIVERSITY OF WISCONSIN-MADISON

1998

Abstract

Industrial refrigeration systems are designed and field-erected for service in factories, warehouses, supermarkets, ice arenas and many other areas where refrigeration is required. These systems are composed of components from many different manufacturers. The components are selected and integrated into one system by a system design engineer using the operational data provided by the component manufacturer. This design process often does not yield an optimal system design, which may result in higher first costs to the owner and usually costs the operator of the system additional expenditures in energy consumption. Additionally, design engineers often design systems with minimal monitoring instrumentation installed in an effort to save on initial equipment and installation costs.

A 20% or more increase in system performance can be achieved by changing the system control algorithms. Additional energy savings can be achieved by changing the system configuration to incorporate dedicated mechanical subcooling. Finally, if the system is equipped with proper monitoring equipment, as much as a 30% reduction in energy expenditures can be realized by the early diagnosis and correction of malfunctioning components.

Acknowledgements

I would like to thank God for giving me guidance and strength to get me where I am today. This was given to me through my Mother and Father and all five of my Brothers and Sisters. Without their continuing support and prayers, I could not have completed this work.

Thank you Sandy and Doug for your patience and help in answering my questions throughout this project. Your continuing guidance allowed me to finish this project, a feat I could not have done without you. Thanks Sandy for the running lessons over the spring and summer.

This research project has been sponsored by the Energy Service, Research, and Education Committee through a grant from the Energy Center of Wisconsin. The project would not have been possible without additional support and cooperation by Fritz Kroncke of the Madison Ice Arena.

List Of Tables

List of Figures

Chapter 1

Introduction

1.1 Background

Commercial and industrial refrigeration systems typically consist of separate components, which are provided by different manufacturers. The system components must be selected by the design engineer based on recommendations from the component manufacturers and catalog equipment performance information. This selection process can lead to non-optimal system configuration and control settings.

A typical commercial refrigeration system consists of one or more evaporators, evaporative condensers, pumps, compressors, refrigerant filters, expansion valves, suction line heat exchangers and suction line accumulators. Additionally, systems may include a secondary cooling solution of ethylene or propylene glycol and water which is typically referred to as brine. This brine solution is used to avoid long runs of refrigerant piping that would require larger charges of refrigerant and larger compressors to overcome the added pressure drop in the system. Figure 1.1 shows a simplified schematic of a typical brine cooled system. The capacity of the evaporator is controlled by the expansion valve, which senses the superheat of the refrigerant at the outlet of the evaporator. When the expansion valve is fully open and can no longer maintain the temperature of the brine returning to the evaporator, another compressor is cycled on to meet the additional load. The evaporative

condenser fan controls the compressor discharge pressure. The fan comes on when the refrigerant pressure

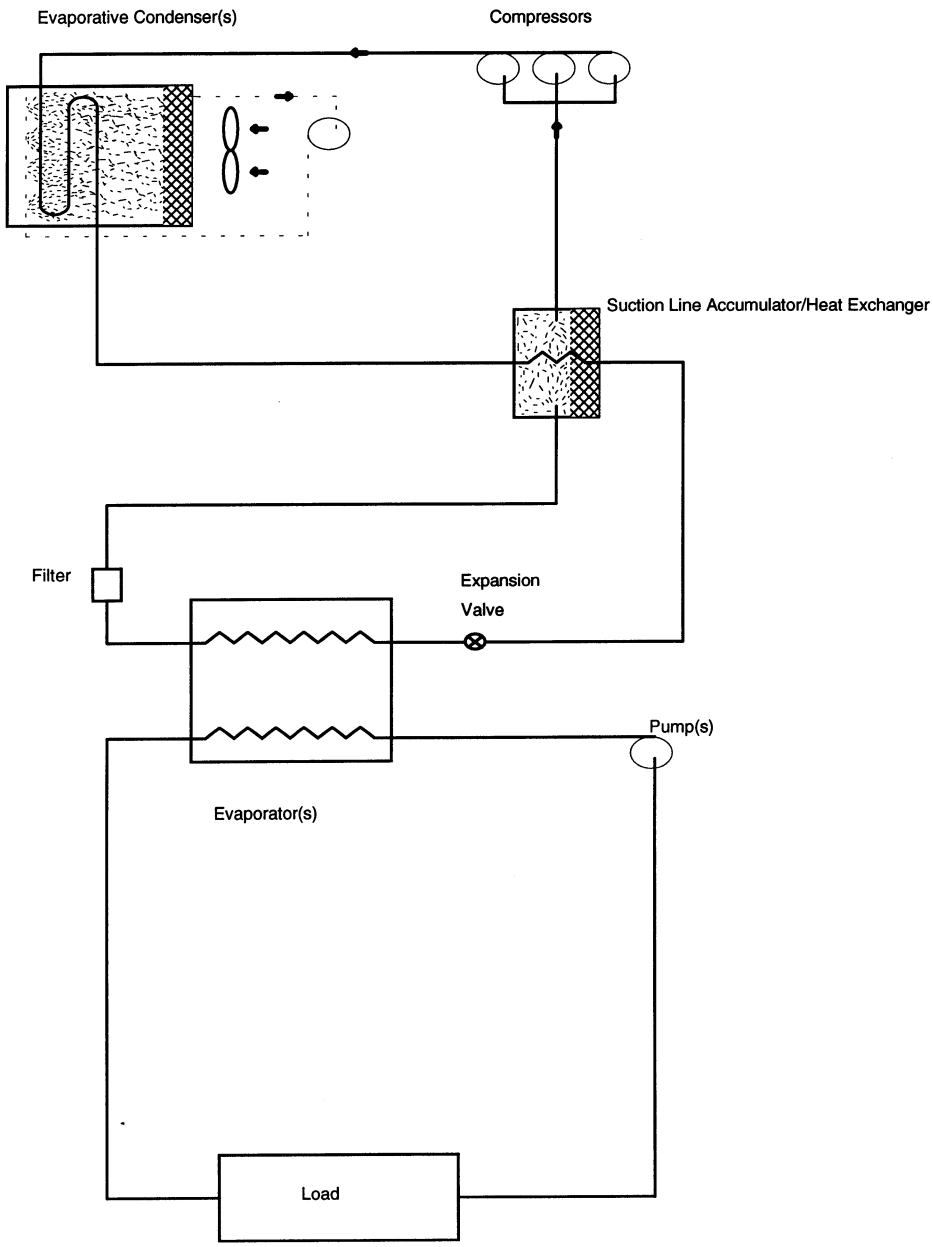

Figure 1.1: Schematic of Typical Brine Cooled System

reaches a predetermined set point and cycles off once the refrigerant pressure is reduced to another predetermined set point. The discharge pressure of the refrigerant is a direct function of the heat transfer from the evaporative condenser (i.e. when the fan is on, the heat transfer from the evaporative condenser is high which decreases the refrigerant pressure). The compressor suction pressure is controlled by the evaporator effectiveness (i.e. the higher the effectiveness of the evaporator, the higher the suction pressure is), the desired temperature of the fluid to be cooled, and the pressure drop between the evaporator outlet and the compressor suction.

Designing a refrigeration system for optimal performance requires the engineer to thoroughly investigate the performance of each proposed piece of equipment to determine how the equipment will perform under all conditions. Additionally, many 'rules of thumb' exist for setting the control setpoints for a system. In most cases, these setpoints build in a factor of safety, which translates into additional operating costs for the system.

1.2 Research Objectives

The objectives of this project are to compare the field performance of large refrigeration systems to design predictions, to identify the cause of differences, and to identify opportunities for reducing energy costs. The areas in which energy savings can be achieved are of a general nature such that they can be applied to a wide range of refrigeration systems.

In order to compare the field performance to design predictions, a computer model of the system was written using the Engineering Equation Solver (EES) (Klein, 1998).

Coefficients were then calculated using actual data of the system to calibrate the model to represent the actual system operating condition. Once calibrated, the model could be used to predict the system performance by varying control settings such as discharge head pressure and varying system configuration to include dedicated subcooling.

1.3 Description of the Madison Ice Arena

The refrigeration system at the Madison Ice Arena is used to cool the ice on two separate rinks for a total of 25,000 ft^2 of ice. The system is rated at 103 tons (362 kW) of refrigerating capacity, which is used to cool a secondary coolant of ethylene glycol water solution. As shown in figure 1.2, the refrigerant side of the system is constructed in two separate loops with the only common components being the evaporative condenser and the evaporator. The refrigerant side of each loop consists of three 35 hp Carlyle semi-hermetically sealed compressors, oil filters, liquid line filters, suction line filters, oil separators, and pressure and temperature controls. A detailed description of these components is included in chapter two.

As shown in figure 1.3, the brine side of the system is constructed in two separate loops with the only common component being the evaporator. The brine side consists of 2 glycol pumps for each rink. The large rink is supplied with brine by either a 10 hp (644 gpm@45ft) or a 5 hp (400gpm@25ft) centrifugal Armstrong pump. The small rink is supplied with brine by either a 7.5 hp (312 gpm@25ft) or a 2 hp (200 gpm@25ft) centrifugal Armstrong pump. Which pump is on is determined by the return glycol temperature from the respective rink. If the return temperature exceeds 17°F, the larger pump is cycled on for that

respective rink. Once the return temperature returns to below 16°F, the smaller pump for the respective rink is cycled back on.

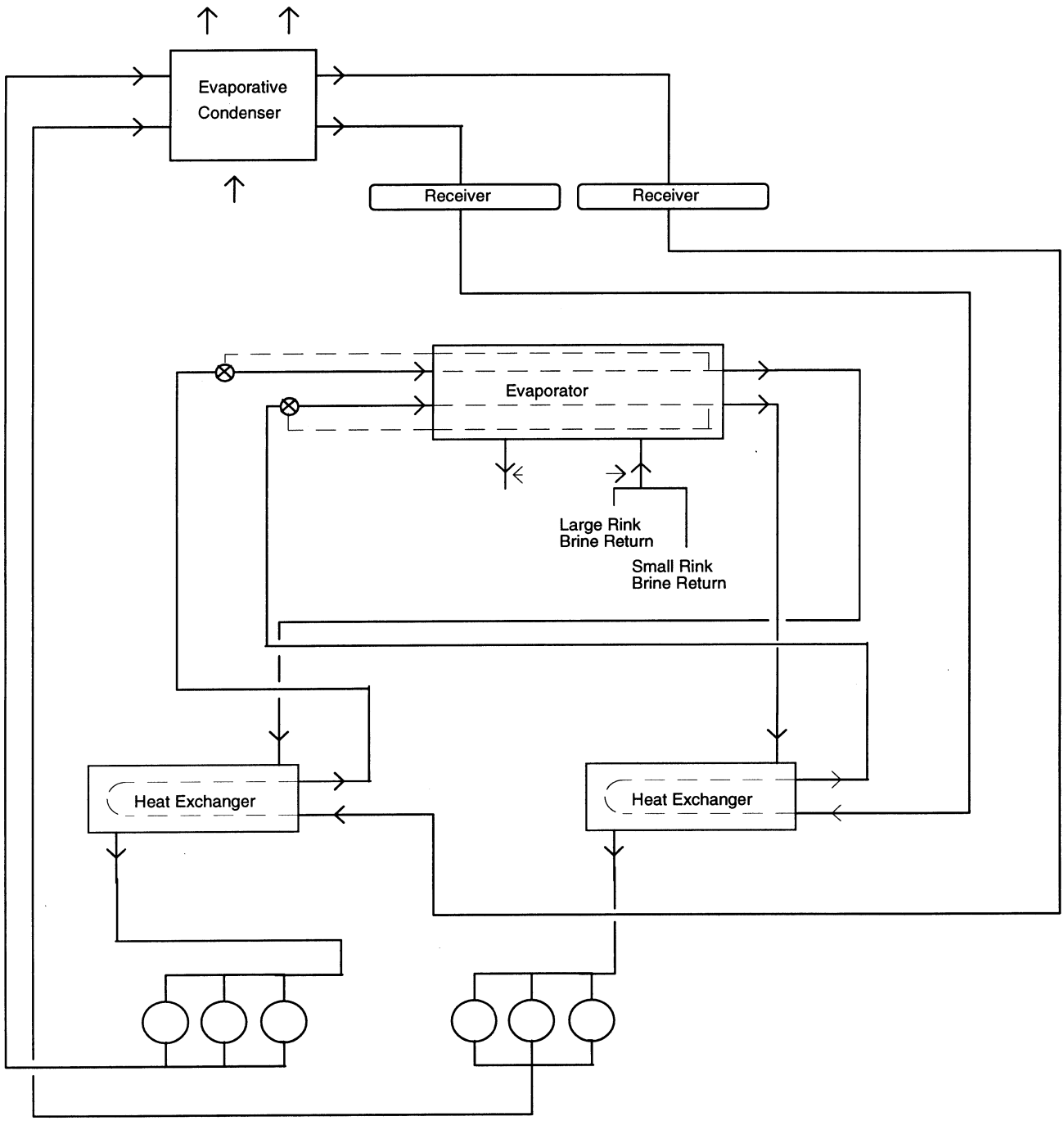

Figure 1.2: Schematic of Refrigerant system

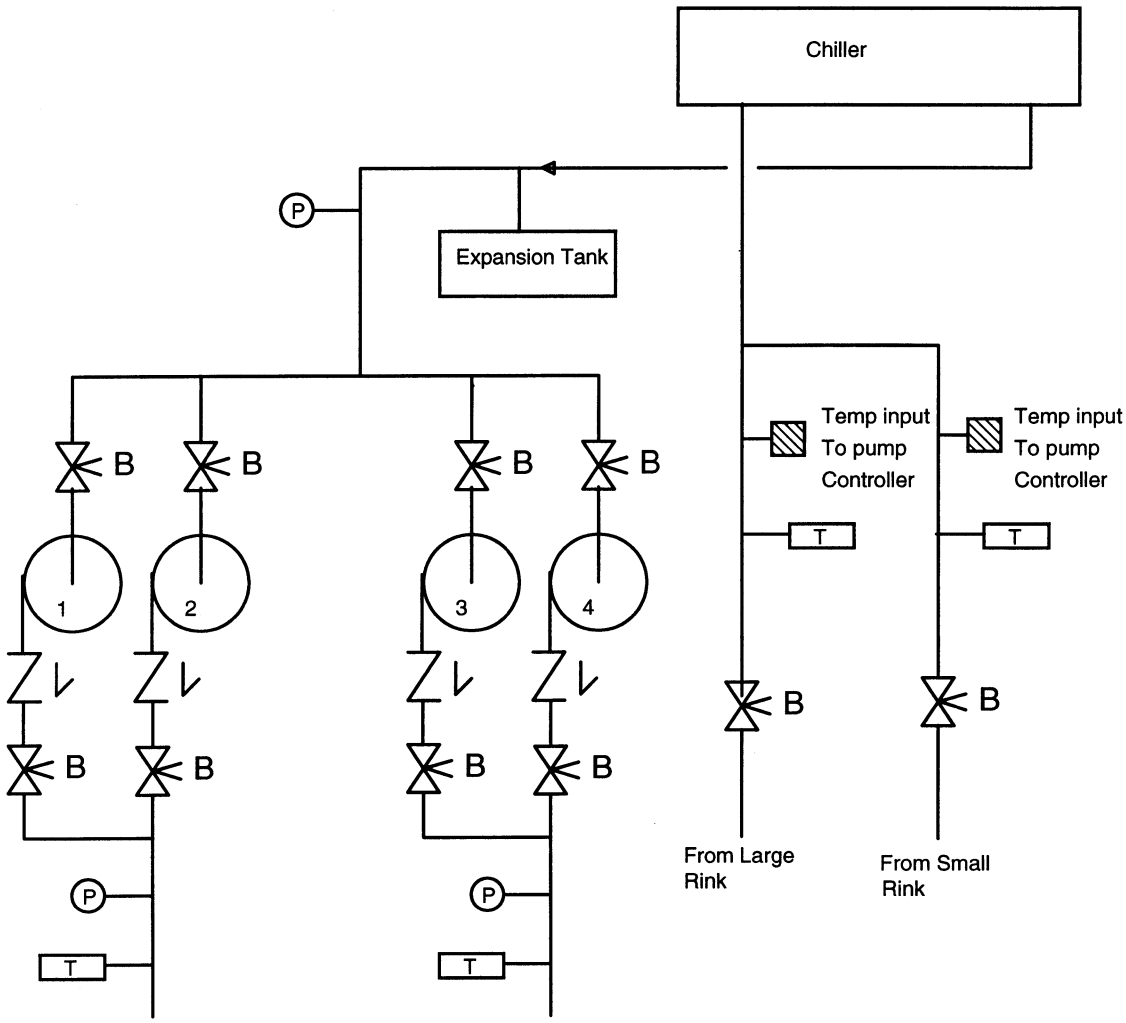

1=10 HP, 1730 RPM, 5x4x8, 644 GPM@45 ft
2=5 HP, 1745 RPM, 5x4x8, 400 GPM@25 ft
3=7.5 HP, 1745 RPM, 5x4x8, 312 GPM@45 ft
4=2 HP, 1725 RPM, 4x3x6, 200 GPM@25 ft

Figure 1.3: Schematic of Brine Side

1.4 Organization

Including this chapter (chapter 1), this thesis is organized into eight separate chapters. Chapter 2 outlines detailed development of individual component models for a refrigeration system. The chapter is written such that these models can be applied to any refrigeration system containing these components. Chapter 3 describes in detail the installation and calibration of sensor equipment for the refrigeration system. Chapter 4 describes the plan for instrumentation of a refrigeration system and how the information obtained from instrumentation will be used to validate the accuracy of the component computer models developed in chapter 2. Chapter 5 describes various problems encountered during the analysis of the system operation. This includes estimated cost savings in electrical consumption by fixing the problem, solutions to the problem and preventative measures to detect the problem in the future before it has a detrimental impact on the system performance. Chapter 6 describes current refrigeration system control strategies used in industry today as well as recommendations for improvement on these control strategies. This chapter also includes the predicted operational savings at Madison Ice Arena should they decide to implement these strategies. Chapter 7 details the effects of reconfiguring the refrigeration system to operate using dedicated mechanical subcooling. Finally, chapter 8 gives conclusions and recommendations on control and configuration of refrigeration systems. Additionally, it provides recommendations for future research concerning refrigeration system component modeling and system design and operation.

Chapter 2

Refrigeration Component Modeling

2.1 Quasi-Steady State vs. Transient Models

Two types of models used to predict refrigeration system performance are the quasi-steady state and transient models. This chapter details the development of a quasi-steady state model for major components in a refrigeration system. Quasi-steady state type models use a steady-state first law analysis to simulate the system operation as shown in equation (2.1). Each component model was programmed using the Engineering Equation Solver (EES) (Klein, 1997). A listing of these programs is provided in appendix A.

$$\dot{Q} - \dot{W} = \sum_{\substack{\text{leaving} \\ \text{system}}} \dot{m}\left(h + \frac{V^2}{2} + gz\right) - \sum_{\substack{\text{Entering} \\ \text{system}}} \dot{m}\left(h + \frac{V^2}{2} + gz\right) \qquad (2.1)$$

2.1.1 Quasi-Steady State Models

In a quasi-steady state model the rate of mass flow, heat transfer and work input are considered independent of time for each simulated condition. Expected system transients such as a fan cycling on and off over a period, are time-averaged to provide composite operational conditions. This type of modeling does not account for the extreme conditions that the system will see; yet, it allows for some consideration of system transients. This is the type of analysis used in the modeling described in this chapter and throughout this thesis.

2.1.2 Transient Modeling

In the transient model, parameters such as mass flow, heat transfer and work input are constantly changing with respect to time. The transient model also includes system capacitance effects that require detailed knowledge of system and component geometry. This type of model was not used to analyze any of the system components. All transients that were encountered in this analysis where time averaged to produce the quasi-steady state model described above.

2.2 Component Modeling

This section describes how specific quasi-steady state models were developed for the equipment installed at the Madison Ice arena. Table 2.2.1 describes the components for which models were developed using manufacturers' data.

Component	Manufacturer	Model No.	Type
Evaporative Condenser	Baltimore Air Coil	VC1-110	Up-draft Blow Through
Compressor	Carlyle	EM199	Semi-hermetic Reciprocating
Evaporator	API-Ketema	DXT-2010-RS-2P-2C	Two Circuit Shell and Tube
Expansion Valve	Sporlan	OVE55E	Direct Expansion
Suction Line Filter	Sporlan	RPE-48-BD	Full Flow
Suction Line Heat Exchanger	Refrigeration Research	HX 3840	Accumulator Type

Table 2.2.1: System Components

2.2.1 Evaporative Condenser

The data provided by the manufacturer of the Baltimore Air Coil, 1617 MBH evaporative condenser (as well as other manufacturers' condensers) are the heat rejection capacity as a function of outside air wetbulb temperature and refrigerant condensing temperature (Baltimore Aircoil, 1978). According to the manufacturer's manual and the manufacturer's representative, the following conditions apply for the equipment installed at the Madison Ice Arena:

- The evaporative condenser fan is operating at its rated 22,000 CFM capacity.
- Rated wet bulb temperatures range from 50 to 76° F
- The rated outside air drybulb remains constant at 91° F.
- The air leaving the evaporative condenser is saturated.

A correlation was developed for the effectiveness of the evaporative condenser using equation (2.2.1). This program is listed in appendix A-1.

$$\varepsilon = \frac{\dot{Q}_{rated}}{\dot{Q}_{max}} \tag{2.2.1}$$

where $\dot{Q}_{rated}$ is the capacity of the evaporative condenser provided by the manufacturer and is based on the refrigerant condensing temperature and the outdoor air wetbulb temperature, $\dot{Q}_{max}$ is the quantity $\dot{m}_{air}\left(h_{air,sat} - h_{air,in}\right)$, and $\dot{m}_{air}$ is the mass flow of air through the evaporative condenser based on a constant volume flow rate and the outdoor air specific

volume at the specified outdoor air condition. Additionally, $h_{air,sat}$ is the specific enthalpy of saturated air at the refrigerant condensing temperature, $h_{air,in}$ is the specific enthalpy of the air at the inlet to the evaporative condenser. A plot of the rated capacity of the evaporative condenser, $\dot{Q}_{rated}$, and the maximum capacity of the evaporative condenser, $\dot{Q}_{max}$, vs. the outdoor air wetbulb temperature is shown in figure 2.2.1.

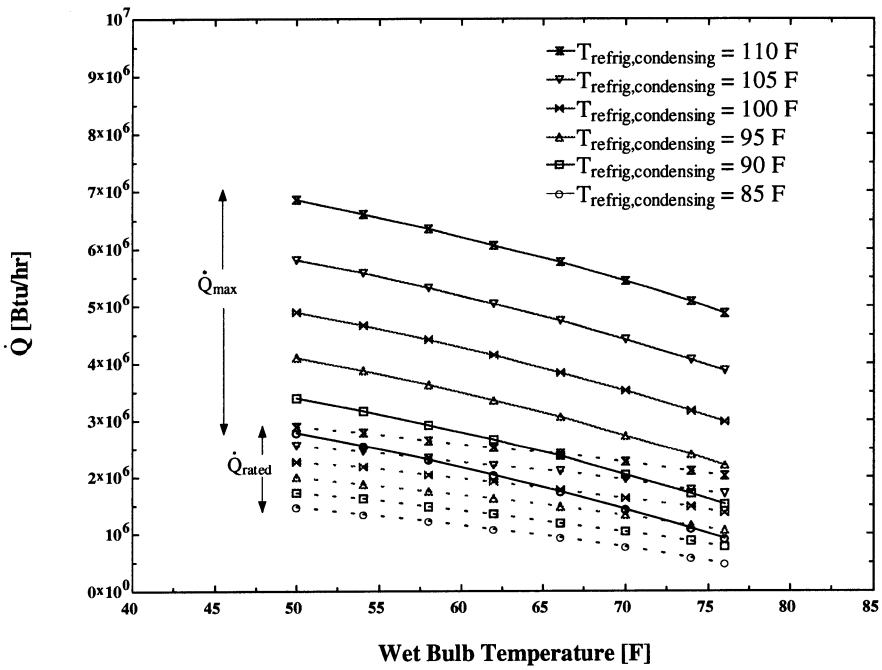

Figure 2.2.1: Evaporative Condenser Heat Transfer Vs. Outside Air Wetbulb Temperature

As depicted in figure 2.2.1, the maximum heat transfer decreases at a slightly greater rate than the evaporative condenser's rated heat transfer at all refrigerant condensing temperatures. Close examination of the trends shown in the plot depict that the ratio of the maximum heat transfer to the rated heat transfer increases significantly as the refrigerant

condensing temperature increases. A plot of the effectiveness vs. the refrigerant condensing temperature for various wet-bulb conditions is shown in Figure 2.2.2.

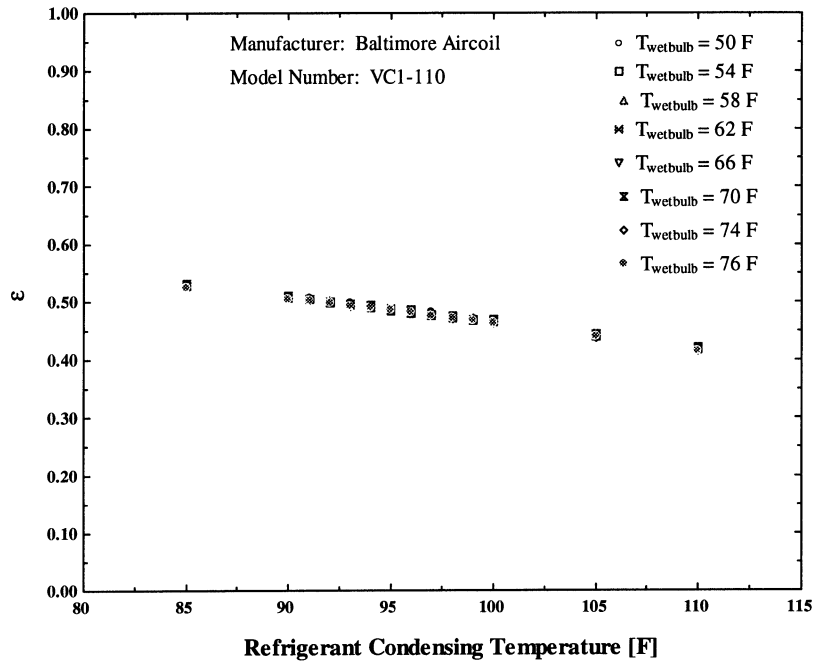

Figure 2.2.2: Evaporative Condenser Effectiveness vs. Condensing Temperature

These data indicate that the effectiveness of the evaporative condenser is a strong function of refrigerant temperature and a weak function of the outdoor air wetbulb temperature. The weak dependence of the effectiveness on air wetbulb temperature is not considered in the model. These data for the evaporative condenser effectiveness fit a first order polynomial as a function of refrigerant condensing temperature as given by equation (2.2.2).

$$\varepsilon = C_1 - C_2 * T_{refrigerant} \qquad (2.2.2)$$

C_1, C2, R^2, RMS, and the number of data points used in the fitting process are shown in Table 2.2.2 for various sizes and manufacturers of evaporative condensers.

Model Number	MFR	Capacity (MBH)	C_1	C_2	R^2(%)	RMS	DATA PTS
VC1-10	Baltimore Aircoil	147	0.62779	0.00308	99.45	1.41E-3	112
VC1-110	Baltimore Aircoil	1617	0.91029	0.00447	99.45	2.05E-3	112
VC1-N357	Baltimore Aircoil	5247.9	0.99838	0.00490	99.45	2.24E-3	112
ATC-50	Evapco	735	0.77164	0.003798	98.06	4.50E-3	102
ATC-105	Evapco	1544	0.96604	0.004755	98.06	5.64E-3	102
ATC-370	Evapco	5439	0.82371	0.004055	98.06	4.81E-3	102
S-110	Frick	1617	0.8004	0.004001	97.84	4.22E-3	47
M-360	Frick	5292	0.95767	0.004787	97.84	5.05E-3	47

Table 2.2.2: Evaporative Condenser Comparison Data

An interesting point is that the values of the effectiveness slope (C2) for the correlations of these evaporative condensers are very similar. The slope is small so changes in refrigerant saturation temperature have little effect on the value of effectiveness. The effectiveness correlations for these condensers are detailed in figure 2.2.3.

If the curves for the rated heat transfer from figure 2.2.1 are extrapolated to accommodate lower wet-bulb temperatures, it appears that the rated heat transfer will be constant for all outside air wetbulb temperatures below 50°F. As the outdoor air temperature (and thus the enthalpy) decreases, the condensing process of the refrigerant in the condenser occurs more rapidly due to an increasing temperature difference between the air and the refrigerant. This increase in the rate of condensation lowers the refrigerant saturated condensing temperature and thus the condensing pressure. As the condensation rate increases, the condenser area required for pure condensation to occur decreases. This causes a greater portion of the condenser to be filled with liquid refrigerant. The resistance to heat transfer increases as the amount of liquid in the condenser increases (Incropera and DeWitt,

1996). At some point, these changes lower the overall thermal conductance (UA) value of the condenser, offsetting the increase in temperature (enthalpy) difference between the air saturated at the refrigerant temperature and the outside air. This keeps the heat rejection capacity of the evaporative condenser relatively insensitive with changing outdoor air wet-bulb temperature at outdoor temperatures below 50°F wet-bulb. It is at this point that the effectiveness of the evaporative condenser may become more dependent on the outdoor air wet-bulb temperatures.

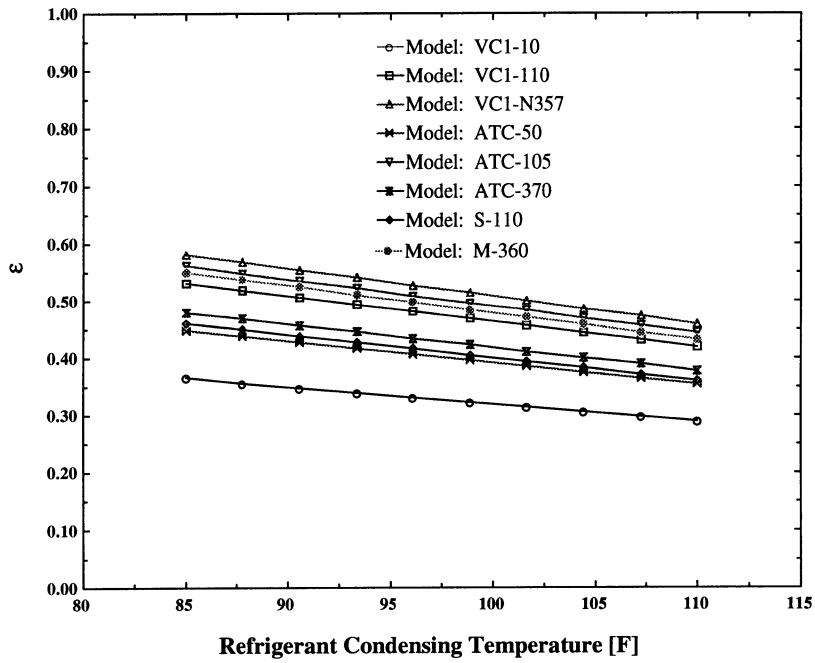

Figure 2.2.3: Effectiveness Correlations for Various Evaporative Condensers

2.2.2 Compressor

The manufacturer of the compressor provides data for the nominal power (kW) and mass flow of refrigerant (lb/hr) based on the saturated suction and saturated discharge

temperatures. These data also assume that the refrigerant suction temperature is at 65°F. Correlations were developed for the Carlyle compressors to determine power and mass flow as shown in equations (2.2.3) and (2.2.4).

$$Pwr = P_1 + P_2ST + P_3ST^2 + P_4CT + P_5CT^2 + P_6ST*CT \quad (2.2.3)$$

$$\dot{m} = \frac{v_{65}}{v_{act}}\left[M_1 + M_2ST + M_3ST^2 + M_4CT + M_5CT^2 + M_6ST*CT\right] \quad (2.2.4)$$

In these equations, ST is the saturated suction temperature (°F) and CT is the saturated condensing temperature (°F). The saturated temperatures are defined as the temperature and pressure where the refrigerant exists in both a vapor and liquid form. The constants for these equations as well as the R^2, RMS, NRMS and number of data points used in the fitting process are shown in Table 2.2.3. The program used to model these power and mass flow correlations is listed in appendix A-2.

POWER (kW)		**MASS FLOW (lb/hr)**	
P_1	7.208	**M_1**	3211
P_2	-0.1977	**M_2**	73.03
P_3	-0.001617	**M_3**	0.9389
P_4	0.3029	**M_4**	-2.852
P_5	-0.001162	**M_5**	-0.04574
P_6	0.005804	**M_6**	-0.06866
R^2	99.99%	**R^2**	100%
RMS	5.37E-02	**RMS**	7.942
NRMS	0.0021%	**NRMS**	0.0031%
DATA PTS	51	**DATA PTS**	51

Table 2.2.3: Compressor Data

The mass flow of refrigerant must be corrected for changes in suction specific volume due to changing suction superheat as indicated by Stoecker, 1988. This correction is

accomplished by multiplying by the ratio of the suction specific volume at the manufacturer rating condition (v_{65}) and the suction specific volume at actual conditions (v_{act}). As the suction superheat increases, the mass flow of refrigerant through the compressor decreases. The power is not affected by changes in suction superheat. A detailed analysis of the corrections to the mass flow rate and power required due to superheat conditions differing from the rated condition is provided in sections 2.2.2.1 and 2.2.2.2.

2.2.2.1 Correction to Mass Flow Correlation

Mass flow of refrigerant is defined by equation (2.2.5), where $\dot{m}_{ref}$ is the compressor mass flow of refrigerant at specified rating conditions, ρ_{ref} is the density of suction gas of the refrigerant at manufacturers' rating conditions, A_{ref} is the inlet area to the compressor, and V_{ref} is the velocity of the refrigerant at manufacturers' conditions.

$$\dot{m}_{ref} = \rho_{ref} A_{ref} V_{ref} \tag{2.2.5}$$

Reciprocating compressors are essentially constant volume flow rate devices. The volume flow rate for the compressor, which is a function of the cylinder sizes and compressor speed, is assumed to remain constant over all operating conditions resulting in the relationship given by equation (2.2.6). The subscript 'act' indicates conditions other than the rating conditions while the subscript 'ref' indicates reference rating conditions.

$$A_{ref} V_{ref} = CFM_{ref} = CFM_{act} \tag{2.2.6}$$

One parameter neglected in this relationship is the change in compressor volumetric efficiency at other than rated conditions. Equation (2.2.7) defines the volumetric efficiency

for a reciprocating compressor which is the ratio of actual displacement rate to maximum possible displacement rate (Stoecker, 1988).

$$\eta_{vc} = 100 - C\left(\frac{v_{suc}}{v_{disch}} - 1\right) \tag{2.2.7}$$

where η_{vc} is the volumetric efficiency (%) of the compressor, C is the percent clearance, v_{suc} is the suction specific volume and v_{disch} is the discharge specific volume. The rated volumetric efficiency was compared to actual volumetric efficiency over a range of operating conditions (see program in appendix A-3). The comparisons were done by using equation (2.2.7) to calculate the volumetric efficiency of the compressor at rated suction and discharge conditions and the volumetric efficiency of the compressor at other than rated suction superheat conditions. Assuming a percent clearance of 4% for the compressor, the difference in the two volumetric efficiencies was taken and determined to be less than 0.5% over a range of suction superheat conditions as shown in figure 2.2.4. Thus, the changes in volumetric efficiency at other than rated suction temperatures were assumed negligible.

Using equations (2.2.5) and (2.2.6), a ratio of mass flows is calculated to determine how the mass flow rate varies from manufacturer ratings at other than the rating conditions. This ratio is shown in equation (2.2.8).

$$\dot{m}_{act} = \dot{m}_{ref}\frac{\rho_{act}}{\rho_{ref}} = \dot{m}_{ref}\frac{v_{1,ref}}{v_{1,act}} \tag{2.2.8}$$

This analysis indicates that the mass flow changes with the ratio of the actual suction specific volume to the reference suction specific volume.

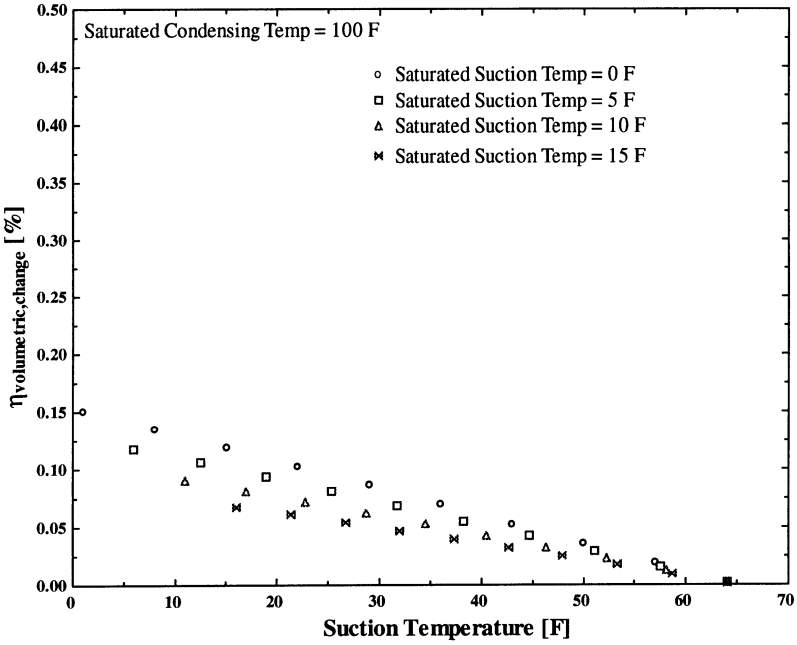

Figure 2.2.4: Change in Volumetric Efficiency

2.2.2.2 Correction to Power Correlation

Power required by the compressors is determined using the compressor correlation shown in equation (2.2.3) which was fitted to manufacturers' data. In order to determine how the power changes at other than rated suction superheat conditions, a relationship between actual power and rated power was developed. The first assumption is to treat the compression process as polytropic such that equation (2.2.9) applies.

$$Pv^n = \text{Constant} \tag{2.2.9}$$

The work per unit mass to compress the refrigerant from a low pressure (state 1) to a high pressure (state 2) is shown in equation (2.2.10) (Threlkeld, 1962).

$$W_{12} = -\frac{n}{n-1} P_1 v_1 \left[\left(\frac{P_2}{P_1} \right)^{\frac{n-1}{n}} - 1 \right] \tag{2.2.10}$$

Taking the ratio of the specific work for the rated conditions to that for the actual conditions and assuming that the discharge and suction pressures remain constant yields equation (2.2.11).

$$\frac{W_{12,act}}{W_{12,ref}} = \frac{v_{1,act}}{v_{1,ref}} \tag{2.2.11}$$

The power required by a refrigeration system can be defined by equation (2.2.12).

$$Pwr = \frac{W_{12}\dot{m}}{\eta_{motor}} \tag{2.2.12}$$

Using equation (2.2.12), the ratio of manufacturers' rated power to the power required at other than design suction superheat is shown in equation (2.2.13). This ratio is derived assuming that the motor efficiency remains constant for the varying suction superheat conditions.

$$\frac{Pwr_{act}}{Pwr_{ref}} = \frac{W_{12,act}}{W_{12,ref}} \frac{\dot{m}_{act}}{\dot{m}_{ref}} \tag{2.2.13}$$

Simplifying equation (2.2.13) with the relationships developed in equations (2.2.8) and (2.2.11) yields equation (2.2.14).

$$Pwr_{act} = Pwr_{ref} \tag{2.2.14}$$

This analysis indicates that no changes in compressor power occur with changing suction superheat.

2.2.3 Evaporator

The mass flow of secondary fluid through the evaporator, the inlet and exit temperatures of the secondary fluid and the specific heat of the secondary fluid solution

determine the evaporator load on the refrigeration system. Using an energy balance for an open system and neglecting changes in kinetic energy (KE) and potential energy (PE), the energy balances and rate equation for the evaporator load are as shown in equations (2.2.15), (2.2.16), and (2.2.17), respectively, where the evaporator effectiveness (ε_{evap}) is calculated from actual data detailed in chapter three.

$$\dot{Q}_{evap} = \dot{m}_{refrig}\left(h_{refrig,out} - h_{refrig.in}\right) \tag{2.2.15}$$

$$\dot{Q}_{evap} = \dot{m}_{brine} Cp_{brine} \Delta T_{brine} \tag{2.2.16}$$

$$\dot{Q}_{evap} = \dot{m}_{brine} Cp_{brine} \varepsilon_{evap}\left(T_{brine,in} - T_{refrig,sat}\right) \tag{2.2.17}$$

$\dot{Q}_{evap}$ is the heat transfer rate across the evaporator, $\dot{m}_{refrig}$ is the mass flow of refrigerant through the evaporator, $h_{refrig,out}$ is the specific enthalpy of the refrigerant leaving the evaporator, $h_{refrig.in}$ is the specific enthalpy of the refrigerant entering the evaporator, $\dot{m}_{brine}$ is the mass flow of secondary fluid through the evaporator, ΔT_{brine} is the temperature change of the secondary fluid across the evaporator and Cp_{brine} is the average specific heat of the secondary fluid in the evaporator. The average specific heat of the secondary fluid is calculated using a correlation developed from ASHRAE data that has inputs of mass fraction ethylene glycol in solution and secondary fluid temperature. The correlation is shown in equation (2.2.18).

$$Cp_{brine} = C_1 + C_2 T - C_3 T^2 - C_4 MF - C_5 MF^2 + C_6 TMF \tag{2.2.18}$$

where Cp_{brine} is the specific heat of the solution, T is the temperature of the solution (°F) and MF is the mass fraction of ethylene glycol in solution. The values for the constants, R^2, RMS and number of data points for this correlation are provided in Table 2.2.4.

C_1	0.972	C_4	0.3863	R^2	100%
C_2	0.0001788	C_5	0.1171	**RMS**	4.27E-4
C_3	$1.304*10^{-8}$	C_6	0.000665	**DATA PTS**	243

Table 2.2.4: Specific Heat Correlation Constants

An assumption is made that the process through the expansion valve (and through the piping due to pressure losses) is isenthalpic. Thus, the inlet enthalpy to the evaporator is assumed equal to the outlet enthalpy of the suction line heat exchanger/accumulator, the calculation of which is described in section 2.2.5.

2.2.4 Expansion Valve

Equation (2.2.19) is used in order to determine the flow coefficient for the expansion valve in a refrigeration system.

$$C_{valve} = \frac{\dot{m}_{refrig}}{A_{inlet}} \sqrt{\frac{1}{2 g_c \rho_{inlet} \; P_{valve}}} \qquad (2.2.19)$$

This equation approximates refrigerant flow through an orifice and has been experimentally validated to model the operation of expansion valves (Vinnicombe and Ibrahim, 1991).

In equation (2.2.19), C_{valve} is the experimentally determined flow coefficient, A_{inlet} is the inlet area of the valve inlet piping, g_c is the acceleration due to gravity, ρ_{inlet} is the density of the refrigerant at the valve inlet, and ΔP_{valve} is the pressure drop across the valve.

Given a constant flow coefficient, the mass flow of refrigerant through a given valve determined with equation (2.2.19) is only dependent on the pressure differential across the

valve and the refrigerant inlet pressure and temperature (which determines the density of the refrigerant).

Manufacturers' data provide expansion valve capacity that depends on:

- the pressure differential across the valve
- entering liquid temperature
- the evaporator temperature

The manufacturers' data are only provided for the valves when they are fully open. Using the manufacturers' data and assuming isenthalpic expansion across the valve, the flow coefficient was determined for the valve at five evaporator temperatures using the program listed in appendix A-4. Since the manufacturers' data did not include mass flow, the mass flow had to be estimated by using an energy balance across the evaporator which assumed no change in potential or kinetic energy across the evaporator, and no work done on or by the evaporator on the refrigerant. The resulting energy balance is shown as equation (2.2.20).

$$\dot{m} = \frac{\dot{Q}_{evap}}{\left(h_{evap,out} - h_{evap,in}\right)} \qquad (2.2.20)$$

Here $\dot{Q}_{evap}$ is the refrigeration capacity given in the valve manufacturers' data, $h_{evap,out}$ is calculated using the manufacturers' saturated evaporator temperature and assuming the refrigerant has a quality of one when leaving the evaporator, and $h_{evap,in}$ is calculated using the pressure and temperature of the refrigerant leaving the condenser if it is subcooled. The manufacturers' data assumes that the refrigerant leaves the condenser as a saturated liquid so the enthalpy of the refrigerant entering the evaporator is calculated using the saturated condensing temperature and a quality of zero.

It is expected that the flow coefficient should remain approximately constant over a varying range of Reynolds numbers (CRANE, 1988). In order to validate this assumption, the Reynolds number is calculated at the inlet condition using equation (2.2.21).

$$\mathrm{Re} = \frac{\dot{m}_{refrig} D_{inlet}}{A_{inlet} \mu_{inlet}} \tag{2.2.21}$$

where D_{inlet} is the diameter of the inlet piping to the expansion valve, A_{inlet} is the inside area of the pipe inlet to the valve, and μ_{inlet} is the viscosity of the fluid which is calculated using the inlet temperature and pressure of the refrigerant.

A plot of the flow coefficient over a range of Reynolds numbers and evaporator temperatures is shown in Figure 2.2.5. As shown in Figure 2.2.5, the flow coefficient for the Sporlan Model OVE55 expansion valve varies as a function of evaporator temperature between 0.022 at an evaporator temperature of -40°F and 0.058 at an evaporator temperature of 40°F. According to CRANE, the flow coefficient should remain constant for a given orifice. In the analysis of the expansion, the opening of the valve was assumed to be constant for the same model valve. However, according to the valve manufacturer, the opening distance of the valve changes with evaporator temperature, thereby changing the inlet area of the valve (BUNDY, 1997).

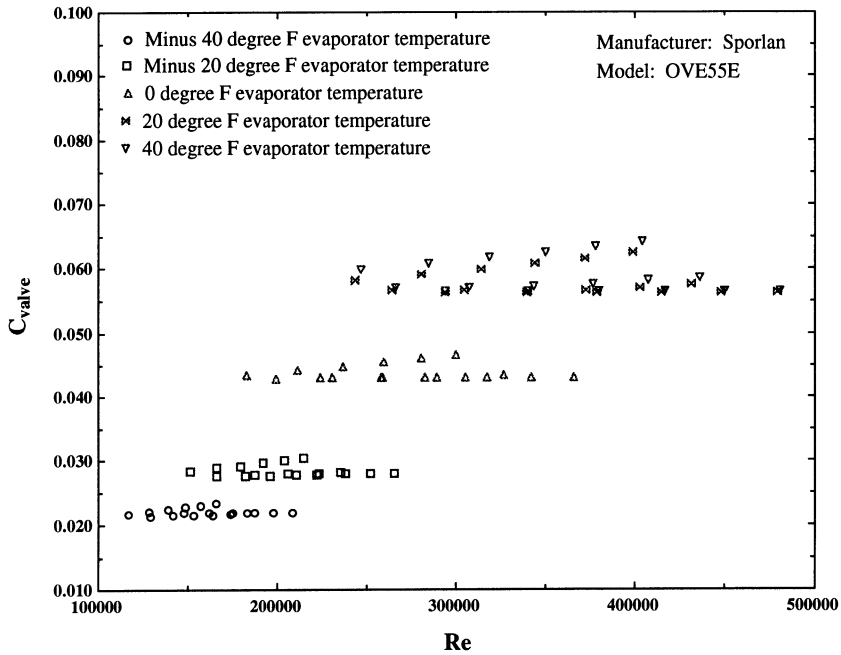

Figure 2.2.5: Flow coefficient Vs. Reynolds Number

This change in inlet area results in a change in flow coefficient for this analysis. Since the evaporator temperatures used in this project were approximately 0°F, a flow coefficient of .043 was used.

This flow coefficient was then used in equation (2.2.22) to ensure that the conditions the valve is subjected to are not outside of its operating range which is 30% to 100% of rated capacity (Vinnicombe and Ibrahim, 1991).

$$\dot{m}_{refrig} = C_{valve} Valve_{open} A_{inlet} \sqrt{2 g_c \rho_{in} \Delta P}_{expansion,valve} \qquad (2.2.22)$$

C_{valve} is the constant flow coefficient for the valve (0.043 for this system) and $Valve_{open}$ is a unit less variable representing the fractional amount that the valve is open for a given condition.

In its application to this research, equation (2.2.22) is used to calculated $Valve_{open}$. The maximum value for this variable is unity with the minimum acceptable being 0.3. Values greater than unity mean that the expansion valve is the restriction in the system and a larger valve is needed to operate at the specified conditions. Values less than 0.3 indicate that the valve is operating at a load much lower than for which it was designed, which in practice can cause the valve to cycle repeatedly open and close. The valve cycling may allow for the introduction of liquid refrigerant to the compressor suction. Any values between 0.3 and unity indicate that the valve is sized properly.

2.2.5 Suction Line Heat Exchanger/Accumulator

The suction line heat exchanger was modeled using an effectiveness model. The effectiveness was determined from experimental data and equations (2.2.23), (2.2.24), and (2.2.25). Equations (2.2.23) and (2.3.25) where derived from equation (2.1) while equation (2.2.24) is a heat transfer rate equation. These equations assume no changes in kinetic or potential energy and that no work was performed on or by the system.

$$\dot{Q}_{HX} = \dot{m}_{refrigerant}\left(h_{in(liquid)} - h_{out(liquid)}\right) \tag{2.2.23}$$

$$\dot{Q}_{HX} = \dot{m}_{refrigerant}\varepsilon_{HX}\left(h_{refrig,max} - h_{refrig,in}\right) \tag{2.2.24}$$

$$\dot{Q}_{HX} = \dot{m}_{refrigerant}\left(h_{out(vapor)} - h_{in(vapor)}\right) \tag{2.2.25}$$

where the effectiveness (ε_{HX}) of the heat exchanger is determined from actual data (detailed in chapter three). The heat exchanger effectiveness determines $h_{out(vapor)}$ and $h_{out(liquid)}$. All other enthalpies and the mass flow of refrigerant are determined by other system components described in this chapter.

2.2.6 Refrigerant Piping pressure drop

In order to determine the piping pressure drop, the simplified form of Bernoulli's Theorem was used as shown in equation (2.2.26) (CRANE 1988). This form of Bernoulli's equation assumes that the density and velocity remain unchanged throughout the section of piping being analyzed.

$$Z_1 - Z_2 + \frac{(P_1 - P_2)}{\rho_{12}} = h_{L12} \tag{2.2.26}$$

Z_1 and Z_2 are the original and final height of the piping section, P_1 and P_2 are the pressure at the entrance and exit of the piping section, ρ_{12} is the average density throughout the piping section, and h_{L12} is the head loss due to friction in the piping section. h_{L12} is calculated using the Darcy equation shown in equation (2.2.27) (CRANE 1988).

$$h_{L12} = \frac{K_{12} Q^2}{d^4} \tag{2.2.27}$$

K_{12} is the total resistance coefficient for the piping (based on configuration, size and material), Q is the flow rate through the piping, and d is the inside diameter of the piping. In order to determine K_{12}, the resistance coefficients for the pipe and elbows are summed as shown in equation (2.2.28).

$$K_{12} = K_{elbow} N_{elbows} + K_{pipe} \tag{2.2.28}$$

where K_{elbow} is the resistance coefficient of each elbow installed. K_{elbow} is known from experimental correlations for standard 90-degree elbows as indicated using equation (2.2.29) (CRANE 1988).

$$K_{elbow} = 30f \tag{2.2.29}$$

where f is the friction factor and is determined using equation (2.2.31) and K_{pipe} was determined by definition using equation (2.2.30).

$$K_{pipe} = f\frac{L}{d} \tag{2.2.30}$$

It is necessary to relate the friction factor to the refrigerant flow rate. Assuming turbulent flow, the Colebrook equation can be applied (MARKS 1996).

$$\frac{1}{\sqrt{f}} = -2\ln\left(\frac{\varepsilon/D}{3.7} + \frac{2.51}{\mathrm{Re}\sqrt{f}}\right) \tag{2.2.31}$$

Here ε/D is the relative roughness of the interior of the pipe wall and is determined based on the diameter of the pipe and the material with which it was constructed and Re is the Reynolds number (CRANE 1988). Preliminary calculations were performed to ensure that the assumption of turbulent flow was valid. These calculations indicated Reynolds numbers in the range of 2.5E5 to 2E6, which ensures turbulent flow.

2.2.7 Suction Line Filter Pressure Drop

In order to determine the pressure drop in the suction line filter, manufacturers' data was used for the Sporlan model RPE-48-BD suction line filter (SPORLAN, 1995). A correlation was developed to predict the pressure drop across the filter based on the mass flow of refrigerant through the filter. The correlation was developed using six manufacturer data points with an R^2 of 99.75% and a RMS of 0.0568. The correlation is shown in equation (2.2.32) with the pressure drop in psi and the mass flow of refrigerant in lb/hr.

$$\Delta P_{filter} = 0.1788 + 0.000197\dot{m}_{refrig} \qquad (2.2.32)$$

The initial analysis of the catalog data for this filter showed an error in the capacity rating for an evaporator temperature of -20°F. The catalog rated the capacity at 32 tons, while the calculations predicted that the capacity should be approximately 22 tons for this condition. After conversation with Sporlan concerning this problem, they agreed that the capacity should indeed be approximately 22 tons at these conditions (Gildehaus, 1997).

Chapter 3

Data Logger Programming and Equipment Calibration

3.1 Programming

Each device installed as described in Chapter 4 required specific programming of the Campbell 21X datalogger to convert the inputs to useful outputs. The logic behind the programming is described in this section with the actual program listed in Appendix B.

3.1.1 Pressure Transducers

The pressure data are measured using three different types of pressure transducers. The discharge pressure transducers have a range of 0-300 psia with an output of 0.5-5.5VDC. One suction line transducer has a range of 0-100 psig with an output of 4-20mA. The other suction line transducer has a range of 0-60 psig with an output of 0.5-5.5VDC.

3.1.1.1 0-300 psia Discharge Pressure Transducer

The output from the discharge transducer is converted to a pressure by taking the range of the transducer (300 psi) and dividing it by the range of output voltage (5000mVDC) to obtain a multiplier of 0.06 psia/mVDC. An offset was calculated to account for the minimum voltage output of 0.5VDC corresponding to zero psia. This offset was calculated by multiplying -500mVDC by the multiplier to obtain –30. This conversion from an output voltage signal to a pressure is shown as equation (3.1.1).

$$P_{discharge} = 0.06 * Output_{signal} - 30 \quad (3.1.1)$$

3.1.1.2 0-100 psig Suction Pressure Transducer

The output from the suction pressure transducer is converted to a pressure by first converting the output current to a voltage. A 270Ω resister was installed in series to convert the 4-20mA signal to a 1080-5400 mVDC signal. The range of the transducer (100 psi) was then divided by the range of output voltage (4320mVDC) to obtain a multiplier of 0.0231 psig/mVDC. An offset was then calculated to account for the minimum voltage output of 1080mVDC corresponding to zero psig. This offset was calculated by multiplying -1080mVDC by the multiplier to obtain –25. This conversion from an output voltage signal to a pressure is shown as equation (3.1.2).

$$P_{suction} = 0.0231 * Output_{signal} - 25 \quad (3.1.2)$$

3.1.1.3 0-60 psig Suction Pressure Transducer

The output from the suction transducer is converted to a pressure by taking the range of the transducer (60 psi) and dividing it by the range of output voltage (5000mVDC) to obtain a multiplier of 0.012 psig/mVDC. An offset was calculated to account for the minimum voltage output of 0.5VDC corresponding to zero psia. This offset was calculated by multiplying -500mVDC by the multiplier to obtain –6. This conversion from an output voltage signal to a pressure is shown as equation (3.1.3).

$$P_{suction} = 0.012 * Output_{signal} - 6 \quad (3.1.3)$$

3.1.2 Thermocouples

The Campbell 21X provides internal temperature measurement with a factory set resistance temperature device (RTD). The data logger is able to convert the voltage output to a temperature through pre-programmed multipliers using the internal RTD as the reference temperature for temperature compensation.

3.1.3 Resistance Temperature Devices

The resistance temperature devices (RTD's) used for measuring the temperature difference of the glycol solution were factory calibrated to output a 4-20 mA signal based on a temperature range from –4 to 68°F. To increase accuracy in measuring temperature differences, they were calibrated as a matched set, to track each other within 0.1°F. Resistors (217.3Ω) are used to convert the 4-20mA signals to a voltage range of 869.2-4346mVDC. The range of the RTD's (72 °F) was then divided by the range of output voltage (3476.8mVDC) to obtain a multiplier of 0.02071 °F /mVDC. An offset was then calculated to account for the minimum voltage output of 869.2mVDC corresponding to -4 °F. This offset was calculated by multiplying -869.2mVDC by the multiplier and adding -4 °F to obtain –22. This conversion from an output voltage signal to a temperature is provided as equation (3.1.4).

$$T_{glycol} = 0.02071 * Output_{signal} - 22 \qquad (3.1.4)$$

Appendix C depicts the exact wiring of the RTD's with the inlet glycol temperature represented by T15 and the exiting glycol temperature represented by T16. One resistor is installed between the high input and ground and one between the low input and ground.

3.1.4 Flow Meter

The flow meter data are obtained using a dual turbine flow meter. This meter is factory calibrated to have an output equivalent to 5.205 pulses/gallon when installed in an 8 inch, schedule 80 PVC pipe. The flow meter output is then converted to give an output of gallons per minute based on data logger input from the flow meter of total pulses/two seconds. The multiplier for the flow meter was calculated by taking the meter output of pulses/second and dividing it by the meter calibration constant of 5.205 pulses/gallon. This gives an output of gallons per second, which is converted to gallons/minute by multiplying by 60 seconds/minute. Therefore, the overall multiplier is calculated as 5.77 with no offset, which can be shown by equation (3.1.5).

$$GPM = \#Pulses * 5.77 \tag{3.1.5}$$

3.1.5 Relative Humidity/Outside Air Temperature Sensor

The output from the relative humidity sensor is converted to a relative humidity (percentage) by first converting the output current to a voltage. A 218.4Ω resister was installed in series to convert the 4-20mA output signal to an 873.6-4368 mVDC signal. The range of the sensor (100%) was then divided by the range of output voltage (3494.4mVDC) to obtain a multiplier of 0.02862 %/mVDC. An offset was then calculated to account for the minimum voltage output of 873.6mVDC corresponding to 0% relative humidity. This offset

was calculated by multiplying -873.6mVDC by the multiplier to obtain –25. This conversion from an output voltage signal to a humidity is shown as equation (3.1.6).

$$RH = 0.02862 * Output_{signal} - 25 \quad (3.1.6)$$

The output from the outside air temperature sensor is converted to a temperature (°F) by first converting the output current to a voltage. A 218.1Ω resister was installed in series to convert the 4-20mA output signal to an 872.4-4362 mVDC signal. The range of the sensor (180°F) was then divided by the range of output voltage (3489.6mVDC) to obtain a multiplier of 0.0516°F /mVDC. An offset was then calculated to account for the minimum voltage output of 872.4mVDC corresponding to 32°F. This offset was calculated by multiplying -872.4mVDC by the multiplier and adding 32°F to obtain –13. This conversion from an output voltage signal to a temperature is shown as equation (3.1.7).

$$OATEMP = 0.0516 * Output_{signal} - 13 \quad (3.1.7)$$

3.1.6 Watt Transducer

The output of the watt transducer is converted to power (kW) using an output constant for the transducer of 306.4 W-hr/pulse. The output constant was multiplied by 3600 seconds/hour and 1 Kw/1000W. Additionally, the new multiplier had to be divided by two to account for the scanning of the channel every two seconds. This gives a multiplier of 551.5 kW/pulse, which is shown in equation (3.1.8).

$$kW = \#Pulses * 551.5 \quad (3.1.8)$$

3.2 Calibration

After calculation of the offsets and multipliers for each component, an attempt was made to validate the performance of the sensors. This section describes how the sensor performance was validated and any field adjustments that were performed.

3.2.1 Pressure Transducers

The factory set calibration of the pressure transducers was validated prior to installation in the system and again once they were installed in the system. The validation prior to installation in the system was performed using pressurized oxygen to apply pressures across the entire range of their operation. The values read from the regulator gage on the oxygen tank corresponded with the pressure gage readings for all transducers. Once the transducers were installed in the system, the suction line transducers could be validated to ensure proper operation. When each compressor bank 'pumps down', pressure controllers on each compressor shut down the compressor when the suction pressure is zero gauge pressure. At these conditions, each of the pressure transducers read a pressure of approximately zero when the compressors shut down. Therefore, no field calibration was applied to the pressure transducers.

3.2.2 Thermocouples

The thermocouples were factory calibrated to read within ±1°F. Since the thermocouples had an adhesive backing, which would be damaged if immersed in water, the thermocouples calibration could not be checked by immersing them in an ice bath. Instead a verification was done to ensure that all the thermocouples tracked each other within 1°F.

This was done by simultaneously exposing the thermocouples to ambient temperatures and ensuring that they all read the same temperature. This test concluded that all thermocouples tracked each other within 0.5°F, thereby supporting the case that field calibration was not necessary.

3.2.3 Resistance Temperature Devices

In order to instill confidence in the RTD calibration, each RTD was placed in the same ice bath. Both RTD's read 32.2-32.5°F with a change in temperature between them of 0.007°F. The RTD's were then both placed in ambient conditions and they tracked each other to within 0.1°F. Additionally, the RTD reading for each sensor was compared to the installed temperature gauges and agreed to within the 0.5°F accuracy of the installed gauges. Therefore, no field calibration was required for the RTD's.

3.2.4 Flow Meter

The factory calibration of the meter is performed using a known flow of water through an eight inch, schedule 80 PVC pipe. The meter is calibrated for an insertion depth of 1/3 the inner pipe diameter. In this case, the insertion depth is two and one-half inches below the top, inner wall of the pipe. This insertion depth is important to ensure that the velocity measurement of the fluid is at the calibrated position on the fluid velocity profile. If the turbine is inserted too far into the pipe, flow rates higher than expected will be measured (due to the higher fluid velocities at the center of the pipe) unless you insert it past the center at which point the measured flow is reduced.

Using a finite difference equation for one dimensional turbulent flow in a pipe, a program was written (listed in appendix A-5) to determine the velocity profiles for both water and ethylene glycol. A comparison of these profiles is shown in Figure 3.1 for the calibrated flow of 1090 GPM. As is apparent in Figure 3.1, the velocity is insensitive to insertion position at the sensor insertion depth. Figure 3.2 depicts the error in readings that can be expected at changes in flow through the piping. As shown, the error does not exceed 5%, which is the rated accuracy of the flow meter.

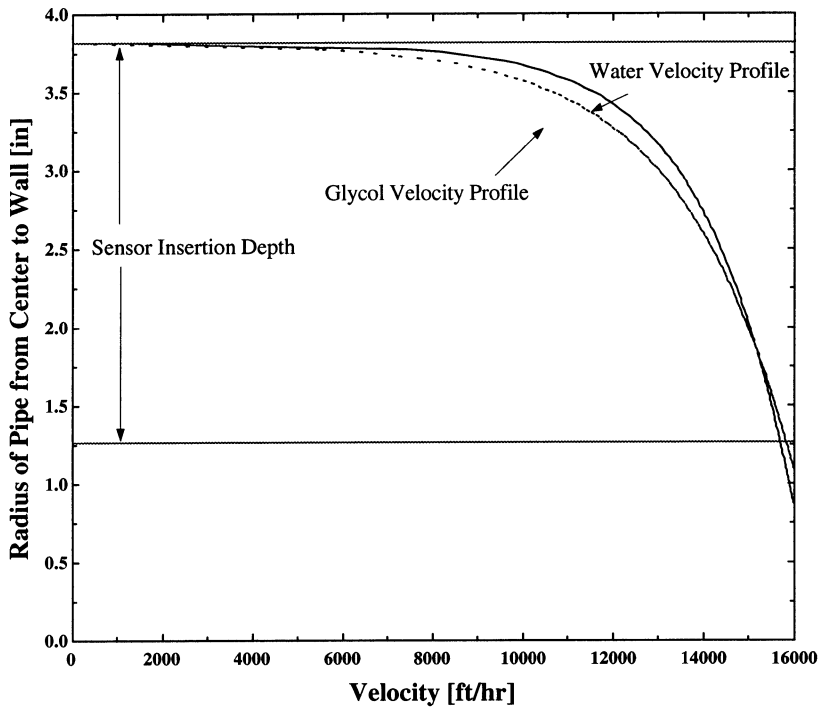

Figure 3.1: Water/Glycol Velocity Profile Comparison

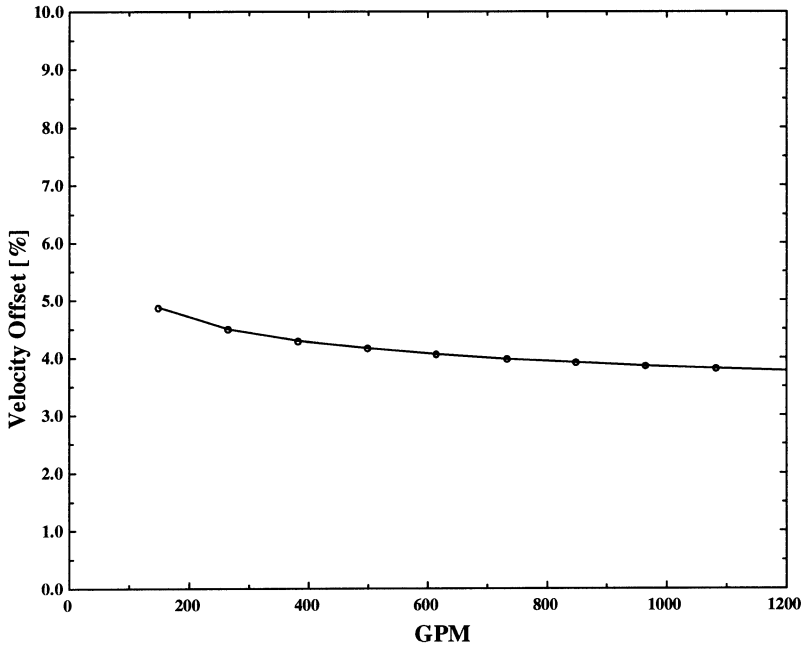

Figure 3.2: Velocity Offset at Varying Flow Rates

3.2.4.1 Use of Flow Meter Output for Energy Balance

The flow meter output is used, in conjunction with the change in temperature of the glycol across the evaporator (recorded by a matched pair of RTD's) and the refractometer data for mass fraction of glycol in solution, to give the brine-side refrigeration load for the system. The refrigerant-side load calculation is performed using a correlation for mass flow of refrigerant (depending on the compressor suction and discharge pressures and suction temperature) and the enthalpy change of the refrigerant across the evaporator. The heat transfer rate from the glycol to the refrigerant should be equal. Equations (4.5.6) and (4.5.9) detail how each of these heat transfer rates are calculated.

3.2.4.2 Analysis of Data

Data collected at two-second intervals has been averaged to one-minute time blocks and used to analyze the system performance. Figure 3.3 depicts data taken and manipulated as described above with four compressors operating.

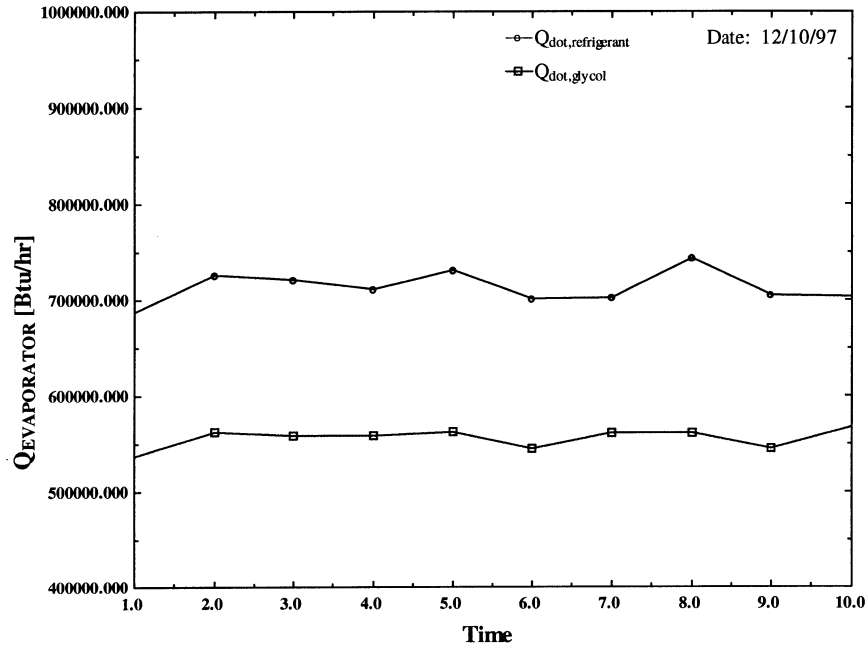

Figure 3.3: Evaporator Load with Four Compressors Operating

As shown in this figure, the calculated loads based on the refrigerant side are approximately different by a factor of 67% of the calculated brine-side load over the entire range of conditions. The glycol side heat transfer has a predicted experimental error of ±5% while the refrigerant side heat transfer has a predicted experimental error of ±7%. An error analysis for these two heat transfer equations is provided in appendix D. The results of the error analysis do not provide an explanation for the discrepancy between the calculated refrigerant and brine-side loads. Another set of data, with two compressors running, is shown in Figure 3.4.

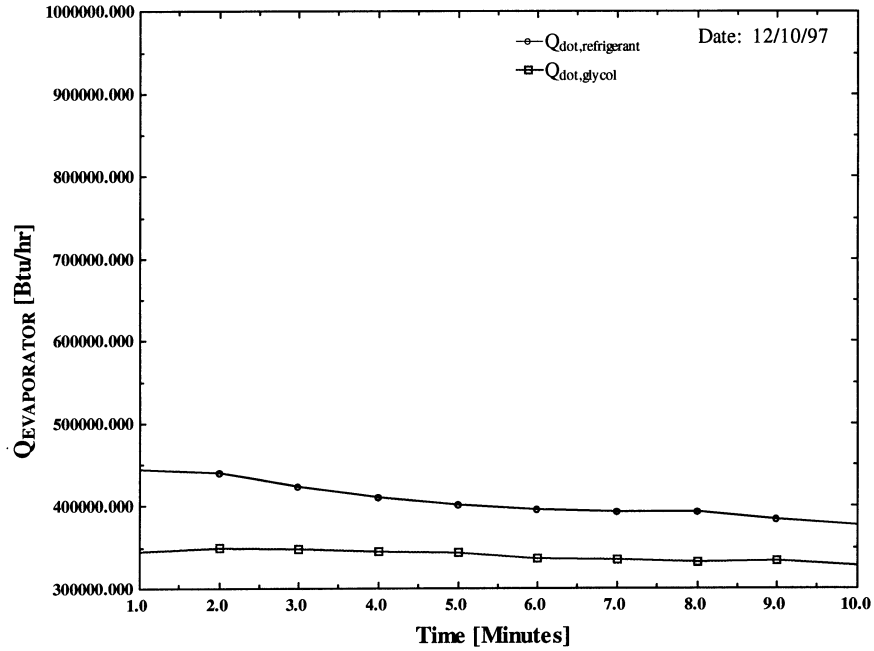

Figure 3.4: Evaporator Load with Two Compressors Operating

The calculated loads depicted in Figure 3.4 differ by a factor of approximately 2/3 $\left(\dot{Q}_{glycol}/\dot{Q}_{refrigerant}\right)$ over the ten minute range of analysis. Both of these energy balances (Figure 3.3 and Figure 3.4) are well outside the expected error bands determined with the error analysis in appendix D.

With both of the energy balances being so far out of balance, other attempts were made to determine if the flow meter was accurately measuring the flow of glycol through the evaporator. The glycol pressure differential across the evaporator was measured over a range of flow rates shown by the flow meter. These pressure differentials were compared to the manufacturers rating for pressure drop across the evaporator at various flow rates (API, 1989). Figure 3.5 depicts these data. As shown in figure 3.5, the measured flow rate is within experimental error of the predicted flow rate for the measured pressure drops. With this information, it was concluded that the experimentally measured flow rate of glycol was

within experimental error and no field calibration was required. The leaves the mass flow of refrigerant predictions using manufacturer data and the RTD calibration as the final possibilities for error. The additional steps performed to find the source of energy imbalance are described in chapter four.

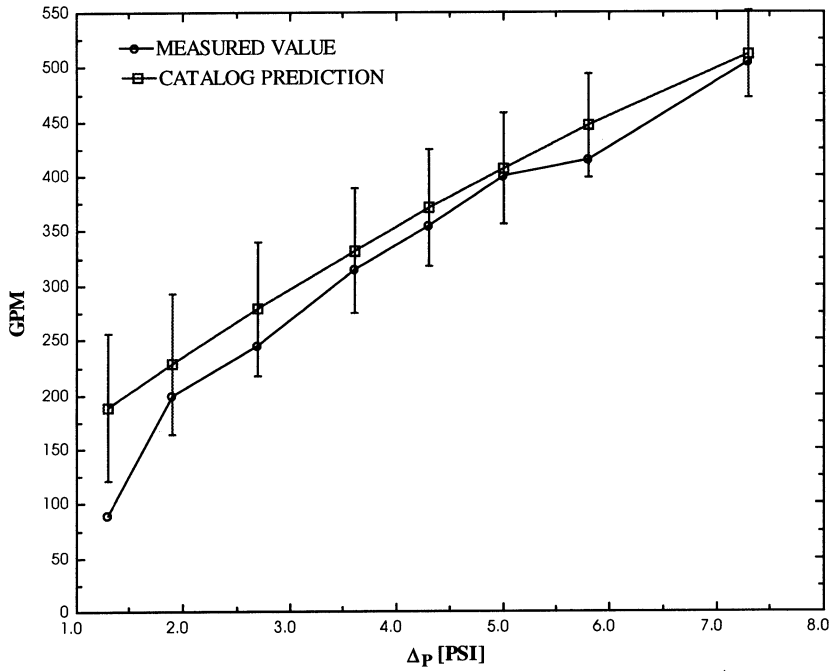

Figure 3.5: Evaporator brine-side flow rate and pressure drop characteristics

3.2.5 Relative Humidity/Outdoor air Temperature

In order to validate the operation of the relative humidity/outdoor air temperature, a sling psychrometer was employed. A problem developed with the operation of the sensor causing it to give extraneous readings. Troubleshooting of the problem was performed with no success. Therefore, all outdoor ambient air conditions where taken with a sling psychrometer and the sensor was abandoned.

3.2.6 Watt Transducer

The watt transducer was validated using the instantaneous readings from another transducer, which was installed temporarily by Madison Gas and Electric (MG&E). The MG&E transducer has a rated accuracy of ±5%. The watt transducer values were also compared to predicted values using the compressor maps and matched to within 5%. Both of these methods validated that the transducer was operating properly so no field calibration was required.

The actual and predicted power consumption of the compressors is compared to ensure that the correlation developed from compressor manufacturer's data is correct. The actual power is obtained from two-second watt transducer data averaged in one-minute blocks with uncertainty of ±5%. The predicted power consumption is based on the compressor suction and discharge saturation temperatures (based on pressure measurements) which are input into a correlation developed from manufacturer's data with an uncertainty of ±7%.

A comparison of the actual and predicted power for four compressors in operation is shown in Figure 3.6. With four compressors running, the average error is 3%, which is well within experimental error. An additional evaluation was performed with six compressors in operation as shown in Figure 3.7. With six compressors running, the average error is less than 2%, which is well within experimental error. With the analysis shown in figure 3.6 and figure 3.7, it was concluded that no field calibration was required for the watt transducer.

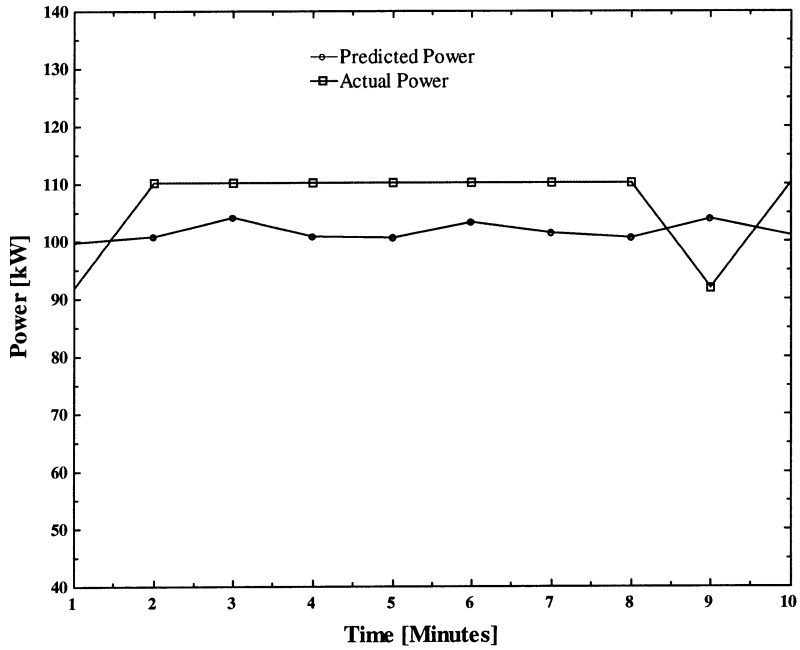

Figure 3.6: Power Comparison with 4 Compressors Operating

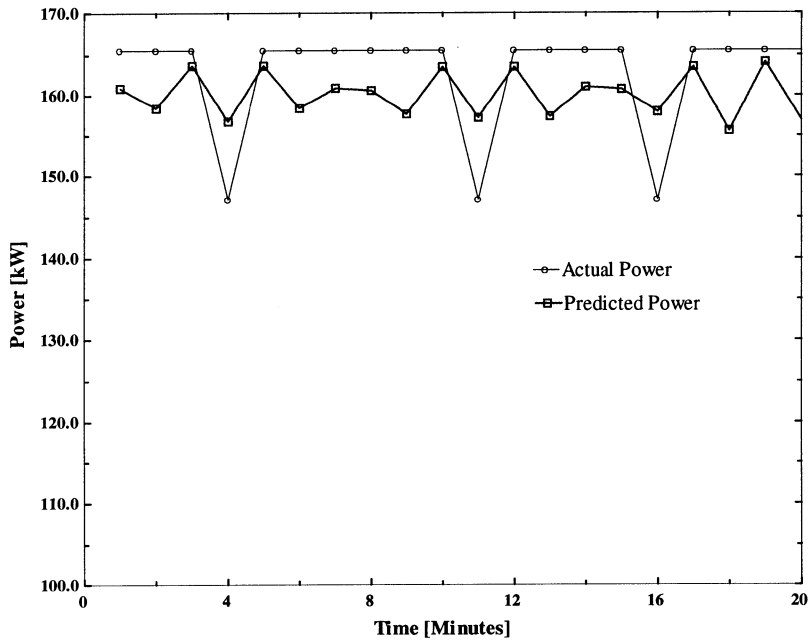

Figure 3.7: Power Comparison With Six Compressors Operating

Chapter 4

Monitoring Plan, Component Validation and System Modeling for the Madison Ice Arena

4.1 Background

Data logging equipment was installed at the Madison Ice Arena (MIA) in locations shown in figure 4.1, in order to validate component performance data for the computer model described in Chapter 2. Once validated, these models were used to predict the performance of the refrigeration system for varying control settings and modified system configurations with results shown in Chapters 5 and 6.

4.2 Installation Requirements

This section discusses the installation requirements for the data logging equipment used in monitoring performance of the refrigeration system. The term 'secured' is used several times in this section and it is defined as the shutting down of the refrigeration system by pumping all of the refrigerant back to the system high pressure receivers and thus removing the refrigerant from the low side of the system.

4.2.1 Thermocouples

The installation of the thermocouples required shutting down one bank of compressors at a time and allowing the piping to warm to ambient conditions. Once the

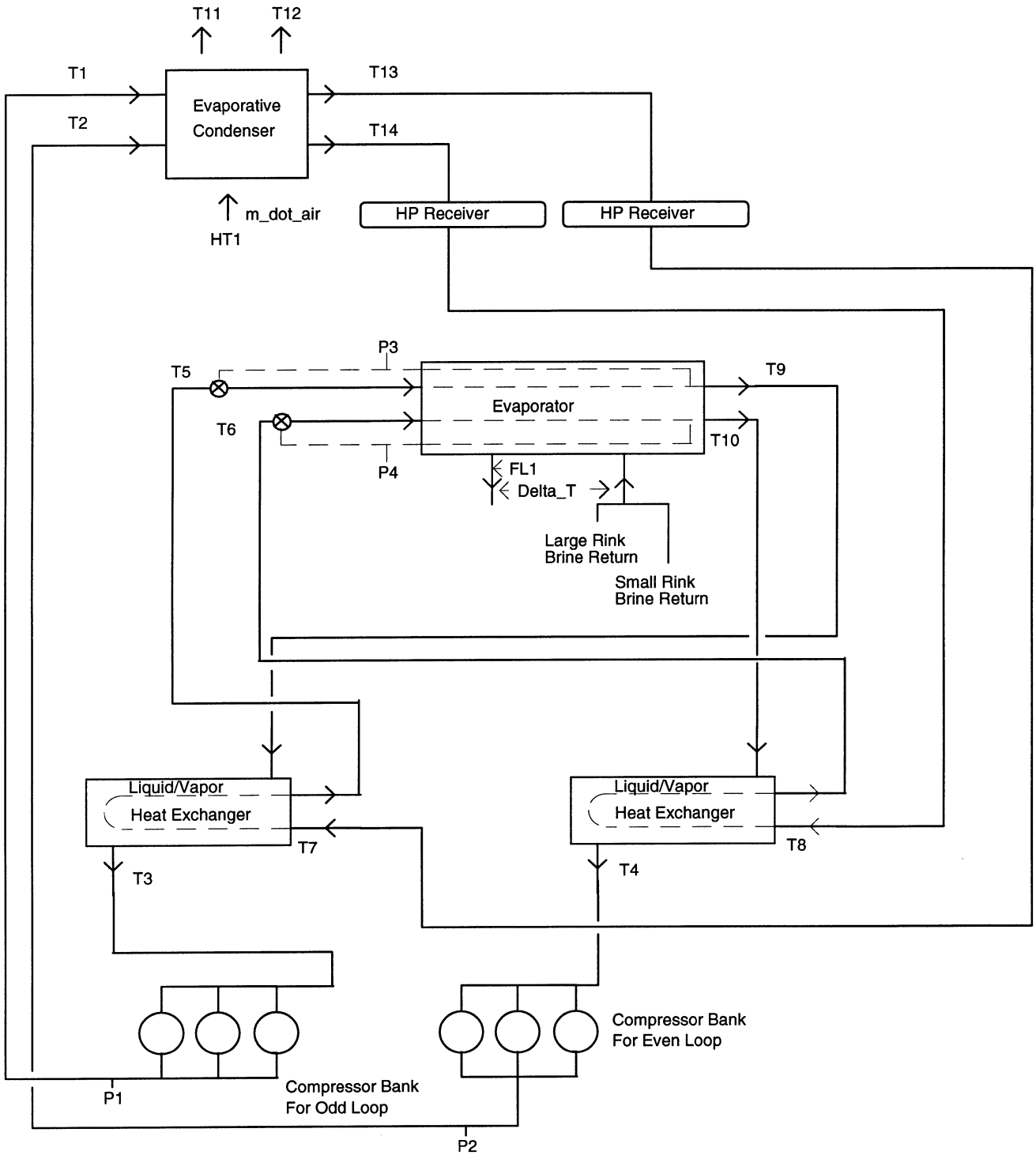

Figure 4.1: MIA Refrigeration System

piping was warm, a patch of insulation was removed from the piping for installation of thermocouples T3 through T8 for a total of six areas. After installation of the thermocouples, the integrity of the insulation system was restored using new insulation and adhesive. The installation of thermocouples T1, T2, and T11-T14 did not require the removal and subsequent repair of insulation.

4.2.2 Pressure Transducers

The installation of the pressure transducers (P1-P4) was accomplished by a refrigeration contractor. Pressure transducers P3 and P4 were installed by disconnecting the external equalizer line and installing a ¼" tee fitting with flare connections for each transducer. Pressure transducers P1 and P2 were installed by closing the valve for the head pressure controls and installing a ¼" tee fitting with flare connections for each transducer. Both of these installations required the system to be briefly secured from operation.

4.2.3 Watt Transducer

The installation of the watt transducer required that the system be completely secured for safety purposes. Once the system was secured, the power to the controller was shut off to facilitate a safe installation of the current transformers. The watt transducer required the installation of two current transformers that convert the measured current draw on two of three phases to a voltage. This was then connected as an input to the watt transducer.

4.2.4 Flow Meter

The installation of a flow meter in the brine side of the system required the entire system to be secured. Once secured, the brine side pumps were shut down and a one inch hole was drilled in the schedule 80 PVC piping between the evaporator and the glycol pumps. A brass pipe saddle with a one inch ball valve was then installed on the pipe. Once installed, the flow meter could be inserted and extracted while the system was operational. The flow meter was installed 16 pipe diameters downstream and six pipe diameters upstream of bends in the piping. This was done to allow a proper velocity profile of the glycol solution to develop.

4.2.5 Brine Side Temperature Difference

The temperature rise on the brine-side was measured using a matched pair of resistance type detectors (RTD, platinum type). The RTDs were installed in existing one-half inch pipe taps on the inlet/exit of the glycol to/from the evaporator. The pipe nipple was insulated to minimize any bias in the temperature difference measurement. However, this insulation was most likely not required as the RTD's only measure temperature at the tip that was completely immersed in the glycol solution. This installation allowed the RTDs to be removed and inserted into the system during operation.

ABBREVIATION	PARAMETER	LOCATION	SENSOR TYPE
T1	Temperature	Odd Evap Cond inlet	Type T Thermocouple
T2	Temperature	Even Evap Cond inlet	Type T Thermocouple
T3	Temperature	Odd Comp suction	Type T Thermocouple
T4	Temperature	Even Comp suction	Type T Thermocouple
T5	Temperature	Odd Evap inlet (Before Exp valve)	Type T Thermocouple
T6	Temperature	Even Evap inlet (Before Exp valve)	Type T Thermocouple
T7	Temperature	Odd Receiver outlet (Before HX)	Type T Thermocouple
T8	Temperature	Even Receiver outlet (Before HX)	Type T Thermocouple
T9	Temperature	Odd Evap outlet (Before HX)	Type T Thermocouple
T10	Temperature	Even Evap outlet (Before HX)	Type T Thermocouple
T11	Temperature	Discharge Air Temp for Evap Cond	Type T Thermocouple
T12	Temperature	Discharge Air Temp for Evap Cond	Type T Thermocouple
T13	Temperature	Odd Refrigerant out of Evap Cond	Type T Thermocouple
T14	Temperature	Even Refrigerant out of Evap Cond	Type T Thermocouple
ΔT	Temperature	Temperature Diff Btwn Evap in/out	RTD (Platinum, 100 ohm nom resistance)
P1	Pressure	Odd Compressor Discharge	Transducer
P2	Pressure	Even Compressor Discharge	Transducer
P3	Pressure	Odd Compressor Suction	Transducer
P4	Pressure	Even Compressor Suction	Transducer
W1	Watts	Power (All compressors)	Transducer
FL1	Flow	Common Brine Inlet to Evaporator	Dual Turbine, Impedance Type
HT1	Temp/Humidity	Outdoor air conditions	Capacitor

Table 3.1: Sensor Points

4.2.6 Data Logger hook-up

The data logger used was a Campbell 21X with eight analog and four pulse input channels. In order to expand the number of analog input channels to accommodate the numerous thermocouples, a Campbell AM25T multiplexer was used. The wiring diagram for the data logger is shown in Appendix C.

4.3 Length of Monitoring

The system was completely installed in early September of 1997 and the last data were taken in January of 1998. During the monitoring, the watt transducer was determined to be faulty and was replaced so data taken during October and November had no power measurements. As of the writing of this thesis, the data logging equipment has not been removed from Madison Ice Arena. However, when the removal of the data logging system is performed, the pipe saddle for the flow meter and the thermocouples will be left in place. All other equipment can be recovered for re-use.

4.4 Time Interval for Readings

Data were taken in two-second intervals to account for the transient system operation and then time-averaged over one-minute intervals to obtain a quasi-steady-state operating condition. These time blocks were taken at varying outdoor air conditions and also at varying system operation (e.g., with two, three, four or six compressors operating and one or two glycol pumps running).

4.5 Energy Balances

The following sections describe how data taken at individual points is used to validate energy balances. Locations with nomenclature of 'odd' and 'even' depict each of the two refrigerant loops in the system. Enthalpy numbering corresponds with the location of the equivalent thermocouple (i.e. h_9 would be the enthalpy at the outlet of the evaporator on the odd loop of the refrigeration system). These energy balances were performed to determine that the data logging equipment was operating properly and add any offsets required for field calibration as detailed in Chapter 3.

4.5.1 Evaporative Condenser

An energy balance was used on both the air-side and refrigerant side of the evaporative condenser. The heat transfer rates were later compared to the effectiveness-based heat transfer analysis developed from manufacturers data. The effectiveness analysis is shown in Chapter 2.

4.5.1.1 Air Side

The air-side heat rejection to ambient used four inputs from the data logging system as shown in equation (4.5.1).

$$Q_{evapcondenser} = \dot{m}_{air}\left(h_{air,out} - h_{air,in}\right)Fraction_{fan\ on} \qquad (4.5.1)$$

where:

- $\dot{m}_{air}$ is determined using manufacturers' data

- $h_{air,out}$ is a function of the average of T11 and T12 with the assumption that the air is saturated (this assumption was validated using a psychrometer)
- $h_{air,in}$ is a function of the outdoor air humidity and temperature (HT1).
- $Fraction_{fan\ on}$ is the fractional amount of time that the fan is on. The heat transfer from the evaporative condenser to the outside air is approximated as zero when the fan is not in operation.

The value of $Fraction_{fan\ on}$ had to be derived from actual data taken. The value of $Fraction_{fan\ on}$ was calculated by determining the amount of time, over a given period, that the values of discharge pressure from the compressors (P1 and P2) were decreasing (which is indicative of cooling which occurs only when the fan is operational). The fan time on was then divided by the total time period to give the $Fraction_{fan\ on}$.

There are several possible sources for error in calculation of this heat rejection rate. The first source is the use of only two thermocouples to measure the discharge air temperature from the evaporative condenser. The discharge area of the evaporative condenser is 57 ft^2. The temperature across this area could have varied substantially from that read by the two thermocouples. Assuming an uncertainty of 5°F in the discharge air temperature, 5% in the discharge humidity and 1°F in inlet dry-bulb and wet-bulb temperatures, the overall uncertainty for equation (4.5.1) was calculated as ±20% using the uncertainty analysis in EES (Klein, 1998).

4.5.1.2 Refrigerant Side

The refrigerant-side heat transfer analysis used ten inputs from the data logger as shown in equation (4.5.2).

$$\dot{Q}_{evapcondenser} = \dot{m}_{refrigerant,odd}(h_1 - h_{13}) + \dot{m}_{refrigerant,even}(h_2 - h_{14}) \qquad (4.5.2)$$

where:

- $\dot{m}_{refrigerant,odd}$ is determined using compressor data and P1, P3 and T3 with pressure drops included for the suction line piping, filter and heat exchanger to predict the actual compressor suction pressure.
- $\dot{m}_{refrigerant,even}$ is determined using compressor data and P2, P4 and T4 with pressure drops included for the suction line piping, filter and heat exchanger to predict the actual compressor suction pressure.
- h_1 is a function of T1 and P1
- h_2 is a function of T2 and P2
- h_{13} is a function of T13 and P1
- h_{14} is a function of T14 and P2

Assuming an uncertainty of 1°F for the temperature readings 1psi for the pressure readings, and 5% for the mass flow of refrigerant, the overall uncertainty for equation (4.5.2) was calculated as ±15%.

4.5.1.3 Effectiveness Model

The effectiveness model for the evaporative condenser used four inputs from the data logger as shown in equations (4.5.3) through (4.5.5).

$$\dot{Q}_{evapcondenser} = \dot{Q}_{evapcondenser,odd} + \dot{Q}_{evapcondenser,even} \tag{4.5.3}$$

$$\dot{Q}_{evapcondenser,odd} = \varepsilon_{evapcond,odd}\dot{m}_{air,odd}\left(h_{air,sat,odd} - h_{air,in}\right)Fraction_{fan,on} \tag{4.5.4}$$

$$\dot{Q}_{evapcodenser,even} = \varepsilon_{evapcond,even}\dot{m}_{air,even}\left(h_{air,sat,even} - h_{air,in}\right)Fraction_{fan,on} \tag{4.5.5}$$

where:

- $\varepsilon_{evapcond,odd}$ is determined using equation (2.2.2) and P1
- $\varepsilon_{evapcond,even}$ is determined using equation (2.2.2) and P2
- $\dot{m}_{air,odd}$ and $\dot{m}_{air,even}$ are equal and determined from manufacturers data
- $h_{air,sat,odd}$ is the enthalpy of the air assuming it leaves the evaporative condenser saturated at the condensing temperature of the odd loop. The condensing temperature of the odd loop is determined assuming a saturated vapor refrigerant temperature at pressure P1.
- $h_{air,sat,even}$ is the enthalpy of the air assuming it leaves the evaporative condenser saturated at the condensing temperature of the even loop. The condensing temperature of the even loop is determined assuming a saturated vapor refrigerant temperature at pressure P2.
- $h_{air,in}$ is determined using a sling psychrometer.

Assuming an uncertainty of 5°F in the discharge air temperature, 5% in the discharge humidity and 1°F in inlet dry-bulb and wet-bulb temperatures, the overall uncertainty for equation (4.5.1) was calculated as ±4%. Two parameters not taken into account for this uncertainty analysis are the mass flow of air through the condenser and the accuracy of the

manufacturers data from which the effectiveness correlations were taken. Assuming a 10% uncertainty in mass flow of air and a 10% uncertainty in the manufacturers data, the overall uncertainty for equation (4.5.1) is ±15%.

4.5.2 Evaporator

An energy balance is developed for both the refrigerant-side and the glycol-side of the evaporator. The heat transfer rates were then compared to each other to gain confidence in the ice arena refrigeration loads.

4.5.2.1 Refrigerant Side

The refrigerant side heat transfer analysis used eight inputs from the data logger as shown in equations (4.5.6) through (4.5.8).

$$\dot{Q}_{evaporator} = \dot{Q}_{act,evap,odd} + \dot{Q}_{act,evap,even} \tag{4.5.6}$$

$$\dot{Q}_{act,evap,odd} = \dot{m}_{refrigerant,odd}(h_5 - h_9) \tag{4.5.7}$$

$$\dot{Q}_{act,evap,even} = \dot{m}_{refrigerant,even}(h_6 - h_{10}) \tag{4.5.8}$$

where:

- h_5 is a function of T5 and P1, which is adjusted for a 7-10 psi pressure drop between where P1 is measured and T5 is measured. This pressure drop was determined using a refrigeration pressure gauge connected to the system approximately 6 feet upstream of the T5 data point and comparing that reading to P1 over a range of refrigerant mass flows.

- h_6 is a function of T6 and P2, which is adjusted for a 7-10 psi pressure drop between where P2 is measured and T6 is measured. This pressure drop was determined using a refrigeration pressure gauge connected to the system approximately 6 feet upstream of the T6 data point and comparing that reading to P2 over a range of refrigerant mass flows.
- h_9 is a function of T9 and P3
- h_{10} is a function of T10 and P4

Assuming an uncertainty of 1°F for the temperature readings 3psi for the pressure readings, and 5% for the mass flow of refrigerant, the overall uncertainty for equation (4.5.2) was calculated as ±15%.

4.5.2.2 Brine Side

The brine-side heat transfer analysis uses two inputs from the data logger as shown in equation (4.5.9).

$$\dot{Q}_{evaporator} = \dot{m}_{Brine,total} Cp_{brine} \Delta T_{brine} \qquad (4.5.9)$$

where:

- $\dot{m}_{Brine,total}$ is determined using the installed flow meter (FL1)
- Cp_{brine} is determined at each point using the average brine temperature and a measured mass fraction of glycol in solution. The mass fraction of glycol in solution was determined using a Misco refractometer and was determined to be 0.48. The average temperature of the brine was determined using the average temperature of the inlet and

exiting glycol. The data were then used in equation (2.2.18) to determine the specific heat.

- ΔT_{brine} was determined using a matched pair of RTD's

Assuming an uncertainty of 0.1°F in the ΔT_{brine} measurement, 5% in the measurement of mass fraction glycol in solution, and 5% in inlet flow measurement, the overall uncertainty for equation (4.5.9) was calculated as ±7%.

4.5.3 Heat Exchanger

A heat transfer analysis on the suction line heat exchanger used an energy balance analysis to compare the vapor-side heat transfer to the liquid-side heat transfer. To accomplish this analysis, twelve inputs from the data logger where used as shown in equations (4.5.10) through (4.5.13).

$$\dot{Q}_{HX,L1} = \dot{m}_{refrigerant,odd}(h_7 - h_5) \tag{4.5.10}$$

$$\dot{Q}_{HX,L1} = \dot{m}_{refrigerant,odd}(h_3 - h_9) \tag{4.5.11}$$

$$\dot{Q}_{HX,L2} = \dot{m}_{refrigerant,even}(h_8 - h_6) \tag{4.5.12}$$

$$\dot{Q}_{HX,L2} = \dot{m}_{refrigerant,even}(h_4 - h_{10}) \tag{4.5.13}$$

where:

- h_7 is a function of T7 and P1, which is adjusted for a 7-10 psi pressure drop between where P1 is measured and T7 is measured. This pressure drop was determined using a refrigeration pressure gauge connected to the system at the same point as T7 and comparing that reading to P1 over a range of refrigerant mass flows.

- h_3 is a function of T3 and P3, which is adjusted for a 1-2 psi pressure drop between where P3 is measured and T3 is measured. This pressure drop was determined using pressure drop predicted across the suction line heat exchanger and the suction line filter.
- h_9 is a function of T9 and P3
- h_8 is a function of T8 and P2, which is adjusted for a 7-10 psi pressure drop between where P2 is measured and T8 is measured. This pressure drop was determined using a refrigeration pressure gauge connected to the system at the same point as T8 and comparing that reading to P2 over a range of refrigerant mass flows.
- h_4 is a function of T4 and P4, which is adjusted for a 1-2 psi pressure drop between where P4 is measured and T4 is measured. This pressure drop was determined using pressure drop predicted across the suction line heat exchanger and the suction line filter.
- h_{10} is a function of T10 and P4

4.6 Determining Actual System Performance

This section outlines the analysis of system capacity, power and overall performance.

4.6.1 Capacity

The capacity of the system can be directly determined using equations (4.5.6) or (4.5.9). Another method for determining capacity is shown in equation (4.6.1).

$$Q_{evaporator} = Q_{evapcondenser} - W_{compressors} \tag{4.6.1}$$

where the capacity of the evaporative condenser is determined using equations (4.5.1), (4.5.2) or (4.5.3) and the work input into the compressors is determined using the power

measurement from W1. These three methods can then be compared and a determination made to identify the best method (based on which method has the smallest amount of uncertainty) for determining the capacity of the system. The best method to calculate the capacity of the system is by using equation (4.5.9). This method has the smallest value of uncertainty when comparing the methods available for this project.

4.6.2 Power

The compressor power requirements can be determined from W1. An indirect method of determining the power is to use P1-P4, T3, and T4 as inputs to equation (2.2.3). The best method of calculating the power is to use the output from the watt transducer. This has an uncertainty of 5% while using the power correlations has an uncertainty of 7%.

4.6.3 COP

The coefficient of performance (COP) can be determined using the values of power and capacity determined above. Equation (4.6.2) is used to determine the COP.

$$COP = \frac{\dot{Q}_{evaporator}}{\dot{W}_{compressors}} \tag{4.6.2}$$

4.7 Validation of Computer Model with Actual Data

All of the parameters are determined using manufacturer's data for mass flow with the exception of the glycol flow that is measured by an Onicon flow meter. In order to gain confidence in the manufacturer's data for the Carlyle, 06EM199 reciprocating compressor, the separate energy balances were compared against each other. If these values were not in

close agreement, the first step was to check the installed thermocouples and pressure sensors to ensure accurate readings as detailed in Chapter 3. Once they have been found to obtain close agreement, this information was then used to determine the actual operation of various system components and how this operation varied from manufacturer ratings. These deviations were then incorporated into the computer model detailed in chapter two. The following operational parameters were validated or determined using the data collected:

- Evaporative condenser heat rejection
- Compressor power consumption
- Compressor mass flow
- Evaporator effectiveness
- Suction line heat exchanger effectiveness

As discussed in Chapter 3, a question exists pertaining to the accuracy of the instrumentation used to determine the energy balance across the evaporator. In this section, in order to evaluate the energy balances across the evaporative condenser and the suction line heat exchangers it is assumed that the refrigerant side energy balance is correct. Further discussion of this energy balance is detailed later in this section.

4.7.1 Evaporative Condenser Effectiveness

In order to validate the effectiveness model developed from manufacturers data, the energy balance described in section 4.4.1 was used. An analysis of this data was performed using the data analysis program listed in appendix A-6. Figures (4.2) and (4.3) depict the heat rejection from the evaporative condenser calculated using equations (4.5.1) through (4.5.3). The analysis used to produce figures (4.2) and (4.3) was done for data taken on the

same day with differing flow rates of glycol. The heat transfer calculated using equation (4.5.1) appears to be erratic in nature due to the error introduced when averaging the discharge air temperature from the evaporative condenser.

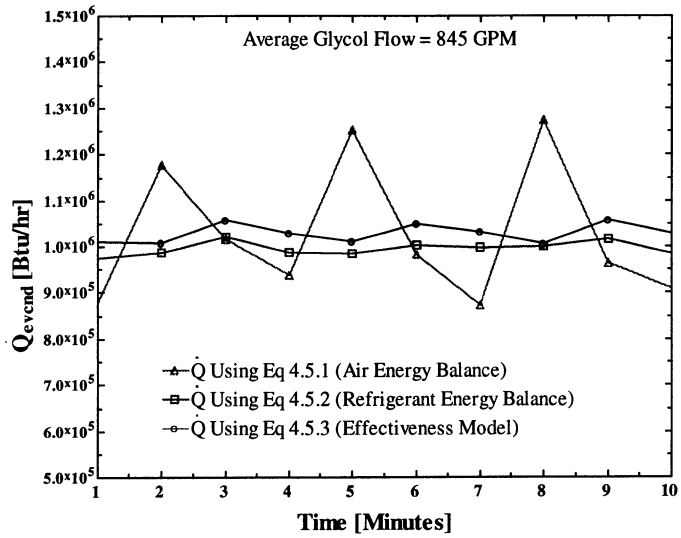

Figure 4.2: Evaporative Condenser Heat Rejection

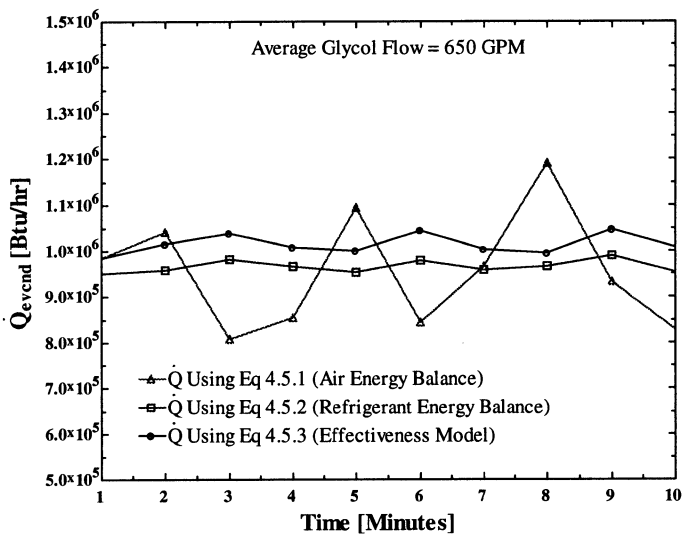

Figure 4.3: Evaporative Condenser Heat Rejection

The results depicted in figure 4.2 and figure 4.3 show the heat transfer to be relatively consistent between the three separate energy balances. They also show that the predicted heat transfer of the evaporative condenser is offset slightly higher than the other two over the entire range of analysis. Some possible explanations for this are:

- The water side of the tubes in the evaporative condenser are scaled, decreasing its heat transfer. A picture of the evaporative condenser tubes in shown in figure (4.4) that indicates some fouling may have occurred.
- The belt drive mechanism for the centrifugal fan is slipping, decreasing the flow of air below rated capacity
- The water is not being distributed properly over the tubes due to scale buildup which clogs the nozzles that disperse the water over the refrigerant tubes

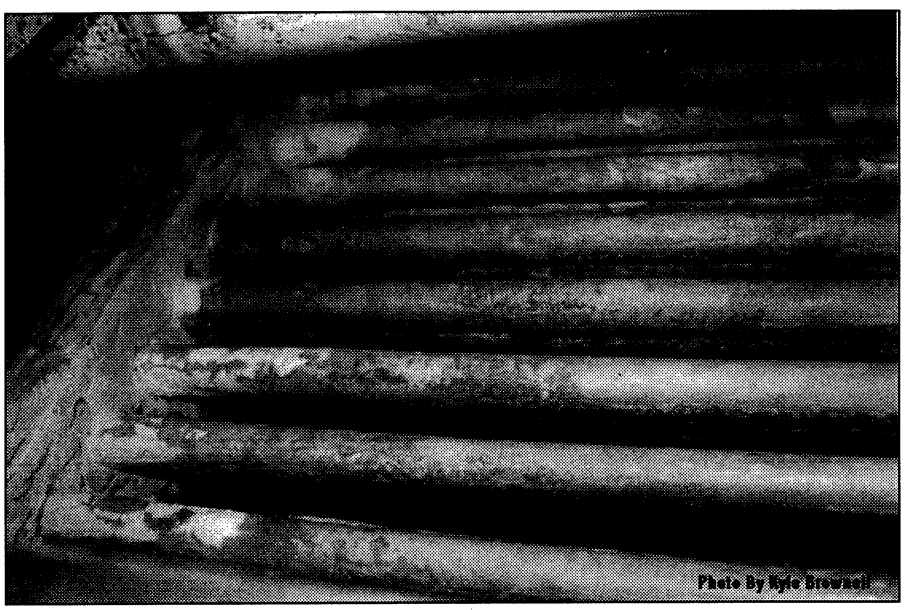

Figure 4.4: Evaporative Condenser Scale

The actual heat rejection is approximately 95% of the calculated heat rejection. This was within experimental error so no correction was required. However, as discussed in chapter two, the effectiveness of the evaporative condenser becomes a stronger function of outdoor air wet-bulb temperature as the temperature decreases below 50°F. These keeps the heat transfer of the evaporative condenser relatively constant at these conditions. Since no data are available to calculate the effectiveness of the evaporative condenser below 50°F, a method was devised to force the heat transfer to remain constant at these operating conditions. When using equation (4.5.3), the inlet air enthalpy was held constant. This forced the heat rejection to stay constant and allowed for accurate simulation of system operation. A test was performed to determine the minimum head pressure attainable when four compressors where operating. The head pressure lowered to approximately 170 psia when the outdoor air temperature was approximately 32°F. This matched to within 3psi of what the computer simulation predicted. To further validate the assumption that the heat rejection capacity remains constant, the test described above was performed when the outdoor air temperature was 15°F. The minimum head pressure attained was approximately 165 psi. This validates this assumption which is used in the remainder of this thesis.

4.7.2 Compressor Power Consumption

Compressor actual power required vs. the predicted power is shown in figures 4.5 and 4.6. The 3.5 kW and 5.5kW differences are within experimental error for the watt transducer and the power correlations which is ±5% for the watt transducer and ±7% for the power correlations. Therefore, no correction was required in the power correlation.

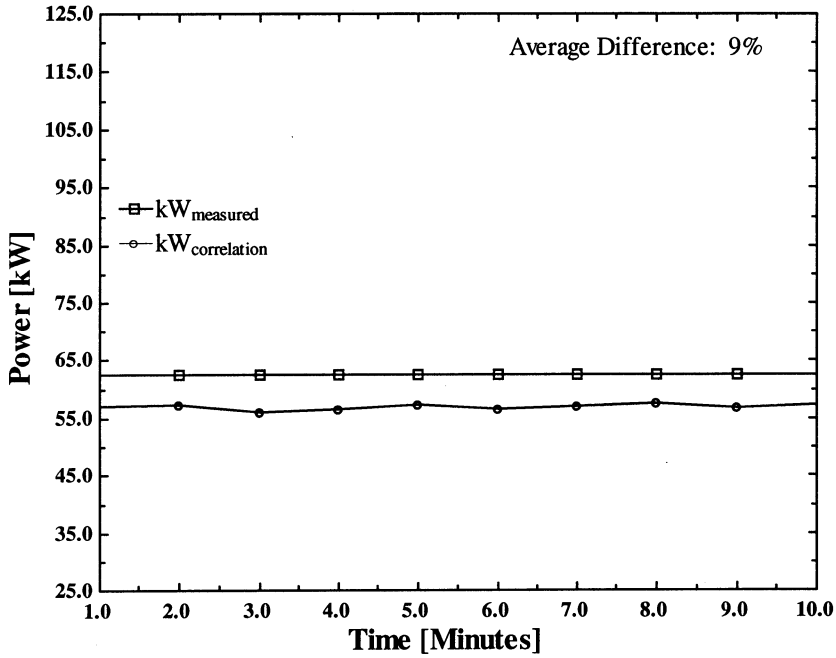

Figure 4.5: Correlated Power vs. Actual with 2 Compressors Operating

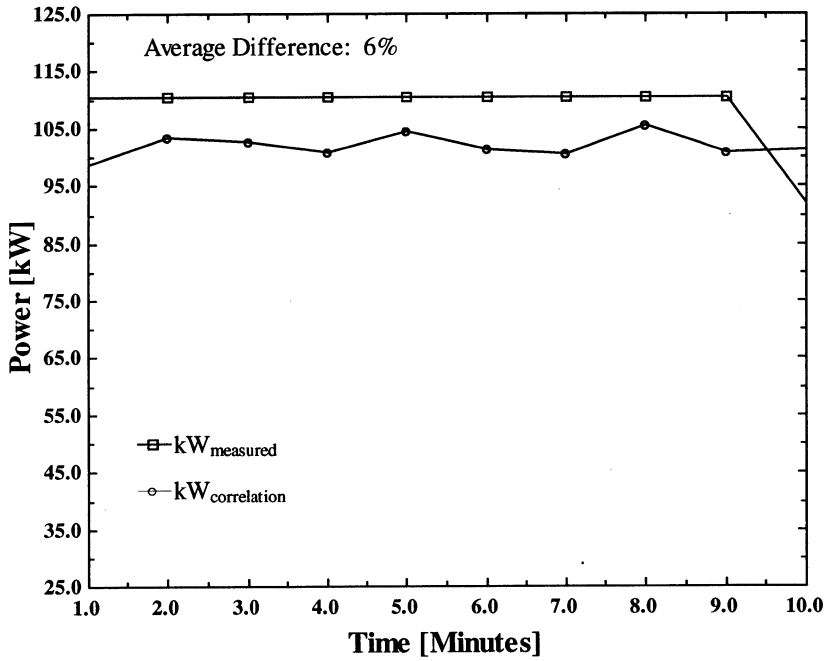

Figure 4.6: Correlated Power vs. Actual with 4 Compressors Operating

4.7.3 Compressor Mass Flow

The correlation for mass flow of refrigerant through the compressor (equation 2.2.4) was validated using an energy balance across the evaporator. Equations (4.5.6) and (4.5.9) were used for this analysis. As discussed in chapter three, the calculated mass flow of refrigerant was approximately 33% higher than the expected value. One possible error is a greater than expected pressure drop between the low side pressure transducer and the compressor suction. This theory was tested in the model by inserting an artificial pressure drop between the low side pressure transducers (P3 and P4) and the compressor. This increase in pressure drop corrected the discrepancy in the heat transfer across the evaporator; however, it decreased the predicted power such that a 25% discrepancy was created between predicted and actual power. This result is shown in figure 4.7 which uses the same data used to create figure 4.6 with the additional pressure drop added.

An additional check was done to determine if the manufacturer incorrectly calculated the refrigerant mass flow data given in the compressor maps. In addition to the mass flow data, the manufacturer gives data pertaining to the cooling capacity of the compressor at zero degrees subcooling, a 65°F compressor suction temperature and various saturated suction and condensing temperatures. These data were used to determine what the mass flow of refrigerant should be for several conditions. The calculated mass flow and the mass flow given in the compressor maps matched to within four significant figures as shown in the program in Appendix A-7.

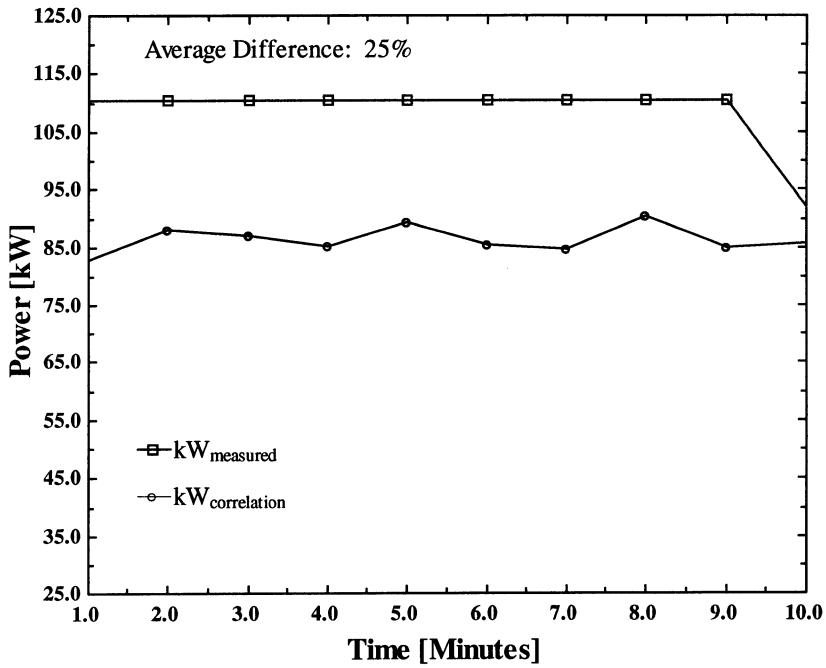

Figure 4.7: Compressor Power Consumption With 4 Compressors Running and a Simulated Additional Suction Line Pressure Drop

These various analysis described above and in Chapter 3 to explain the discrepancy in the energy balance across the evaporator have failed to yield an explanation for the 33% difference in glycol and refrigerant energy balances. As discussed in the beginning of this section, the refrigerant side energy balance was assumed to be correct in order to evaluate the remaining energy balances on the system. In the remaining chapters of this thesis, the average of the glycol side loads and refrigerant side loads is used for the system load. This load is 53 tons which is the average load for the system during the course of this project. It is also assumed that the refrigerant mass flow data from the compressor maps is correct due to lack of sufficient data to discredit this theory.

4.7.4 Evaporator Effectiveness

Equations (4.7.1) through (4.7.4) were used in order to determine the effectiveness for each loop of the evaporator.

$$\varepsilon_{evap,odd} = \frac{\dot{Q}_{act,evap,odd}}{\dot{Q}_{max,evap,odd}} \tag{4.7.1}$$

$$\varepsilon_{evap,even} = \frac{\dot{Q}_{act,evap,even}}{\dot{Q}_{max,evap,even}} \tag{4.7.2}$$

$$\dot{Q}_{evap,max,odd} = \dot{m}_{glycol,odd} Cp_{brine} \left(T_{brine,in} - T_{sat,refrig,odd}\right) \tag{4.7.3}$$

$$\dot{Q}_{evap,max,even} = \dot{m}_{glycol,even} Cp_{brine} \left(T_{brine,in} - T_{sat,refrig,even}\right) \tag{4.7.4}$$

where:

- $\dot{Q}_{act,evap,odd}$ and $\dot{Q}_{act,evap,even}$ are the actual heat transfers from the refrigerant in the odd and even loops to the glycol and are determined from equations (4.4.7) and (4.4.8)
- $\dot{Q}_{evap,max,odd}$ and $\dot{Q}_{evap,max,even}$ are the maximum heat transfer rates possible on the odd and even loops given the actual operating conditions
- $T_{sat,refrig,odd}$ and $T_{sat,refrig,even}$ are the saturation temperatures of the refrigerant in the evaporator

Plots of calculated effectiveness values are shown in figures (4.8) and (4.9).

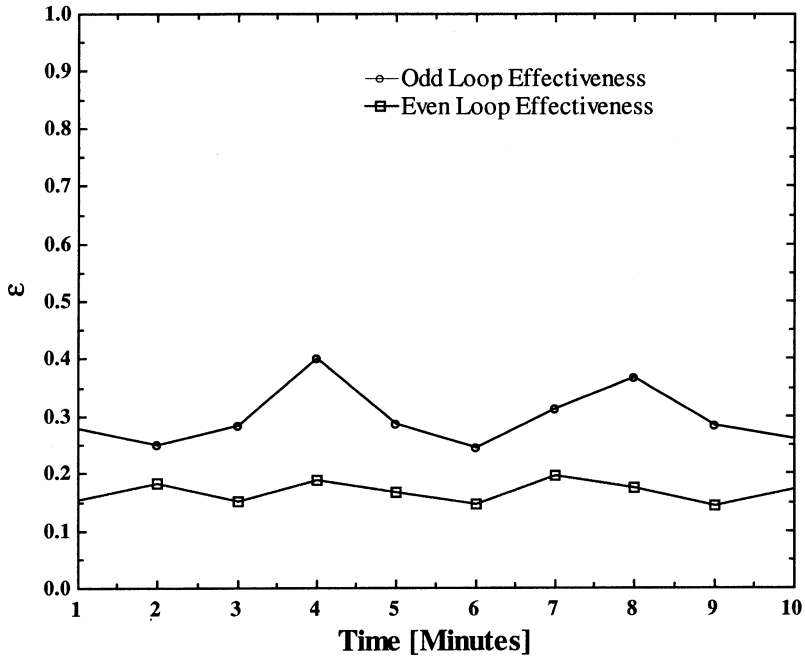

Figure 4.8: Evaporator effectiveness values with one compressor on the odd loop and three compressors on the even loop

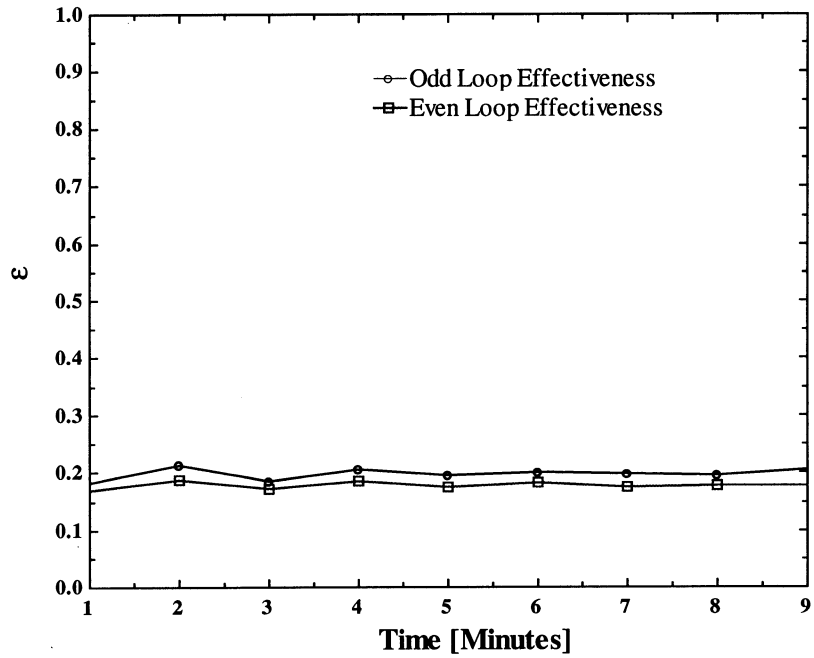

Figure 4.9: Evaporator effectiveness values with one compressor on the even loop and three compressors on the odd loop

Numerous analysis on the evaporator effectiveness values were performed and the median values were determined to be an effectiveness of 0.248 for the odd loop and an effectiveness of 0.17 for the even loop. With these values, the actual system operation can be modeled quite accurately. Although the loop effectiveness values should be nearly identical, no explanation was found to explain the differences. One possible explanation is a malfunctioning expansion valve on the odd loop that artificially raises the evaporator pressure, thereby increasing the effectiveness. The faulty expansion valve is discussed in chapter five.

4.7.5 Suction Line Heat Exchanger Effectiveness

In order to determine the suction line heat exchanger effectiveness values, equations (4.7.5) through (4.7.8), (4.5.10) and (4.5.12) were used.

$$\varepsilon_{HX,odd} = \frac{\dot{Q}_{HX,ODD}}{\dot{Q}_{HX,MAX,ODD}} \tag{4.7.5}$$

$$\varepsilon_{HX,even} = \frac{\dot{Q}_{HX,EVEN}}{\dot{Q}_{HX,MAX,EVEN}} \tag{4.7.6}$$

$$\dot{Q}_{HX,MAX,ODD} = \dot{m}_{refrig,odd}\left(h_9 - h_{3,max}\right) \tag{4.7.7}$$

$$\dot{Q}_{HX,MAX,EVEN} = \dot{m}_{refrig,even}\left(h_{10} - h_{4,max}\right) \tag{4.7.8}$$

The effectiveness value for both heat exchangers was calculated as approximately 0.03.

4.8 System Modeling

In modeling the overall Madison Ice Arena refrigeration system, the following factors where considered:

- Heat transfer from the evaporative condenser as a function of outdoor air temperature.
- Mass flow (compressor) as a function of saturated suction/discharge temperatures and suction superheat.
- Expansion valve operation (percent open and degrees superheat).
- System load as a function of glycol flow and temperatures.
- Suction line accumulator/heat exchanger operation.
- Pressure drop in the piping due to friction and elevation.
- Pressure drop in the suction line filter

The individual component models developed in Chapter 2 were put in one EES program to model system operation. This program is listed in Appendix A-8. The program has inputs of glycol flow rate, glycol inlet temperature, outside air temperature, outside air humidity, and compressor minimum head pressure. Additionally, effectiveness values and correction factors for various components that where calculated from actual data are entered in as constants. The output of this program is system coefficient of performance that can be used directly to evaluate the operational cost of the refrigeration system as detailed in Chapter 6.

Chapter 5

Component Troubleshooting

5.1 Background

The system at the Madison Ice Arena was installed in the winter of 1996. Although it is a relatively new system, several problems with system operation were discovered during analysis of the system performance during the course of this project. This chapter describes the detection and resolution of those problems. Unless specified otherwise, all simulations performed in this chapter assume a 53 ton refrigeration load, a fixed head pressure of 235 psia and an average electrical cost of $.047/kw-hr with no demand charges. All yearly cost analysis were done using typical bin weather data for Madison, WI.

5.2 Plugged Suction Line Filter

Each of the two independent refrigeration system loops at the Madison Ice Arena are equipped with a refrigerant side suction line filter. This filter is located at the exit of the evaporator and before the suction line accumulator. The purpose of the filter is to remove foreign debris that may become mixed with the refrigerant and are carried throughout the system. Since the refrigeration system is a closed hermetic system, dirt can enter the system only if it is opened up for maintenance, if a compressor problem develops (such as a compressor burn-out), or any other unusual operating circumstance. When the system is operating in accordance with its design, the filters should remain clean. During the analysis

of system performance for the Madison Ice Arena, one of the suction line filters was determined to have an excess pressure drop and was replaced with a new filter.

5.2.1 Identifying the Problem

No direct method of measuring the pressure drop across the suction line filters was available with the equipment installed in order to determine that the filter had an excessive pressure drop. As described in Chapter 3, the suction side pressure transducers sense the pressure at the outlet of the evaporator. This pressure should be within approximately three psi of the pressure at the compressor suction port based on the pressure drop in the suction line filter, accumulator and suction line piping detailed in Chapter 2. When both the odd and even loop were operating at the same evaporator pressure, it was noticed that the suction isolation valves at the inlet to the odd loop compressors were frosting up with ice. This was the first indication of a lower pressure and thus a lower temperature at the suction to the odd loop compressors. Additional analysis was performed to validate the problem of a clogged suction line filter by installing a pressure gauge to measure the pressure at the compressor suction port. Comparing this gauge to the pressure measured at the pressure transducer indicated a pressure drop 3-5 psi higher than the 3 psi drop expected.

Upon identification of the problem, personnel at the Madison Ice Arena, arranged for a refrigeration contractor to replace the suction line filter. Figure 5.1 is a photo showing the contrasts of the dirty filter (bottom) with the clean replacement filter (top). As apparent by visual inspection, the filter is severely contaminated with debris.

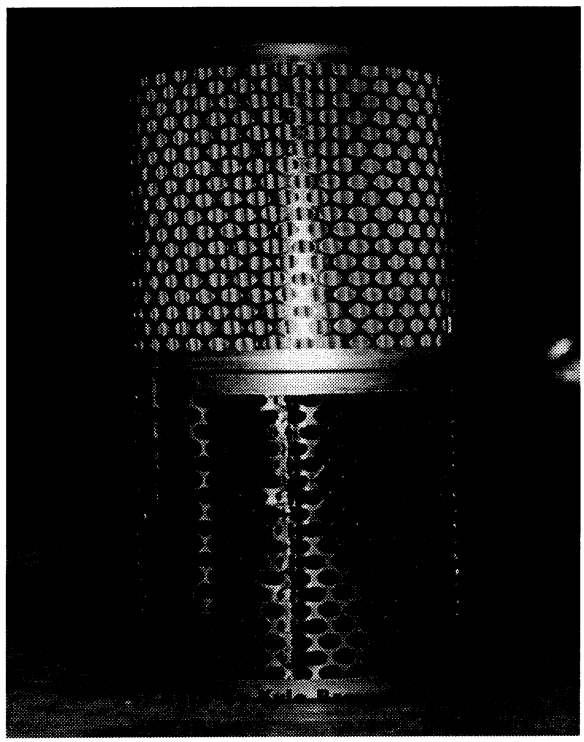

Figure 5.1: Suction Line Filters

5.2.2 Effect on System Performance and Operating Cost

The additional pressure drop caused by the suction line filter was included in the computer model detailed in chapters 2-4 to calculate a yearly operational cost penalty. Figure 5.2 compares the cost of system operation under normal conditions to the cost of system operation with an additional 4 psi pressure drop in the suction line filter for each bin condition in Madison. By integrating the cost data depicted in the figure, the additional pressure drop results in increased operation costs of $2,289 per year.

This operating cost penalty could have been avoided by installing proper monitoring equipment on the system. The recommended additional monitoring equipment is detailed later in this chapter.

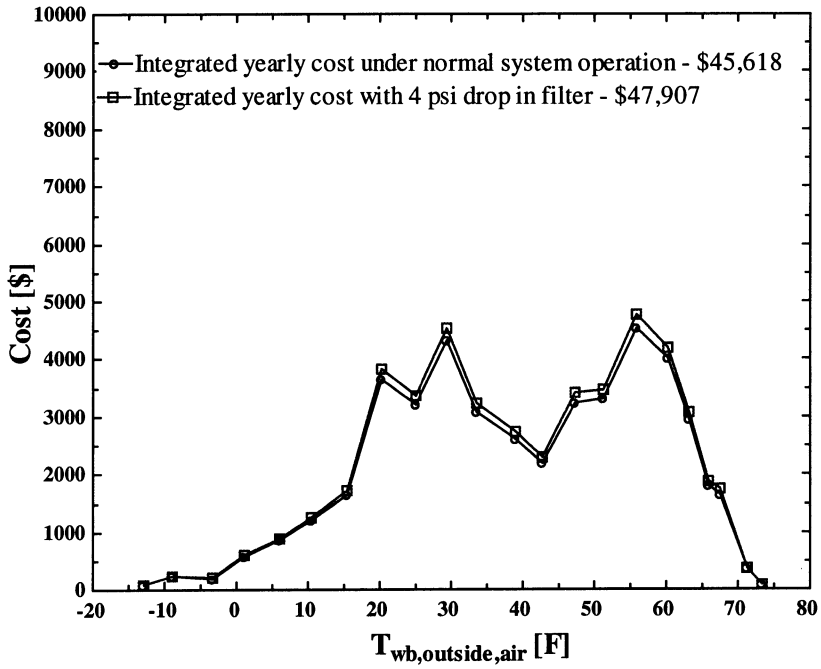

Figure 5.2: Cost Comparison for Operating With and Without a Plugged Suction Line Filter

5.3 Low Refrigerant Charge

The system at Madison Ice arena has two separate refrigeration loops and thus two separate charges of refrigerant. Refrigeration systems are designed to operate with the refrigerant in liquid form between the outlet of the condenser and the inlet to the expansion valve. A sufficient charge of refrigerant must be provided in the system to fill the volume of the piping and components between the condenser and a portion of the high pressure receiver with liquid refrigerant. Assuming the system is initially supplied with a proper charge of refrigerant, a low charge will eventually result if refrigerant leaks to the atmosphere from some point in the system. In order to ensure that the refrigerant is in the liquid form prior to entering the expansion valve, a sight glass is installed in the liquid line just upstream of the

expansion valve. Vapor present in the sight glass is one indicator of low refrigerant charge. Another indication is excessively high compressor suction superheat.

5.3.1 Identifying the Problem

Two methods were used to determine if vapor was present in the liquid line. The first method was a visual observation of the sight glass to see if vapor "bubbles" were present. If bubbles were present, the liquid line has vapor in it and the specific cause needs to be investigated further. The second method was to monitor the evaporator pressure and outlet refrigerant temperatures. Floating pressure and/or high outlet superheat indicates that the evaporator is being starved of refrigerant. Figure 5.3 depicts actual data showing the fluctuating pressure in the odd loop due to the presence of vapor in the liquid line compared to the normal operation of the even loop. The fluctuating pressure is a direct result of the vapor in the liquid line. The expansion valve is sized to admit only liquid, which has a much higher density and therefore requires a smaller flow area to admit a given maximum amount of refrigerant. As shown in equation (2.2.19), the mass flow of refrigerant is proportional to the square root of the inlet density times the pressure drop across the expansion valve. This is shown in equation (5.3.1).

$$\dot{m}_{refrigerant} \propto \sqrt{\rho_{inlet} \Delta P_{valve}} \tag{5.3.1}$$

Figure 5.4 represents the refrigerant superheat at the evaporator outlet.

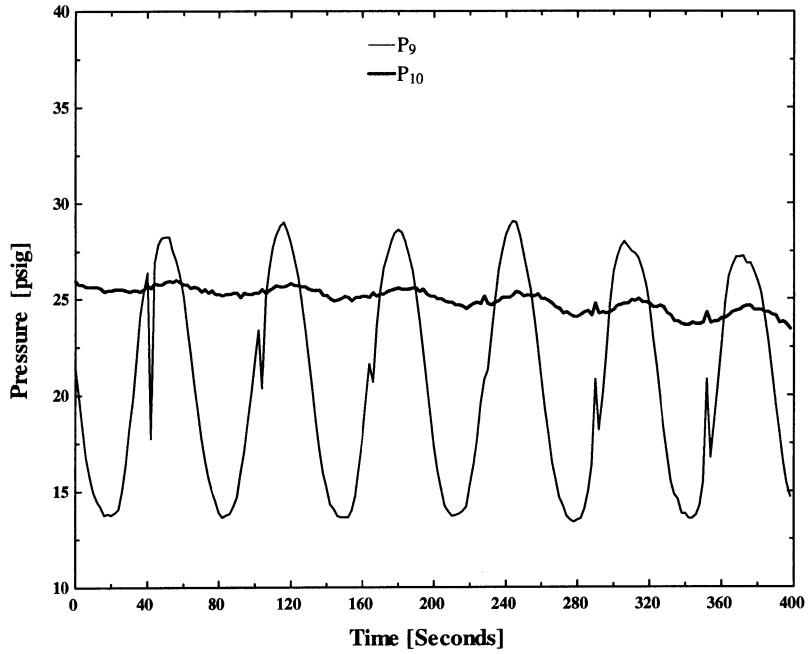

Figure 5.3: Evaporator pressure for even and odd loops

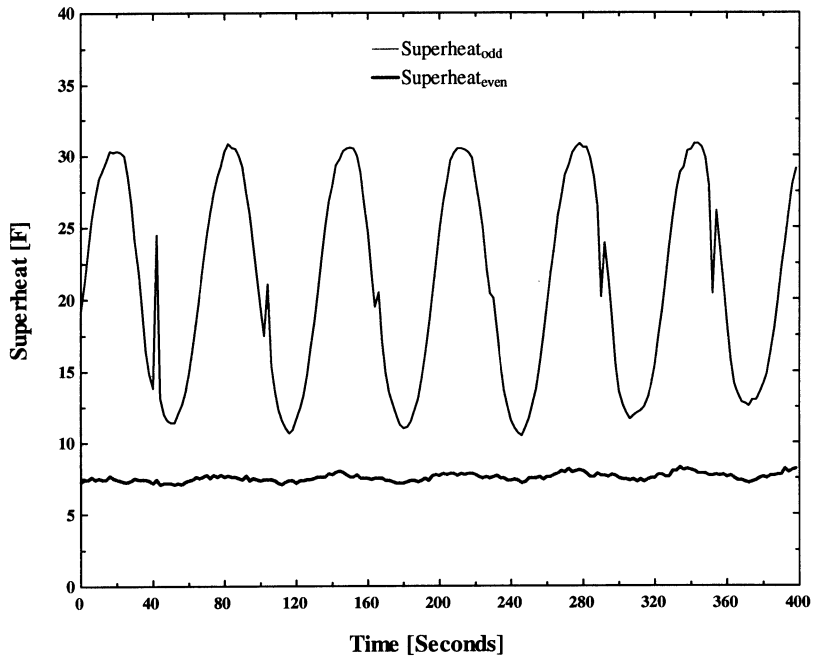

Figure 5.4: Refrigerant superheat at outlet of evaporator

The superheat for the evaporator outlet on all systems is maintained by an expansion valve. In this system, the design superheat is 7-8°F. Figure 5.4 shows that the superheat on the even loop is maintained at design operating conditions while the odd loop superheat fluctuates between 10 and 30°F. This is an indication that the evaporator is being starved of refrigerant on the odd loop.

Since the expansion valve is unable to maintain proper refrigerant feed, it is likely to hunt. During normal expansion valve operation, the valve modulates the flow of refrigerant to the evaporator to control the outlet superheat. In this case, when the valve is always wide open, the outlet superheat and thus the mass flow of refrigerant, is controlled only by the pressure drop across the valve. Figure 5.5 depicts the pressure drop across the valve and the corresponding superheat.

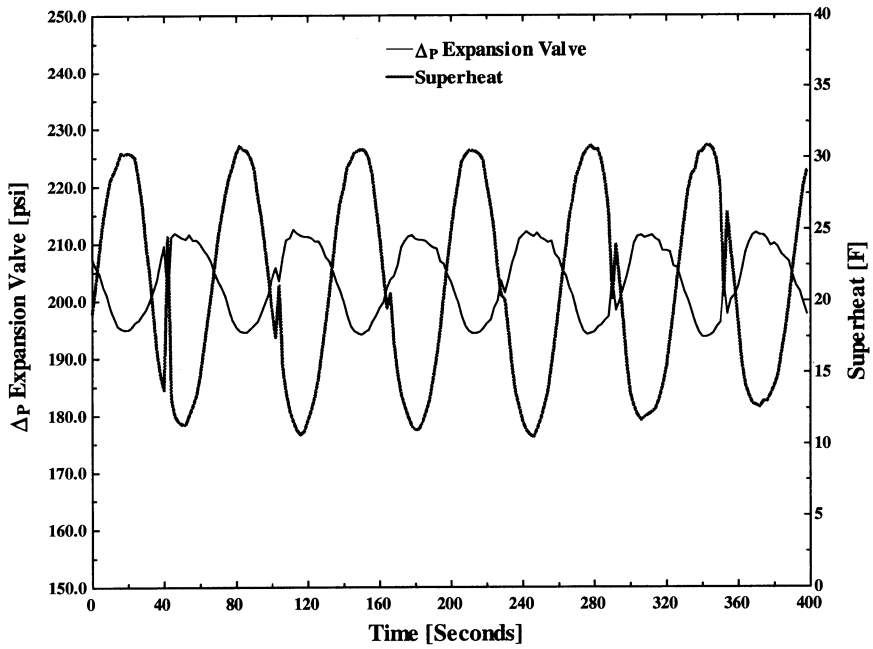

Figure 5.5: Pressure drop and superheat relationship with vapor in the liquid line

As is evident in the figure, the superheat increases as the pressure drop decreases, indicating the mass flow of refrigerant is decreasing with decreasing pressure drop. As the pressure drop increases, the superheat decreases, indicating the mass flow of refrigerant is increasing with increasing pressure drop.

The vapor in the liquid line can be caused by two problems. The first problem is an excessive pressure drop between the condenser and the sight glass causing some refrigerant to flash into vapor. The second problem is a low refrigerant charge in the system. In order to validate that the problem was a low refrigerant charge and not excessive pressure drop, the liquid line pressure was measured using a pressure gage and compared to the transducer pressure measurement. From this information, a pressure drop was determined and compared to the calculated pressure drop between these two points. The calculated pressure drop and measured pressure drop were in close agreement so the problem was determined to be a low refrigerant charge and not excessive pressure drop.

In order to fix the problem of low refrigerant charge, a leak check was performed on the entire system until the leak was isolated and repaired. An additional 135 pounds of R22 was then added to the system by a refrigeration contractor.

5.3.2 Effect on System Performance and Operating Cost

Using actual data, the effect on the system performance was calculated. The coefficient of performance (COP) for the system when it is operating properly is approximately 1.7. When the system is operating with vapor in the liquid line on one bank of compressors, the system COP is reduced to approximately 1.0. This is a 33% reduction in overall system performance. The reduction in system performance is a direct relation to the

operating cost for the system. Since only one of the two refrigerating loops had this problem, the overall system performance was reduced by 17%. This equates to a $7,800 increase in yearly operating cost.

This additional cost could have been avoided by installing proper monitoring equipment on the system. The recommended additional monitoring equipment is detailed later in this chapter.

5.4 Faulty Expansion Valve

When operating properly, the expansion valve should maintain a relatively constant outlet superheat temperature (7-8°F at the Madison Ice Arena). Large deviations from the set point may indicate a faulty expansion valve.

5.4.1 Identify the Problem

A faulty expansion valve can be detected by determining how well the expansion valve controls the outlet superheat at varying refrigerant mass flow rates. The best way found to determine how well the expansion valves controlled outlet superheat was to decrease the mass flow of refrigerant to its minimum level. This was done at the Madison Ice Arena by having only one compressor operate on the specified loop. Figures 5.6 and 5.7 compare the superheat control of the expansion valves at the Madison Ice Arena during high and low mass flow operation. As shown in the figures, the odd loop superheat is very low at low flow rates and has a 5°F fluctuation at higher flow rates.

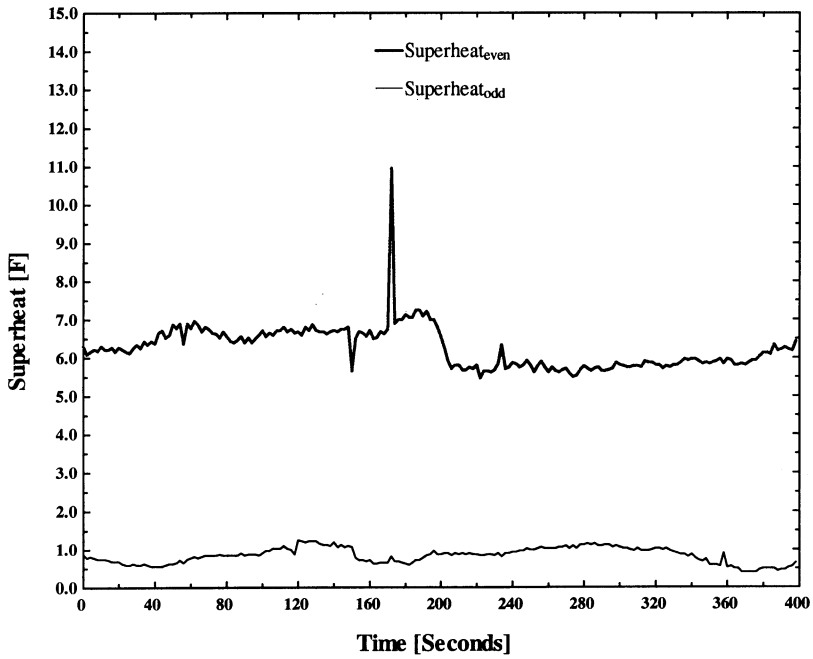

Figure 5.6: Evaporator outlet superheat with low flow on the odd loop and high flow on the even loop

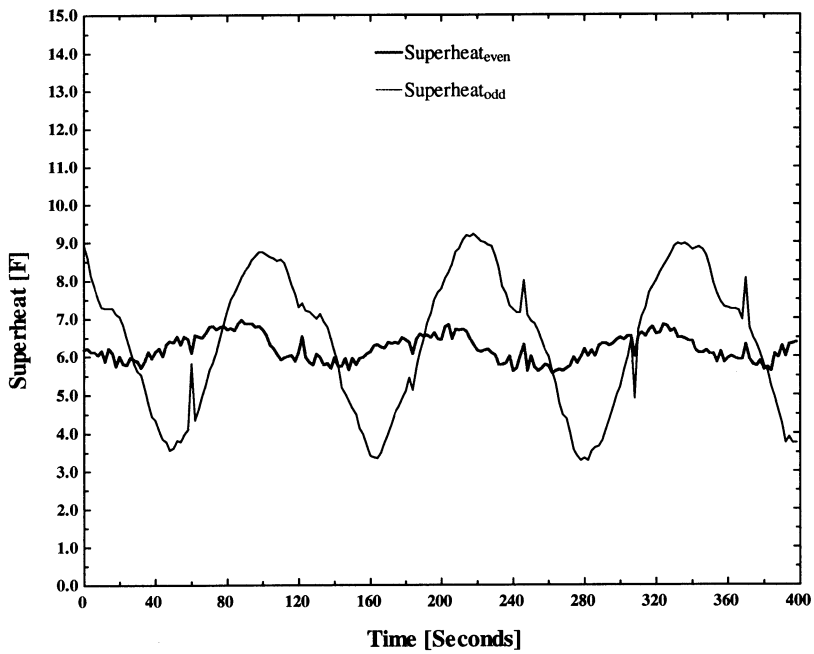

Figure 5.7: Evaporator outlet superheat with high flow on the odd loop and low flow on the even loop

The even loop expansion valve is shown to be operating properly by maintaining a constant superheat at high and low refrigerant flow rates. This analysis of actual data indicates that the odd loop expansion valve is in need of replacement. The odd loop expansion valve loses superheat control at lower flow rates most likely due to a worn valve seat that admits more refrigerant than required.

5.4.2 Effect on System Performance and Operating Cost

The effect of the faulty expansion valve on system performance and operating cost is not significant. However, if the valve seat is worn further, which would admit a greater amount of refrigerant when it is not required, the risk of liquid refrigerant flooding back to the compressor greatly increases. As currently operating, the saturated vapor refrigerant leaving the evaporator is superheated in the suction line heat exchanger before reaching the suction side of the compressors.

This problem can be detrimental to the compressor operation. If the seat becomes further worn, a greater amount of excess refrigerant will be admitted to the evaporator. If the excess liquid refrigerant leaving the evaporator becomes greater than the capacity of the suction line heat exchanger/accumulator, the liquid refrigerant will enter the suction side of the compressor. This could cause a total compressor failure.

5.5 Recommended Additional Monitoring Equipment

Table 5.1 details additional monitoring equipment recommended for installation in each of the compressor banks. The pressure gages are to be installed on the upstream and downstream side of the suction and liquid line filters. These are necessary to detect any

excessive pressure drop across the filter (indicating when it should be changed). The pressure switch is to be installed after the relief valve on the high pressure receiver. This will indicate if the relief valve opens (indicating refrigerant from the high pressure receiver has been vented) so the ice arena personnel are aware of potential system problems. The receiver liquid level column, liquid level indicators, and angle valves are to be installed on the receivers. These indicate the level of refrigerant in the receiver during normal system operation. These components allow the operator to monitor the level of refrigerant in the receiver. If the level decreases below a pre-determined level, this indicates that a refrigerant leak may be present in the system which allows detection and repair of the leak before significant quantities of refrigerant have been lost to the atmosphere.

Component	Model	Location	Number Required	Unit Cost	Extended Cost
Pressure Gage	Sentry G25	Liquid Line Filter	2	$36	$72
Pressure Gage	Sentry G25	Suction Line Filter	2	$36	$72
Pressure Switch	Sentry SW56	Receiver Relief Valves	1	$52	$52
Receiver Liquid Level Column	Henry LCF12	Receiver	1	$103	$103
Liquid Level Indicator	Henry LL5	Liquid Level Column	3	$10	$30
Seal Cap Angle Valve	Henry 7775	Liquid Level Column Shut-Off	2	$39	$78

Table 5.1: Components for System Monitoring

The material cost of these components comes to a total of $407 per bank of compressors for a total system cost of $814. The Pressure Switch needs to be wired into the existing alarm system. Assuming an installation cost of $2,000 for these components, the net

savings for Madison Ice Arena (due to early detection and resolution of problems) could have been $7,475. This assumes that the problems indicated and corrected existed for one year.

5.6 Refrigeration System Head Pressure Control

Refrigeration system head pressure is the pressure against which the compressors discharge refrigerant. This pressure is a function of (and controlled by) the condenser and interconnecting piping in all refrigeration systems by varying methods. The method employed for head pressure control at the Madison Ice Arena is by cycling the evaporative condenser fan on and off as needed to maintain the head pressure.

5.6.1 Assessing the Existing Control Strategy

The evaporative condenser fan cycles off at a head pressure of 220 psia. With the condenser fan off, the heat transfer from the condenser is reduced to almost zero, causing the system head pressure to increase permitting heat to be rejected from the system. The fan then cycles on at a head pressure of 250 psia, increasing the heat transfer and lowering the head pressure. Thus, the average head pressure seen by the compressors during operation is 235 psia.

5.6.2 Impact on System Performance and Operating Cost

Using the program shown in Appendix A-8, the yearly operational cost of the Madison Ice Arena with its current control strategy was calculated to be $45,505 with the 5 hp and 2 hp glycol pumps running on each rink. The yearly operational cost with the 10hp

and 7.5hp glycol pumps running was calculated to be $45,618. The difference in these costs is due to a lower evaporator pressure on the refrigerant side. This is caused by a higher temperature change of glycol across the evaporator (due to the lower flow rate) which creates a lower average glycol temperature. If the head pressure is designed to 'float' to the minimum head pressure attainable on each loop and the 10hp and 7.5hp glycol pumps are used, the total annual operating cost should be $36,021. This is an $9,597 yearly savings by decreasing the head pressure. This savings equates to a 21% decrease in energy costs. Figure 5.8 depicts this savings.

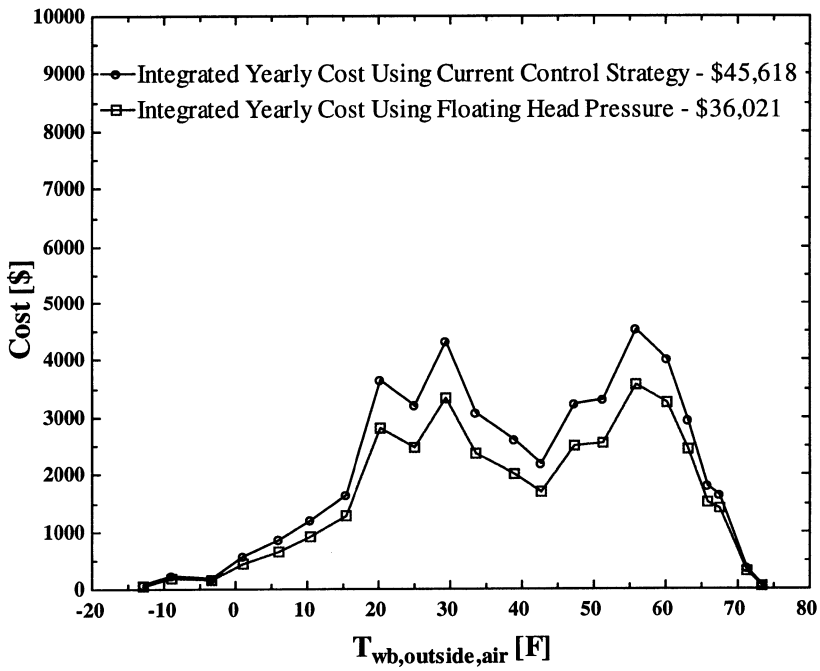

Figure 5.8: Annual cost of fixed head pressure vs. floating

5.6.3 Developing a Refined Control Strategy

Developing a refined control strategy for the Madison Ice Arena requires that all aspects of the current system operation be investigated. As detailed above, allowing the compressor head pressure to "float" to a lower average pressure increases system

performance that decreases operational costs. Another change that affects operational costs is the flow of glycol through the evaporator. The current system configuration allows for two different flow rates of glycol for each of the two ice rinks at the arena. Using the larger pumps (and thus the higher flow rate) increases the average temperature of glycol in the evaporator, increasing the pressure of the refrigerant in the evaporator. This increase in evaporator pressure, increases the capacity and efficiency of the compressors. This increase in compressor performance offsets the increase in energy required for the larger pump operation. However, the change is so small that it could be due to errors in calculating the effectiveness values for the evaporator. Thus, the use of the larger and smaller pumps is determined to equally effect the system performance under normal system operation. The advantage of using the higher flow rates is an even temperature distribution throughout the ice field. This is important in order to maintain a uniform ice temperature and thus a uniform skating surface.

The final control strategy recommended for the Madison Ice Arena is to use the smaller pumps during low load periods and to use the larger pumps during high load periods. The head pressure should be allowed to 'float' under all conditions with a minimum being set at 110 psia. This control strategy would cause the fan to cycle on and off at only conditions of extremely high ice arena loads and extremely low outside air temperatures, a combination which is unlikely to occur.

Chapter 6

Optimum Control Settings

6.1 Background

Refrigeration system designs vary drastically depending on the type of load for the system and the geographical location of the system. ASHRAE is generally considered the authority on guidelines for systems design throughout the industry. However, the actual system designs are tailored to meet specific application needs and operation may or may not result in optimum system performance. According to ASHRAE, (1990), the following are some typical considerations for the design engineer in refrigeration system development:

- Year-round operation regardless of outdoor ambient conditions
- Possible wide load variations (0 to 100% capacity) during short periods without seriously disrupting the required temperature levels
- Frost control for continuous performance applications
- Oil management for different refrigerants under varying load and temperature conditions
- A wide choice of heat exchange methods, e.g., direct expansion, liquid overfeed, or flooded feed of the refrigerants, and the use of secondary coolants such as salt brines, alcohol, and glycol
- System efficiency, maintainability, and operating simplicity
- Initial and operating costs

- Operating pressures and pressure ratios that might require multi-staging, cascading, and so forth

Although all areas are important in system development, only certain areas have been focused on to optimize system performance in this project. For the purpose of this project, it was assumed that the basic system configuration was constrained and all increases in system performance would be due to control changes. Chapter seven details the effect on system performance due to changes in system design/configuration.

6.2 Industry Standard

Industry standards for basic ice arenas system designs is to use a secondary coolant of ethylene glycol and water that is cooled by a refrigeration system using R-22 or ammonia (ASHRAE, 1990). The glycol is then circulated through a portable pipe network or permanent field of piping over which water will flood and freeze to create the ice rink.

6.2.1 Brine Side

According to ASHRAE, flow rates which provide temperature changes of three to five degrees Fahrenheit are normal (ASHRAE, 1990). This low temperature difference is imperative to ensure a near constant temperature for the ice field.

The original design of the brine side for the Madison Ice Arena was to use one large pump on each arena (studio and main) during high load and pull down conditions and a small pump on each arena to maintain the load during normal operation. However, during evaluation of system operation, it was noted that the large pumps for each rink ran almost continuously. The glycol is designed to return from the rink to the evaporator at a

temperature of 17°F with a supply brine temperature of 14°F which is maintained by the number of compressors in operation. These design parameters are within the design recommendations developed by ASHRAE.

6.2.2 Refrigerant Side

Components on the refrigerant side of the system are selected based on design refrigeration loads and design ambient conditions. ASHRAE recommends two or more compressors for the system with multistage thermostats used to control the compressor sequence of operation. Compressors should be selected with capacities to allow for the 'pull-down' of the rink during system start-up.

ASHRAE recommends selecting condensers based on:

- Maximum expected outdoor air wet-bulb temperature
- Suitable controls to cover a wide range in capacities
- Freeze protection for the water (for evaporative condensers and cooling towers)

One way to account for the extreme outdoor operating conditions is to maintain an artificially high head pressure in the condenser that ensures proper refrigerant flow through the expansion valve. During the course of this project, it was found that ice arenas throughout the world are designed in this manner (Cox, 1998). This practice also provides built-in freeze protection for the evaporative condenser by maintaining a high refrigerant condenser temperature and thus a high condenser water temperature. Additionally, it gives the expansion valve high-pressure drops and favorable control characteristics.

The Madison Ice Arena is designed with six compressors, which are sequenced by a four stage Honeywell controller. The condenser is designed to maintain a year-round

discharge pressure between 220-250 psia (103-113°F). These design parameters are within the design recommendations developed by ASHRAE.

6.2.3 Suction Line Heat Exchanger

Suction line heat exchangers are commonly installed in refrigeration systems to increase system performance and insure proper system operation. ASHRAE (1990) states that these heat exchangers are effective in: 1) increasing the system performance, 2) subcooling the liquid refrigerant to prevent flash gas at the expansion valve and 3) evaporating any liquid in the suction line prior to it reaching the compressor(s). The system at the Madison Ice Arena has one suction line heat exchanger/accumulator installed in each refrigeration loop. These suction line heat exchangers provide an additional refrigerant superheat of 12-14°F, which results in an additional subcooling of 1-3°F. These design parameters are within the design recommendations developed by ASHRAE.

6.3 Recommended Settings and Sizing

As detailed above, ASHRAE provides guidelines for the design engineer to assist in system design. Most refrigeration systems, including the one at Madison Ice Arena, are designed using these guidelines as a basis; however, in many cases, the design engineer will use past experience on a 'similar' system to determine the control strategy for the system being designed. Most often, this method of design results in a "working" operational design for the end user; however, it generally results in lower system operating efficiencies. If care is not taken in the development of the control strategy for the system, the end user may see operating efficiencies as much as 25% lower than a similar, optimally designed and

controlled system. This section provides areas, which the engineer should thoroughly investigate when developing the system control strategy.

6.3.1 Glycol Side

As detailed in chapter five, the glycol flow rate has a small impact on overall system performance. By increasing the glycol flow rate for a given system, the increase in pump power required may be offset by increasing the evaporator pressure on the refrigerant side of the system (this increases compressor efficiency, decreasing compressor power consumption). The data on the increase in flow rate taken at Madison Ice Arena are inconclusive on the effects of high flow rate vs. low flow rate. The recommendations based on this project are to maintain the flow rate required to maintain the ice at the desired temperatures. No optimum flow rate can be recommended based on this study. However, it has been determined that the pump power becomes more important under floating head pressure conditions.

6.3.2 Refrigerant Side

An area often approximated using the engineer's past experience in the design of refrigeration systems is the head pressure control strategy. A minimum head pressure is needed to maintain the required pressure drop across the expansion valve for proper operation. It is designing for this pressure drop where engineers often make the mistake of "over-designing" the system. As discussed in Chapter 2, expansion valves are supplied with rated mass flows for given pressure drops. According to manufacturers data and studies done by Vinnecombe and Ibrahim, expansion valves have an approximately 25% greater capacity

than stated in the manufacturers catalog (called reserve capacity by manufacturers). It is recommended to determine the minimum condenser pressure in the system design by examining the minimum required expansion valve pressure drop as provided by the manufacturer. This will allow for the reserve capacity of the expansion valve to be used as the system design margin of safety.

The design is based on using a floating head pressure. With this design, the head pressure changes based on outside air temperature. Assuming a constant load, this change in head pressure based on outdoor air wet-bulb temperature is shown in Figure 6.1. This figure depicts that the head pressure reaches a minimum at approximately 55°F.

A comparison of the coefficient of performance (COP) for the system with a yearly load of 53 tons using fixed and floating head pressure is shown in Figure 6.2. As depicted in the analysis, the system coefficient of performance is significantly greater when using floating head pressure than when using fixed head pressure. The COP values depicted above translate directly into energy savings. Therefore, the recommendation for improvement is to allow the head pressure to float to a set minimum. The expansion valve installed in the system or the maximum heat rejection capacity of the condenser may determine this minimum.

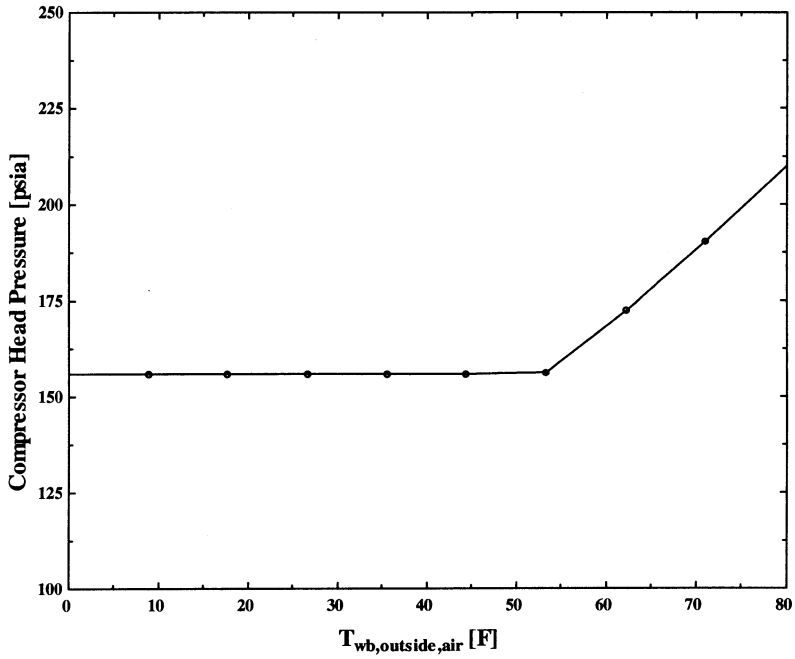

Figure 6.1: Head Pressure Vs. Outdoor Air Wet Bulb Temperature

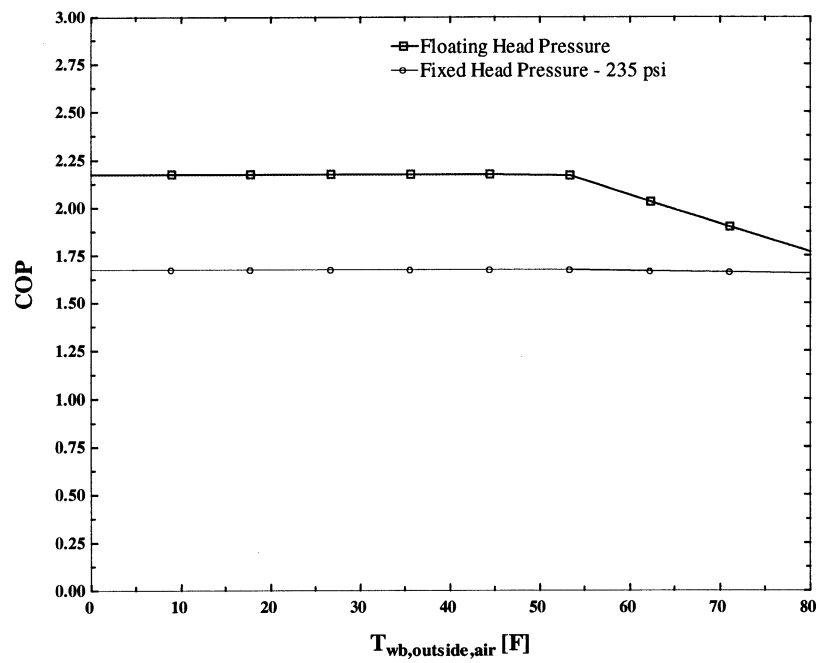

Figure 6.2: COP comparison using floating and fixed head pressure control

When designing a system to use floating head pressure, the engineer must ensure that the capacity of the expansion valve is not exceeded. If the selected expansion valve is undersized, it will starve the evaporator of refrigerant during low outside air temperature conditions. If the expansion valve is oversized, it may cause liquid refrigerant to enter the compressor as well as extreme fluctuations in evaporator pressure.

6.3.3 Suction Line Heat Exchanger

Suction line heat exchangers are installed in the suction line of refrigeration systems for various reasons. An analysis was performed on suction line heat exchangers to determine their effect on system capacity and performance. This analysis included the comparison of the heat exchanger effect when using various refrigerants.

6.3.3.1 Heat Exchanger Effectiveness

In order to determine the effect of a suction line heat exchanger on system performance, varying effectiveness where used for the heat exchanger. The effectiveness for the suction line heat exchanger is defined in equation (6.3.1).

$$\varepsilon = \frac{T_3 - T_1}{T_2 - T_1} \qquad (6.3.1)$$

where the temperature (T) values correspond to locations depicted in figure 6.3.

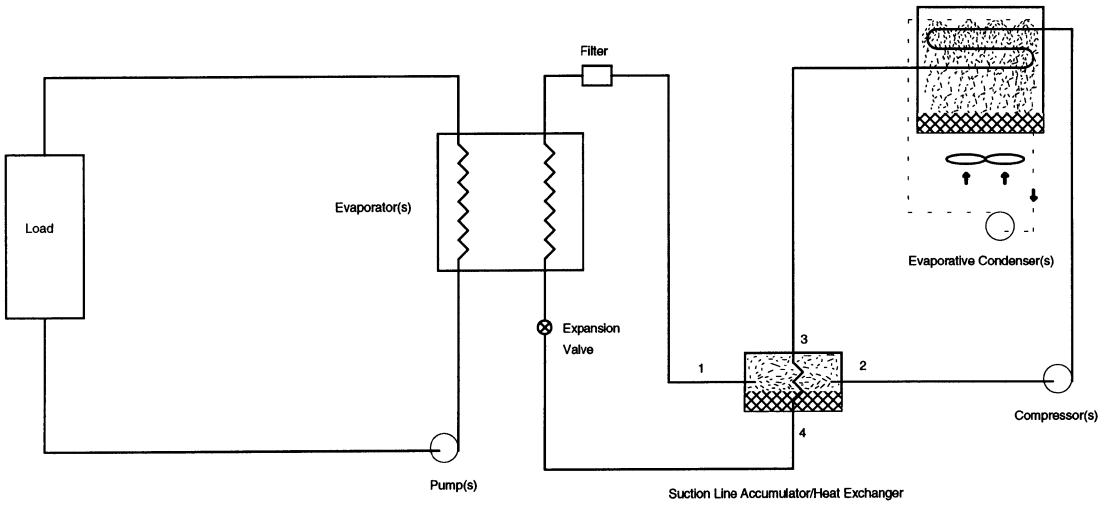

Figure 6.3: Schematic of Typical Refrigeration System

In this analysis, the refrigerant is assumed to exit the evaporator (1) at a quality of one, and exit the condenser (3) at a quality of zero. The maximum temperature at state 2 is if the refrigerant leaves the heat exchanger at the same temperature as the refrigerant entering at state 3.

The suction line heat exchanger effects the performance of the refrigeration system in the following two areas: 1) it superheats the suction line vapor, decreasing mass flow of refrigerant through the compressor and 2) it subcools (or decreases the enthalpy of) the refrigerant entering the expansion valve, thereby increasing the refrigerating effect of the evaporator. Figure 6.4 depicts the effect of the heat exchanger using a pressure enthalpy diagram.

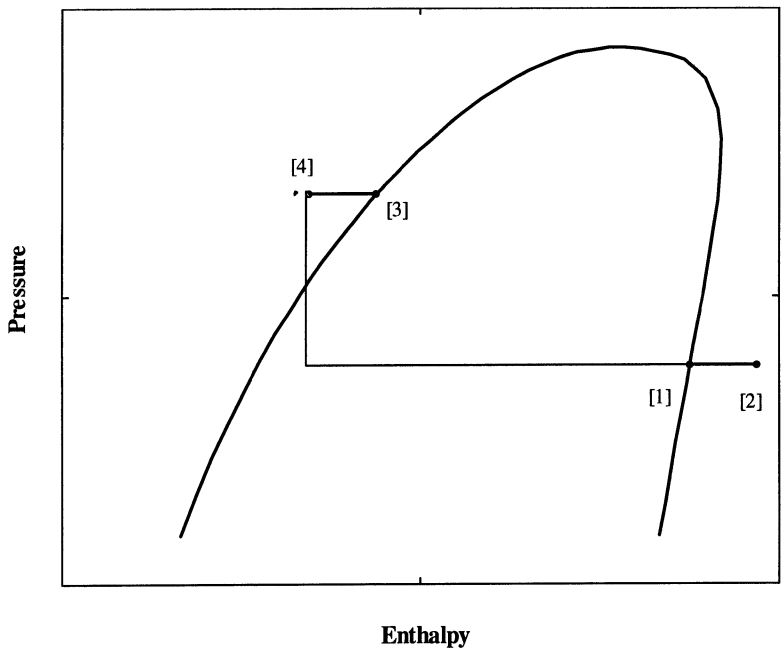

Figure 6.4: Pressure Enthalpy Diagram

6.3.3.2 Heat Exchanger Effect on Capacity Without Correction For Mass Flow Rate

When the suction line heat exchanger is not installed in the system, the refrigerating effect per unit mass of refrigerant is the difference between the enthalpies at states 1 and 3. It is readily apparent that when the heat exchanger is installed, the refrigeration effect per unit mass can be increased to be the difference between points 1 and 4. A simplified analyses on the effects of a suction line heat exchanger assumes the mass flow of refrigerant to be remaining constant when analyzing the effects of a suction line heat exchanger. Using this assumption, Figure 6.5 compares the change in system capacity for various values of effectiveness using different refrigerants. It is interesting to note that the capacity increase for refrigerant R502 is as much as 45% while the increase in capacity for R717 at these design conditions is only 10%. All of these analyses assumed an evaporating temperature of

0°F and a condensing temperature of 105°F. The varying refrigerant properties cause the difference in effect that the heat exchanger has on refrigerating effect. An example of this is that when the evaporator temperature is decreased to –20°F, the capacity increase for R502 is 55% while the capacity increase for R717 remains at approximately 10%.

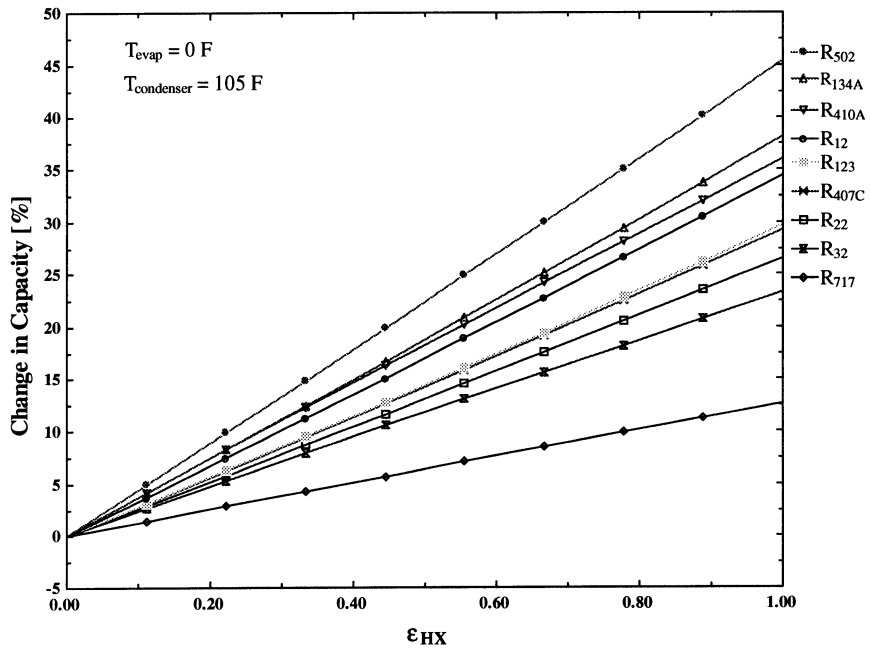

Figure 6.5: Change In Capacity Without Correction For Mass Flow

6.3.3.3 Heat Exchanger Effect on Capacity With Correction for Mass Flow Rate

A critical element not included in the analysis depicted in Figure 6.5 is the effect of superheating the suction gas on the mass flow of refrigerant through the compressor. As described in Chapter 2, the mass flow of refrigerant through the compressor is a function of changes in suction specific volume. Assuming that the reference specific volume and mass

flow is at a quality of one, equation (6.3.2) can be used to determine the capacity of a system at reference conditions with no suction line heat exchanger installed.

$$\text{Capacity}_{\text{reference}} = \dot{m}_{\text{reference}}(h_1 - h_3) \tag{6.3.2}$$

To determine the capacity of a system at conditions with a suction line heat exchanger installed which increases the suction superheat and refrigerating effect, equation (6.3.3) was used.

$$\text{Capacity}_{\text{actual}} = \dot{m}_{\text{reference}} \frac{v_{\text{reference}}}{v_{\text{actual}}}(h_1 - h_4) \tag{6.3.3}$$

Due to varying refrigerant properties, it was found best to compare the effect a suction line heat exchanger has on system capacity for different refrigerants on a percentage basis. This was done by dividing the actual capacity by the system capacity to obtain the relationship shown in equation (6.3.4).

$$\text{Capacity}_{\text{change},\%} = \frac{(h_1 - h_4)v_{x=1}}{(h_1 - h_3)v_{\text{actual}}} * 100 - 100 \tag{6.3.4}$$

Accounting for the decrease in mass flow resulting from changes in suction specific volume, the change in capacity of systems with various refrigerants is shown in Figure 6.6 through Figure 6.8. The capacity change can be directly related to the change in system COP. As discussed in Chapter 2, the compressor power does not change significantly with changing suction superheat. Therefore, the percentage of change in the system COP is equal to the percentage of change in system capacity.

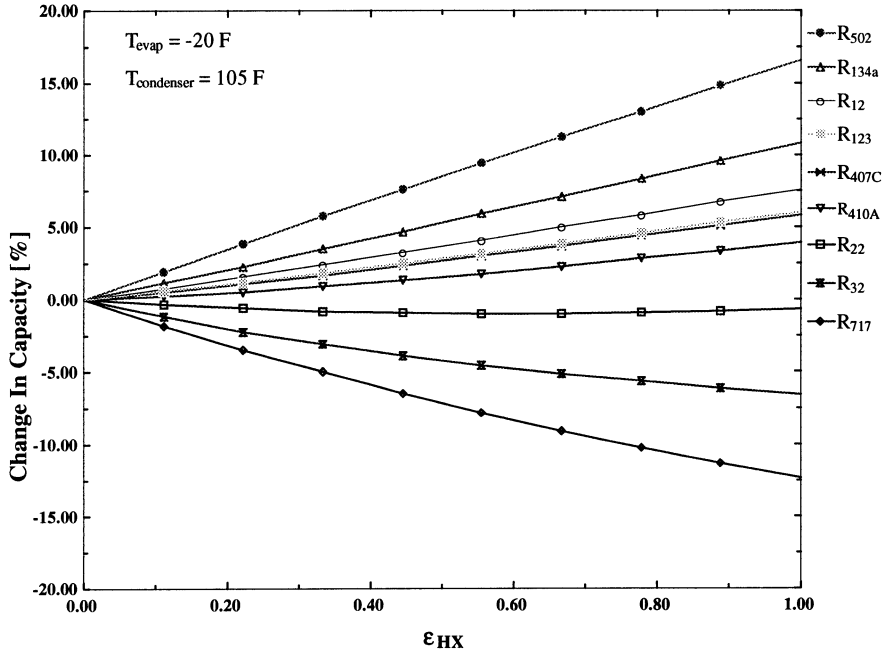

Figure 6.6: Change in Capacity at -20°F Evaporator Temperature

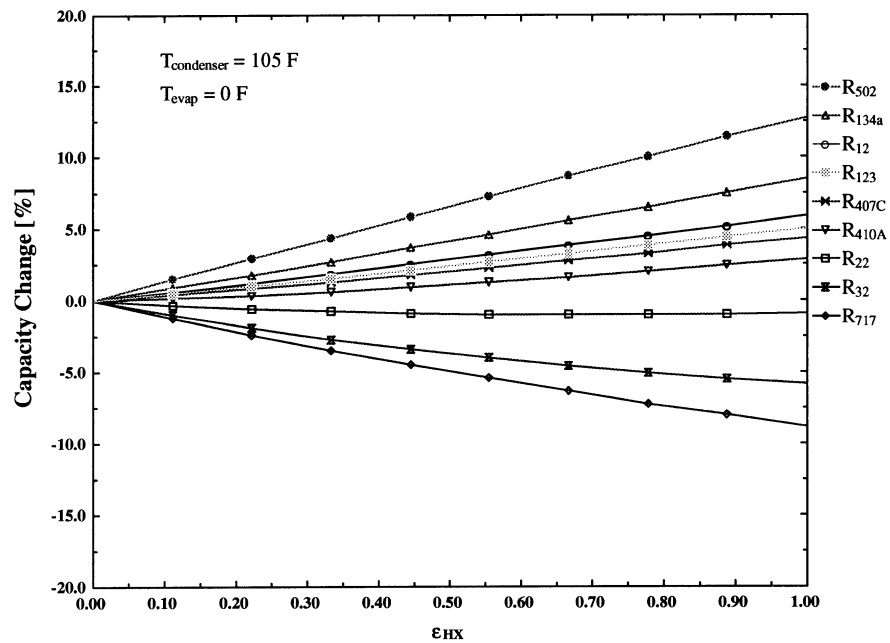

Figure 6.7: Change in Capacity at 0°F Evaporator Temperature

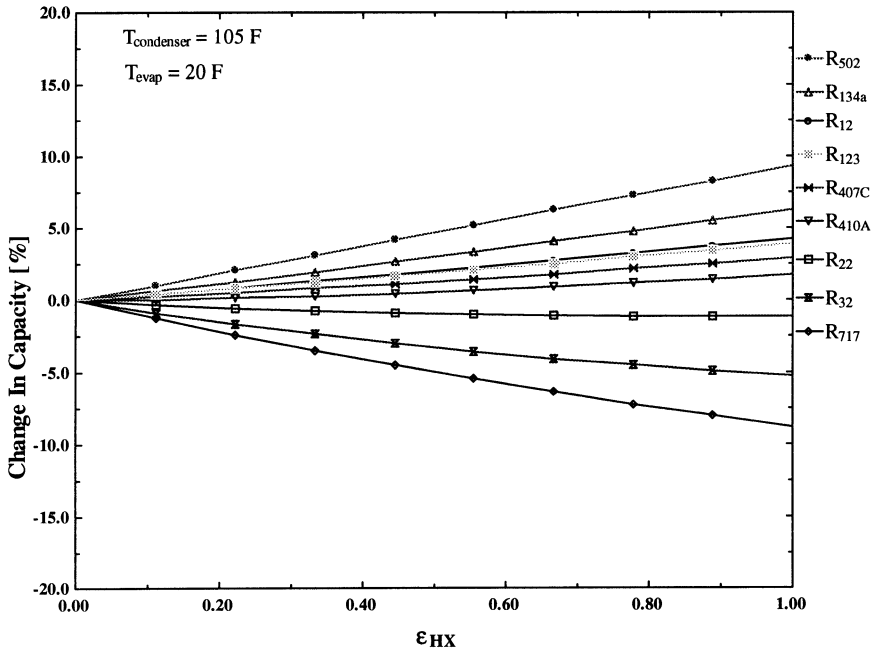

Figure 6.8: Change in Capacity at 20°F Evaporator Temperature

6.3.3.4 Conclusions

From this analysis, it can be concluded that suction line heat exchangers are useful components for systems using R502, R134a, R12, R123, R407C, and R410A. The heat exchanger is detrimental to system performance in systems using R22, R32, and R717. The results obtained for R134a, R12 and R22 follow the same trends as the results of Domanski and Didion, (1992). Most suction line heat exchangers in use in R22 systems have effectiveness less than 0.1 that minimizes the effect on system capacity. However, in large systems, a one or two- percent decrease in system performance can cost a large amount in added energy costs for system operation. The system designer must be very careful in choosing when to install suction line heat exchangers in the system.

The system at the Madison Ice Arena uses R22 as the refrigerant. Based on this study of suction line heat exchangers, it is not recommended to install a suction line heat exchanger in this system. However, the heat exchangers currently installed have effectiveness values lower than 0.1 so the overall effect on this systems performance is negligible. As discussed in section 6.2.3, even though the suction line heat exchanger has a negative impact on system performance, the system does benefit from the heat exchanger by preventing vapor in the liquid line before the expansion valve (discussed in chapter five) and liquid entering the suction side of the compressor.

Chapter 7

Performance Enhancement Option - Dedicated Subcooling

7.1 Background

Currently the system at Madison Ice Arena is configured similar to many vapor compression refrigeration systems. This chapter describes reconfiguration of the system to increase the system COP with the addition of dedicated mechanical subcooling. The premise behind subcooling is to depress the temperature of liquid refrigerant before it enters the expansion valve, thereby, increasing the capacity of the system.

7.2 System set-up

Additional equipment is required for reconfiguration to operate with mechanical subcooling. Figure 7.2.1 depicts the refrigeration system installed at the Madison Ice Arena. The subcooler and associated components are to be added between the liquid/suction heat exchangers and the expansion valves. The boxed area in Figure 7.2.1 is the area to be modified for mechanical subcooling and is shown in detail in Figure 7.2.2. A complete refrigeration system including a compressor, receiver, piping, expansion valve, and condenser is required to complete the dedicated subcooling system.

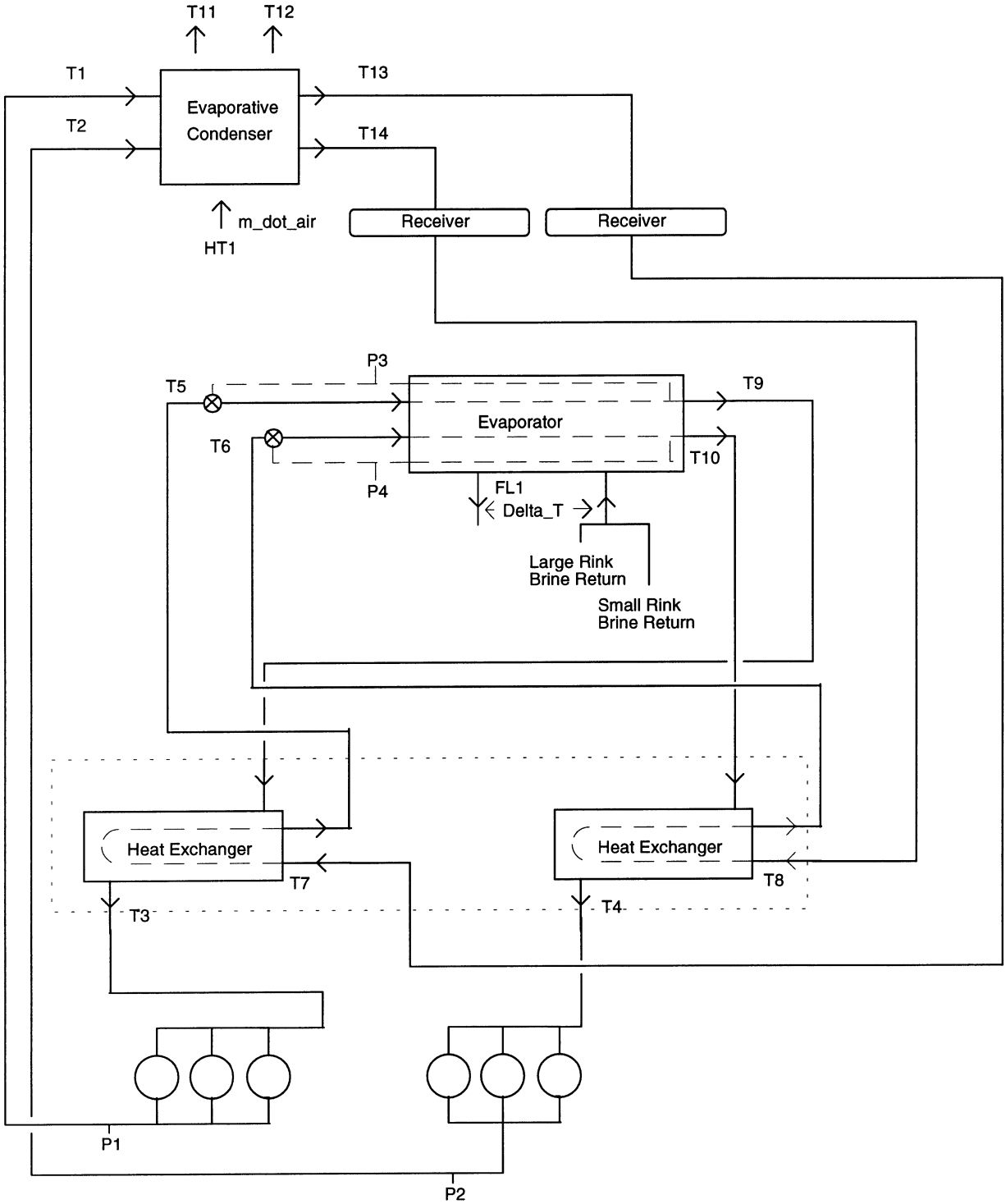

Figure 7.2.1: Madison Ice Arena Refrigeration System

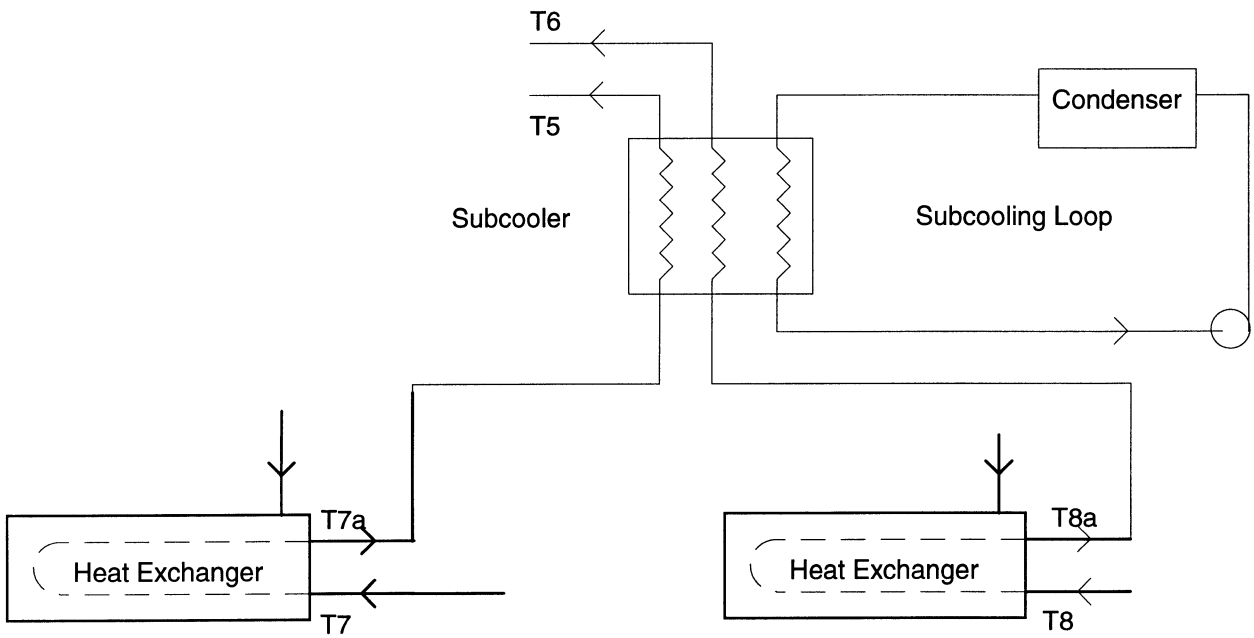

Figure 7.2.2: Subcooling Equipment Schematic

The compressor chosen for modeling mechanical subcooling of the system at Madison Ice Arena is a Carlyle model 06DM808 reciprocating compressor which has a refrigerating capacity of approximately 3 tons. The refrigerant used is R22. The computer model for this set-up is listed in appendix A-9.

7.3 Effects on System Performance

The effect of mechanical subcooling has been determined to increase system performance for vapor compression refrigeration systems (Thornton, et al., 1994). This increase in performance is based on the premise that the COP of the subcooling system is much higher than the COP of the main refrigeration system. This section details the design process for selecting adequately sized components for the dedicated subcooling system.

7.3.1 Capacity

Dedicated mechanical subcooling increases the capacity of any refrigeration system. However, if the settings for the subcooling system are not optimized, it may not increase the COP. It accomplishes this by decreasing the enthalpy of the refrigerant prior to it entering the expansion valve. Figure 7.3.1 uses a pressure enthalpy diagram to depict the effect that mechanical subcooling has on system capacity.

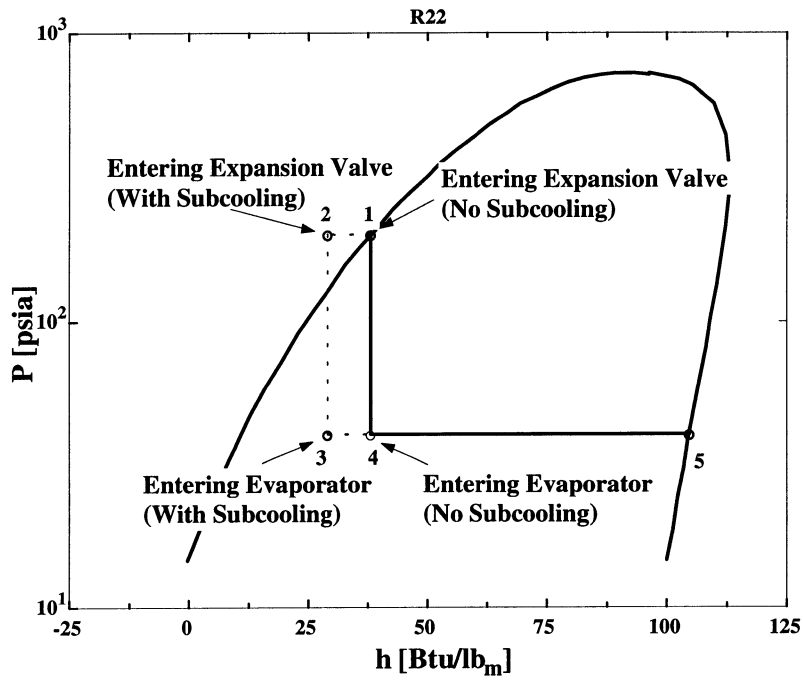

Figure 7.3.1: Effects of Mechanical Subcooling on P-h diagram

Without mechanical subcooling, the system refrigeration capacity is proportional to the difference in enthalpies between states five and four. With the addition of mechanical subcooling, the system refrigeration capacity proportionally increases to the difference between states five and three. This figure represents a 30°F subcooling of the liquid refrigerant from a temperature of 95°F down to 65°F. The amount of subcooling (and

corresponding increase in refrigeration capacity) is chosen and should be optimized by the design engineer. The optimum selection of the amount of subcooling is discussed in section 7.3.3.

7.3.2 Power Required

In addition to increasing the capacity of the refrigeration system, dedicated mechanical subcooling also increases the power requirements. In order to calculate the additional power required for the subcooling system evaporative condenser, it was assumed that the subcooling system condenser power was a fraction of the power required by the main system condenser (this includes the fan and pump). This fraction was calculated by taking the ratio of the heat rejection required by the subcooling system and the heat rejection required by the main system. The compressor power was taken from the compressor maps provided by the manufacturer (Carlyle, 1995).

7.3.3 Coefficient of Performance

The COP of a refrigeration system without mechanical subcooling is represented by equation (7.3.1).

$$COP = \frac{Q_{evap}}{W_{comp,main} + W_{cond,main} + W_{pumps}} \tag{7.3.1}$$

The COP of a refrigeration system with mechanical subcooling can be represented by equation (7.3.2).

$$COP = \frac{Q_{evap}}{W_{comp,main} + W_{cond,main} + W_{pumps} + W_{comp,subcool} + W_{cond,subcool}} \tag{7.3.2}$$

The optimum COP for the system was determined based on the saturated evaporating temperature in the subcooler. As shown in figure 7.3.2, the optimum COP for the overall system occurs at a subcooler saturation temperature of approximately 47°F for both of the Carlyle compressors evaluated. The next step was to choose which compressor to use in the subcooling system. As depicted in figure 7.3.2, the Carlyle model DM808 provides the better overall system performance so this compressor was selected as the subcooling compressor. The evaluation was only performed up to a 60°F subcooler temperature due to the limits set by the manufacturers rating of the compressors. Unless otherwise specified, the system performance and cost predictions are modeled using a constant evaporator load and bin weather data for Madison, WI.

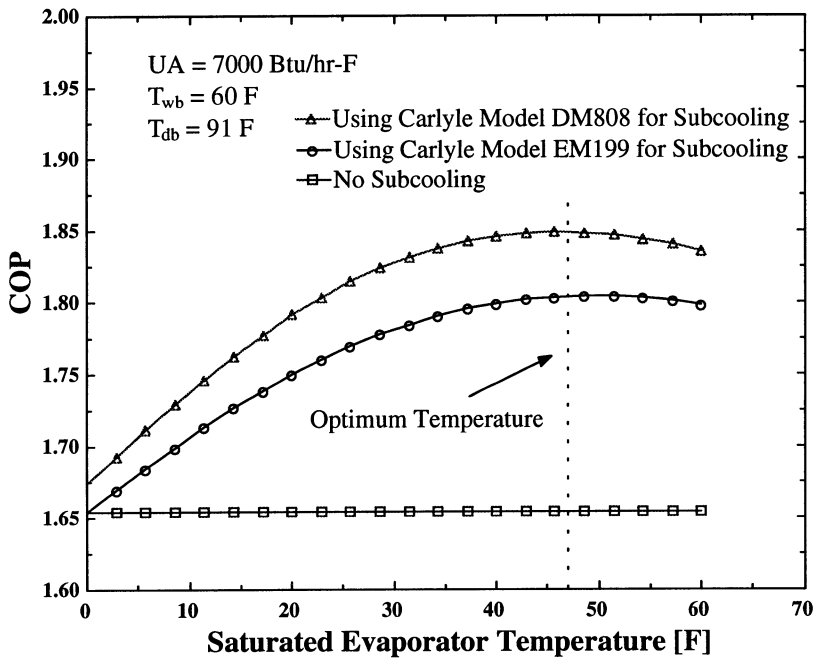

Figure 7.3.2: Optimization of COP

Once the optimum subcooler saturated evaporator temperature was chosen, an optimum and reasonable thermal conductance (UA) value needed to be selected. The yearly cost savings, calculated using equation (7.3.3), was determined for different UA values.

$$\text{Savings} = \text{Cost}_{\text{no subcooling}} - \text{Cost}_{\text{subcooling}} \tag{7.3.3}$$

This was done using both the floating and fixed head pressure models detailed in chapter six. Figures (7.3.3) and (7.3.4) depict decreasing savings for increasing UA values for both fixed and floating head pressure, respectively. To give a good perspective on the size requirements for these heat exchangers, the evaporator in the system at the Madison Ice Arena has a UA value of approximately 70,000 Btu/hr-F which would make these heat exchangers anywhere from 1% to 10% the size of the installed evaporator.

As the UA value for the fixed head pressure model increases, one subcooling compressor is required for values up to 900, two compressors between 900 and 2100 and three compressors between 2100 and 8000. As the UA value for the floating head pressure model increases, one subcooling compressor is required for values up to 3000 and two compressors are required for values above 3000.

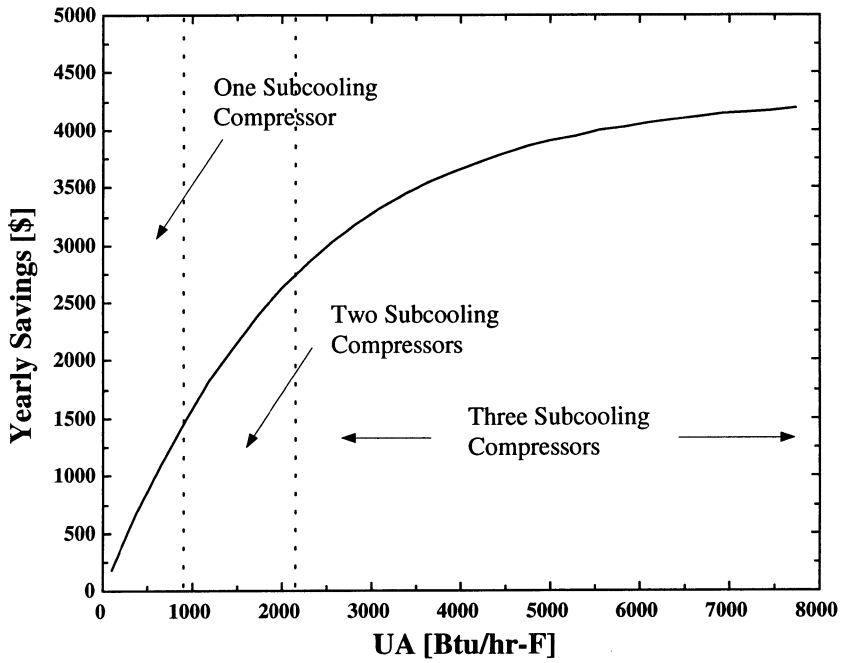

Figure 7.3.3: Cost Savings for Fixed Head Pressure

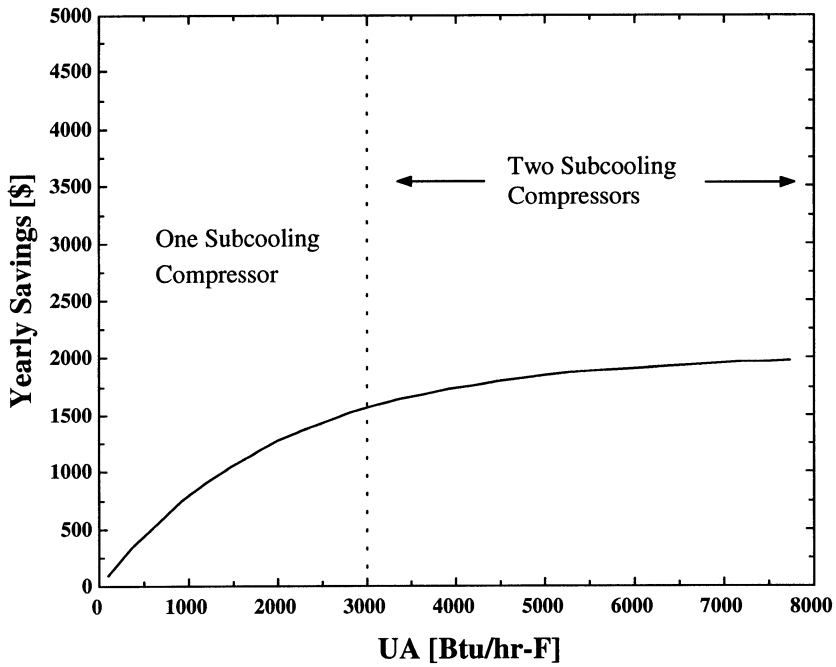

Figure 7.3.4: Cost Savings for Floating Head Pressure

Increases in subcooler UA value relate to increases in subcooler size, which translates into increased installation cost. Increases in the number of compressors required or the capacity of the compressor also translates directly into increased installation cost. Additionally, increasing the amount of machinery in a given system increases the yearly maintenance cost of the system. The savings in electrical consumption must be weighed against the added initial and lifetime costs to determine if installing a dedicated subcooling system is economically viable.

As discussed in Chapter 6, floating the head pressure is the optimal way to control system operation. This strategy also provides the smallest return for installation of a dedicated mechanical subcooling system.

Assuming that the initial system installation for the mechanical subcooling system costs $25,000 with a subcooler that provides a UA of 2400 Btu/hr-F, a life cycle cost analysis was used to determine if the system would be beneficial to install at the Madison Ice Arena (Mitchell and Braun, 1997). The analysis concluded that the installation and equipment costs would have to be less than $7,000 to be economically feasible. Therefore, the installation of a dedicated subcooling system at the Madison Ice Arena is not recommended provided that the current control strategy is changed from fixed to floating head pressure.

Chapter 8

Conclusions and Recommendations

8.1 Compressor Head Pressure Control

The design minimum head pressure set point on any refrigeration system is a critical parameter in terms of operation and maintenance costs. The design engineer must thoroughly investigate the component operating parameters to determine a set point, which will insure proper and efficient system operation. Many system designs focus on the expansion valve as the single critical element which determines the minimum head pressure setting. Although the expansion valve is an important consideration in system design, a careful investigation of the valve operation (in most cases) will indicate that the valve is not the limiting factor in head pressure design set points. The system should be designed with adequately sized components such that the head pressure changes based on the condenser's maximum available heat rejection rate and not a system control setting. Improper head pressure settings (i.e. too high) can decrease system performance by as much as 25%.

8.2 Suction Line Heat Exchanger Sizing

Suction line heat exchangers should be sized based on the impact the heat exchanger has on system performance. These heat exchangers can effect the system performance in both negative and positive ways depending on the refrigerant being used. Suction line heat exchangers with high effectiveness values are recommended for systems using R502, R134a, R12, R123, R407C, and R410A because of their increase in system performance. Suction

line heat exchangers are not recommended for use in systems using R22, R32 and R717 because they actually decrease system capacity and coefficient of performance.

8.3 Dedicated Subcooling

Dedicated mechanical subcooling increases system performance for all refrigeration systems regardless of the type of refrigerant used in the system. However, this increase in performance has to be balanced with the additional costs of machinery, maintenance and installation. The level of subcooling can be optimized by considering the subcooling heat exchanger size and the evaporation temperature of the subcooling heat exchanger. This optimal thermal performance point may not coincide with the optimal (minimum) cost of the subcooling system. In large properly controlled refrigeration systems configured and operated in a similar manner to the Madison Ice Arena, the reduced energy expenditures associated with mechanical subcooling do not appear to outweigh, the added installation, maintenance, and equipment cost of a mechanical subcooling system. However, a subcooling system integrated into the initial system design may prove to provide greater value in energy savings than expenditures for the equipment and installation. Additionally, a subcooling installation proposed for a system with lower evaporator temperatures than the zero degree temperature at Madison Ice Arena may prove to be cost effective.

8.4 Permanently Installed Monitoring Equipment

During the course of this project, numerous problems such as a plugged suction line filter, faulty expansion valve, refrigerant leak and a fouled condenser were discovered during refrigeration system monitoring at the Madison Ice Arena. These problems are commonly

seen on refrigeration systems around the world. Although (in many cases) these problems do not prevent the system from meeting the refrigeration requirements they were designed for, they can decrease the system performance by as much as 30% before being detected. This decrease in system performance translates directly into increased energy costs. Systems may operate for years with performance problems such as plugged filters or bad expansion valves before the problem is detected and rectified which can cost thousands of dollars in increased electrical bills. It is recommended to installed basic (and relatively inexpensive) monitoring equipment on the refrigeration system to allow for the detection and correction of these problems in a timely manner. Most likely, this monitoring equipment will pay for itself within the first few years of system operation.

8.5 Recommendations For Future Work

Several areas for which additional work is recommended are:

- A detailed analytical investigation into the heat transfer characteristics for an evaporative condenser when the outside air wet-bulb temperature is below manufacturers rating criteria
- A continuing investigation into the discrepancy in energy balances found at the Madison Ice Arena which may include the use of a mass flow meter to directly measure refrigerant flow rates
- Investigation into reducing the refrigeration load on the ice arena system by using different air flow rates and ice arena construction methods

- Investigation into varying secondary fluid flow rates and mass fraction of glycol in solution to optimize system performance especially under floating head pressure conditions
- Simplified methods for analyzing system performance with minimal system instrumentation

Appendix A-1

Baltimore Aircoil Effectiveness Program

"The variables Factor, T_wb, and T_refrigerant are taken from mfr data"

```
T_db=91
V_dot_air=22000
P=14.7
h_air_in=enthalpy(airh2o,T=T_db,P=P,B=T_wb)
v_air_in=volume(airh2o,T=T_db,P=P,B=T_wb)
h_air_sat=enthalpy(airh2o,T=T_refrigerant,P=P,R=1)
m_dot_air=V_dot_air/v_air_in*60
Q_dot_max=m_dot_air*(h_air_sat-h_air_in)

"Calculate the effectiveness of the heat exchanger at design conditions"
Q_dot_catalog=epsilon*m_dot_air*(h_air_sat-h_air_in)
Q_dot_catalog=1617*1000/Factor

"Calculate Evap Condenser COP"
COP=Q_dot_catalog/P_fan
P_fan=30*convert(hp,Btu/min)
```

Appendix A-2

Carlyle Model EM199 Mass Flow and Power Program

```
function PowerR22EM199(SCT,SST)
POWERr22em199=(7.208419-1.9771E-01*SST-1.6172E-
03*SST^2+0.3028965*SCT-1.1624E-03*SCT^2+0.00580433*SST*SCT)
end

function mflowR22EM199(SCT,SST,ST)
PSST=PRESSURE(R22,T=SST,x=1)
v_65=volume(r22,T=65,P=PSST)
v_act=volume(r22,T=ST,P=PSST)
mflowr22em199=v_65/v_act*(3211.161+73.03042*SST+0.9389134*SST^2-
2.8520E+00*SCT-4.5740E-02*SCT^2-6.8658E-02*SST*SCT)
end
```

Carlyle Model DM808 Mass Flow and Power Program

```
function PowerR22dm808(SCT,SST)
POWERr22dm808=0.1773069+0.02957389*SCT-1.1619E-04*SCT^2-3.2785E-
02*SST-2.9773E-04*SST^2+5.7545E-04*SCT*SST
end

function mflowr22dm808(SCT,SST,ST)
PSST=PRESSURE(R22,T=SST,x=1)
v_65=volume(r22,T=65.01,P=PSST)
v_act=volume(r22,T=ST,P=PSST)
mflowr22dm808=v_65/v_act*(277.0146-2.6948E-01*SCT-5.0529E-
03*SCT^2+6.350815*SST+0.0854907*SST^2-6.5811E-03*SCT*SST)
end
```

Appendix A-3

Compressor Volumetric Efficiency Comparison Program

```
module etavchange(SST,SCT:eta_vc)
ST=65
eta_vc=100-m*(v_suct/v_disch-1)
m=4                    "Assume a 4% clearance for the compressor"
P_suct=pressure(r22,T=SST,x=1)
P_disch=pressure(r22,T=SCT,x=1)
v_suct=volume(r22,P=P_suct,T=ST)
v_disch=volume(r22,P=P_disch,h=h_disch)

h_suct=enthalpy(r22,P=P_suct,T=ST)
h_disch=h_suct+power*convert(kw,btu/hr)/m_dot
m_dot=mflowR22EM199(SCT,SST,ST)
Power=PowerR22EM199(SCT,SST)
end
```

```
call etavchange(SST,SCT:eta_vc_ref)
SST=15
SCT=100
{ST=30}
eta_vc=100-m*(v_suct/v_disch-1)
m=4            "Assume a 4% percent clearance for the compressor"
P_suct=pressure(r22,T=SST,x=1)
P_disch=pressure(r22,T=SCT,x=1)
v_suct=volume(r22,P=P_suct,T=ST)
v_disch=volume(r22,P=P_disch,h=h_disch)

h_suct=enthalpy(r22,P=P_suct,T=ST)
h_disch=h_suct+power*convert(kw,btu/hr)/m_dot
m_dot=mflowR22EM199(SCT,SST,ST)
Power=PowerR22EM199(SCT,SST)

Percent_offset=eta_vc-eta_vc_ref
```

Appendix A-4

Sporlan Expansion Valve Determination of Flow Coefficient

```
"P_cond is a function which determines the condenser pressure based on the
specified entering liquid temperature, the specified evaporator temperature (uses
pressure) and the required pressure drop across the expansion valve"

Function P_cond(P_evaporator, DELTA_P_expansion_valve, T_liquid)
Trans_temp=temperature(r22,P=P_evaporator+DELTA_P_expansion_valve,X=0
)
if T_liquid<Trans_temp then
P_cond=P_evaporator+DELTA_P_expansion_valve
else
P_cond=pressure(r22,T=T_liquid,x=0)
endif
end

"h_1 is a function which returns the outlet enthalpy of the condenser based on
the condenser pressure, the specified liquid temperature, pressure drop across
the expansion valve and evaporator temperature (uses a pressure input)"
Function h_1(p_condenser,T_liquid,DELTA_P_expansion_valve,P_evaporator)
Trans_temp=temperature(r22,P=P_evaporator+DELTA_P_expansion_valve,X=0
)
if T_liquid<Trans_temp then
h_1=enthalpy(r22,T=T_liquid,P=P_condenser)
else
h_1=enthalpy(r22,T=T_liquid,x=0)
endif
end

"Inputs"
T_liquid=100
DELTA_P_expansion_valve=75
T_evaporator=0
Q_evap=50

"Define Pressures"
P_condenser=P_cond(P_evaporator,DELTA_P_expansion_valve,T_liquid)
P_condenser=P_evaporator+DELTA_P_2+DELTA_P_expansion_valve
DELTA_P_1=0
P_evaporator=pressure(R22,T=T_evaporator,x=1)

"Temperature calculations"
```

```
Trans_temp=temperature(r22,P=P_evaporator+DELTA_P_expansion_valve,X=0
)
T_2=T_liquid
T_condenser=temperature(r22,P=P_condenser,x=0)

"Enthalpy Calculations"
h_1=h_1(p_condenser,T_liquid,DELTA_P_expansion_valve,P_evaporator)
h_2=h_1
h_3=h_1
h_4=h_1
h_evap_out=enthalpy(r22,T=T_evaporator,x=1)

"Calculate the density at the Inlet of the expansion valve"
rho_2=density(r22,T=T_2,h=h_2)

"Calculate the Area at the inlet of the expansion valve"
A_inlet=pi*r_inlet^2/144    "Ft2"
r_inlet=1.025/2     "Based on 1-1/8 OD type L copper tubing"

"Calculate the mass flow rate based on manufacturers data"
Q_evap*12000=m_dot_refrig*(h_evap_out-h_4)

"Calculate the flow coefficient based on manufacturers data"
C_valve=m_dot_refrig/(rho_2*A_inlet)*sqrt(rho_2/(2*g_c*DELTA_P_expansion_
valve))*1/43200
g_c=32.2

"Calculates the specified capacity at each operating condition based on the
manufacturers data"
Q_table*factor=Q_evap

"Calculates the Reynolds Number based on the inlet dimensions of the
expansion valve"

Re=m_dot_refrig*D_inlet/(A_inlet*mu_inlet)
D_inlet=2*r_inlet/12          "Ft"
mu_inlet=VISCOSITY(R22,T=T_2,P=P_condenser)
DELTA_P_TOTAL=P_condenser-P_evaporator
```

Appendix A-5

Velocity Profile Program

```
"Water velocity profile"

"Knowns"

D_pipe=7.625/12  "ft"
{GPM=600      "Gal/min"}
T_water=40          "F"
P_water=14.7  "psia"
dradius=D_pipe/2*12
N=200

"Equations"

m_dot=rho_water*A_pipe*V_mean
A_pipe=pi*D_pipe^2/2
V_mean=GPM/A_pipe*convert(gal/ft^2-min,ft/hr)
rho_water=DENSITY(Water,T=T_water,P=P_water)

"V_mean Profile"
Re=rho_water*V_mean*D_pipe/mu_water
mu_water=VISCOSITY(Water,T=T_water,P=P_water)

1/sqrt(friction_factor)=-2*ln(2.51/(Re*sqrt(friction_factor)))

r[N]=dradius
rwall[N]=dradius
V[N]=0
V_glycol[N]=0
Duplicate i=1,N-1
r[i]=dradius/(N+1)*i
V[i]/V_mean=1+1.43*sqrt(friction_factor)+2.15*sqrt(friction_factor)*ln(1-
r[i]/dradius){2*(1-r[i]/dradius)}
V_glycol[i]/V_mean_glycol=1+1.43*sqrt(friction_factor_glycol)+2.15*sqrt(friction_
factor_glycol)*ln(1-r[i]/dradius){2*(1-r[i]/dradius)}
rwall[i]=dradius
rsensor[i]=dradius/3
Percent_diff[i]=V[i]/V_glycol[i]
end
offset=V[67]/V_glycol[100]*100-100
Percent_diff[N]=0
rsensor[N]=dradius/3
"Glycol Calculations"
```

"Equations"

m_dot_glycol=rho_glycol*A_pipe*V_mean_glycol
V_mean_glycol=GPM/A_pipe*convert(gal/ft^2-min,ft/hr)
rho_glycol=67.7

"V_mean Profile"
Re_glycol=rho_glycol*V_mean_glycol*D_pipe/mu_glycol
mu_glycol=11*convert(centipoise,lbm/ft-hr)

1/sqrt(friction_factor_glycol)=-2*ln(2.51/(Re_glycol*sqrt(friction_factor_glycol)))

Appendix A-6

Evaporative Condenser Data Analysis

```
"Constants"
P_atm=14.7
N_comp_odd=1
N_comp_even=3
T_glycol_avg=(T_gly_in+T_gly_out)/2
MF_glycol=.48
P_loss_odd=0
P_loss_even=0
Flow_offset=1/2

"Inputs"
t_1=dummy;t_2=dummy2;t_3=dummy3;t_4=dummy4;t_5=dummy5;t_6=dummy6
;t_7=dummy7
t_8=dummy8;t_9=dummy9;t_10=dummy10;t_11=dummy11;t_12=dummy12;t_13
=dummy13;t_14=dummy14
p_1=dummyp1;p_2=dummyp2;fan=dummyf1;t_water=dummy15;x_axis=dummy
x
T_gly_in=dummytglyin;t_gly_out=dummytglyout
p_3=p_atm+p_suct_3
p_4=p_atm+p_suct_4
kW_act=dummykw1

"Compressor Data"
m_dot_refrig_odd=mflowR22EM199(SCT_odd,SST_odd,T_3)*N_comp_odd
m_dot_refrig_even=mflowR22EM199(SCT_even,SST_even,T_4)*N_comp_even
SCT_odd=temperature(r22,P=P_1,x=1)
SCT_even=temperature(r22,P=P_2,x=1)
SST_odd=temperature(r22,P=P_3_calc,x=1)
SST_even=temperature(r22,P=P_4_calc,x=1)
Power_comp_odd=PowerR22EM199(SCT_odd,SST_odd)*N_comp_odd
Power_comp_even=PowerR22EM199(SCT_even,SST_even)*N_comp_even
Power_comp_total=Power_comp_odd+Power_comp_even

"Suction Line Filter Pressure Drop"
P_3_calc=P_3-DELTA_P_FILTER_ODD
P_4_calc=P_4-DELTA_P_FILTER_EVEN
DELTA_P_FILTER_ODD=.1788+.000197*m_dot_refrig_odd
DELTA_P_FILTER_EVEN=.1788+.000197*m_dot_refrig_even


"Evaporator Energy Balance"
```

```
Q_dot_refrig=Q_dot_refrig_even+Q_dot_refrig_odd
Q_dot_refrig_odd=m_dot_refrig_odd*(h_9-h_5)
Q_dot_refrig_even=m_dot_refrig_even*(h_10-h_6)
Q_dot_glycol=m_dot_glycol*C_p_glycol*(DELTA_T_GLYCOL)
m_dot_glycol=FL_ACTUAL*rho_glycol*convert(Gal-lbm/min-
ft^3,lbm/hr)*Flow_offset

"Coefficient of Performance"
COP_odd=Q_dot_refrig_odd/(Power_comp_odd*convert(kw,btu/hr))
COP_even=Q_dot_refrig_even/(Power_comp_even*convert(kw,btu/hr))

"Enthalpies"
h_1=enthalpy(r22,P=P_1,T=T_1)
h_2=enthalpy(r22,P=P_2,T=T_2)
h_5=enthalpy(r22,P=P_1-P_loss_odd,T=T_5)
h_6=enthalpy(r22,P=P_2-P_loss_even,T=T_6)
h_9=enthalpy(r22,P=P_3,T=T_9+2)
h_10=enthalpy(r22,P=P_4,T=T_10)
h_13=enthalpy(r22,P=P_1,T=T_13)
h_14=enthalpy(r22,P=P_2,T=T_14)

"Evaporative Condenser Heat Transfer"
fan_on=.48
Q_dot_evcnd_theory=Q_dot_evcnd_theory_odd+Q_dot_evcnd_theory_even
Q_dot_evcnd_theory_odd=epsilon_evcnd_odd*m_dot_air*(h_air_sat_odd-
h_air_in)*fan_on
Q_dot_evcnd_theory_even=epsilon_evcnd_even*m_dot_air*(h_air_sat_even-
h_air_in)*fan_on
epsilon_evcnd_odd=(0.9102917-4.4703E-03*SCT_ODD)
epsilon_evcnd_even=(0.9102917-4.4703E-03*SCT_EVEN)
h_air_out=enthalpy(airh2o,P=P,R=1,T=T_12)
T_db=32
RH=50
V_dot_air=11000
P=14.7
T_wb=WETBULB(AirH2O,T=T_db,P=P,R=RH/100)
h_air_in=enthalpy(airh2o,T=T_db,P=P,B=T_wb)
v_air_in=volume(airh2o,T=T_db,P=P,B=T_wb)
h_air_sat_even=enthalpy(airh2o,T=SCT_EVEN,P=P,R=1)
h_air_sat_odd=enthalpy(airh2o,T=SCT_ODD,P=P,R=1)
m_dot_air=V_dot_air/v_air_in*60

Q_dot_evcnd_actual_refrig=Q_dot_refrig+Power_comp_total*convert(kw,btu/hr)
Q_dot_evcnd_actual_glycol=Q_dot_glycol+kW_act*convert(kw,btu/hr)
```

```
Q_dot_evcnd_eq442=m_dot_refrig_odd*(h_1-h_13)+m_dot_refrig_even*(h_2-
h_14)
Q_dot_evcnd_eq441=m_dot_air*2*(h_air_out-h_air_in)*Fan_on
Q_dot_evcnd_eq443=Q_dot_evcnd_theory_odd+Q_dot_evcnd_theory_even

"Glycol Info"
C_p_glycol=0.9720026+1.7876E-04*T_glycol_avg-1.3049E-08*T_glycol_avg^2-
3.8625E-01*MF_glycol-1.1706E-01*MF_glycol^2+6.6653E-
04*T_glycol_avg*MF_glycol
RHO_glycol=62.72192-3.3326E-03*T_glycol_avg-4.7155E-
05*T_glycol_avg^2+11.59591*MF_glycol-2.4576E+00*MF_glycol^2-1.0900E-
02*T_glycol_avg*MF_glycol


"Misc Equations"
Superheat_even=T_10-SST_even
Superheat_odd=T_9-SST_odd

"Evaporator Effectiveness values"
Q_dot_max_odd=m_dot_glycol*1/4*C_p_glycol*(T_gly_in-T_sat_evap_odd)
Q_dot_max_even=m_dot_glycol*3/4*C_p_glycol*(T_gly_in-T_sat_evap_even)
T_sat_evap_odd=temperature(r22,P=P_3,x=1)
T_sat_evap_even=temperature(r22,P=P_4,x=1)
epsilon_evap_odd=Q_dot_refrig_odd/Q_dot_max_odd
epsilon_evap_even=Q_dot_refrig_even/Q_dot_max_even
```

Appendix A-7

Compressor Map Validation Table

SST	SCT	Power Map	Power Curve Fit	Mass Flow Map	Mass Flow Curve Fit
0	80	23.91	24	2679	2690
0	90	25.02	25.05	2571	2584
0	100	25.92	25.87	2455	2469
0	110	26.61	26.46	2331	2344
5	80	25.24	25.29	3056	3051
5	90	26.59	26.64	2945	2942
5	100	27.74	27.75	2826	2823
5	110	28.67	28.63	2698	2695
5	120	29.36	29.27	2561	2558
10	80	26.5	26.51	3470	3460
10	90	28.1	28.14	3356	3346
10	100	29.51	29.54	3233	3224
10	110	30.7	30.71	3101	3093
10	120	31.65	31.64	2960	2952
10	130	32.33	32.35	2811	2802
15	80	27.68	27.64	3923	3915
15	90	29.55	29.56	3806	3798
15	100	31.23	31.25	3680	3672
15	110	32.68	32.71	3543	3537
15	120	33.9	33.94	3398	3393
15	130	34.86	34.93	3245	3240
20	80	28.77	28.69	4420	4417
20	90	30.92	30.9	4299	4297
20	100	32.87	32.88	4169	4167
20	110	34.61	34.63	4029	4029
20	120	36.11	36.15	3880	3882
20	130	37.35	37.43	3722	3725
25	80	29.76	29.66	4962	4966
25	90	32.19	32.16	4839	4842
25	100	34.44	34.43	4705	4709
25	110	36.47	36.47	4562	4568
25	120	38.26	38.28	4409	4417
25	130	39.8	39.85	4247	4257
30	80	30.64	30.54	5553	5561
30	90	33.37	33.34	5427	5435
30	100	35.91	35.9	5291	5299
30	110	38.24	38.23	5144	5153

30	120	40.34	40.33	4989	4999
30	130	42.18	42.19	4824	4836
35	80	31.38	31.35	6197	6204
35	90	34.42	34.44	6069	6074
35	100	37.27	37.29	5930	5934
35	110	39.92	39.91	5781	5786
35	120	42.33	42.29	5623	5628
35	130	44.49	44.45	5456	5461
40	80	31.99	32.08	6897	6894
40	90	35.35	35.45	6767	6760
40	100	38.52	38.6	6627	6617
40	110	41.49	41.51	6477	6465
40	120	44.23	44.18	6317	6304
40	130	46.72	46.63	6149	6134

Appendix A-8

System Modeling Program

```
module
deltaP(P_in,Z_in,Z_out,L_pipe,D_pipe,m_dot,epsilon\D_pipe,N_elbow_section,x
:P_out)

{P_in=the pressure at the inlet of the section evaluated (lb/in2)
Z_in=the elevation above the system baseline at the inlet of the section
evaluated (ft)
Z_out=the elevation above the system baseline at the outlet of the section
evaluated (ft)
L_pipe=the length of pipe being evaluated (ft)
m_dot=the mass flow of r22 through the section of pipe being evaluated (lb/hr)
epsilon\D_pipe=relative roughness of the section being evaluated
N_elbow_section=number of 90 degree elbows in the section being evaluated
x=quality of the fluid in the section being evaluated (zero for liquids, 1 for
vapors)}

"Basic Calcs"
A_pipe=pi*(d_pipe/2)^(2)

"Inputs for piping between sections "

rho_avg=density(r22,P=P_in,x=x)
mu_avg=viscosity(r22,P=P_in,T=T_in)
T_in_sat=temperature(r22,P=P_in,x=1)
T_in=T_in_sat+x*5-2
"Bernoulli's Equation"

Z_in-Z_out+144/rho_avg*(P_in-P_out)=h_L_section

"Solve for head loss"

h_L_section=(.00259*K_T_section*(m_dot/rho_avg*convert(ft3/hr,gal/min))^2)/d
_pipe^4

"Calculate Resistance Coefficient"

K_T_section=K_elbow_section*N_elbow_section+K_pipe_section
K_elbow_section=30*f_section
K_pipe_section=f_section*(L_pipe*12/d_pipe)

"Calculate Friction Factor and Reynolds Number"
```

```
1/sqrt(f_section)=-2*ln(epsilon\D_pipe/3.7+2.51/(Re_section*sqrt(f_section)))
        "Colebrook equation for Turbulent flow"
Re_section=rho_avg*V_section*d_pipe/(mu_avg*12)
m_dot=rho_avg*A_pipe*V_section*convert(in2,ft2)
end
```

```
"General Inputs"
P_discharge_setting_odd=235
P_discharge_setting_even=235
"The following two equations are needed for runs 1 through 20 when using
floating head pressure"
{P_discharge_setting_even=P_discharge_setting_odd}
{P_discharge_setting_even=165}
{Fraction_fan_on=1}
"The following two equations are needed for runs 21 and 22 when using floating
head pressure and should be commented out at all other times"
{Valve_open_odd=1
Valve_open_even=1}

T_brine_in=17
Load_evaporator=53      "Tons"
P_air=14.7              "psia"
MF_glycol=.48
evap_superheat=7        "F"
Cost_kwhr=.047          "$/kw-hr"
V_dot_air=11000
{N_hours=2000
T_wb_outside_air=64     "F"
T_db_outside_air=70}

{enter one to simulate the pump operating or zero to simulate the pump in a
shutdown condition}
Pump_10hp_running=1     "487 GPM"
Pump_7.5hp_running=1    "257 GPM"
Pump_5hp_running=0      "327 GPM"
Pump_2hp_running=0      "120 GPM"

"Flow Rate Calculation"
GPM_glycol=flow_10hp*Pump_10hp_running+flow_7.5hp*Pump_7.5hp_running
+flow_5hp*Pump_5hp_running+flow_2hp*Pump_2hp_running
flow_10hp=487
flow_7.5hp=257
flow_5hp=327
```

```
flow_2hp=120
"Experimentally determined effectiveness values"
epsilon_evaporator_even=.17
epsilon_evaporator_odd=.248
epsilon_suct_heat_exch_even=.03
epsilon_suct_heat_exch_odd=.03
evcnd_offset=1

"Correlations and functions"
epsilon_evcnd_odd=evcnd_offset*(0.9102917-4.4703E-03*SCT_odd)
epsilon_evcnd_even=evcnd_offset*(0.9102917-4.4703E-03*SCT_even)
m_dot_comp_even=mflowR22EM199(SCT_even,SST_even,T_4)*N_comp_eve
n
m_dot_comp_odd=mflowR22EM199(SCT_odd,SST_odd,T_3)*N_comp_odd
Power_comp_even=PowerR22EM199(SCT_even,SST_even)*N_comp_even
Power_comp_odd=PowerR22EM199(SCT_odd,SST_odd)*N_comp_odd
C_p_glycol=CPEG(T_glycol_avg,MF_glycol)
Rho_glycol=RHOEG(T_glycol_avg,MF_glycol)

"Assumptions"
x_13=0
x_14=0
P_1a=P_discharge_setting_odd
P_2a=P_discharge_setting_even
h_13=h_7
h_14=h_8

"Energy Balances"

"Evaporator"
Q_dot_evap_odd=Load_evaporator/2*12000
Q_dot_evap_even=Load_evaporator/2*12000
m_dot_glycol=GPM_glycol*convert(gal/min,ft3/hr)*Rho_glycol
m_dot_glycol_odd=m_dot_glycol/2
m_dot_glycol_even=m_dot_glycol/2
T_glycol_avg=(T_brine_in+T_brine_out)/2
Load_evaporator*12000=m_dot_glycol*C_p_glycol*(T_brine_in-T_brine_out)
Q_dot_evap_odd=m_dot_glycol_odd*epsilon_evaporator_odd*C_p_glycol*(T_bri
ne_in-T_sat_evap_odd)
Q_dot_evap_even=m_dot_glycol_even*epsilon_evaporator_even*C_p_glycol*(T
_brine_in-T_sat_evap_even)

Q_dot_evap_odd=Q_dot_refrig_odd
Q_dot_evap_even=Q_dot_refrig_even
```

```
Q_dot_refrig_odd=m_dot_comp_odd*(h_9-h_5)
Q_dot_refrig_even=m_dot_comp_even*(h_10-h_6)

"Suction Line Heat Exchangers"

epsilon_suct_heat_exch_odd*(h_3_max-h_9)=h_3-h_9
epsilon_suct_heat_exch_even*(h_4_max-h_10)=h_4-h_10
h_3-h_9=h_7-h_5
h_4-h_10=h_8-h_6

"Evaporative Condenser"
Q_dot_evcnd_max=Q_dot_evcnd_odd_max+Q_dot_evcnd_even_max
Q_dot_evcnd_even_max=m_dot_air*epsilon_evcnd_even*(h_air_sat_even-
h_air_in)
Q_dot_evcnd_odd_max=m_dot_air*epsilon_evcnd_odd*(h_air_sat_odd-
h_air_in)
v_air_in=volume(airh2o,T=T_db_outside_air,P=P_air,R=Humidity_outside_air/10
0)
Humidity_outside_air=RELHUM(AirH2O,T=T_db_outside_air,P=P_air,B=T_wb_
outside_air)*100
h_air_sat_even=enthalpy(airh2o,T=T_14,P=P_air,R=1)
h_air_sat_odd=enthalpy(airh2o,T=T_13,P=P_air,R=1)
h_air_in=enthalpy(airh2o,T=T_db_outside_air,P=P_air,R=Humidity_outside_air/
100)
m_dot_air=V_dot_air/v_air_in*60
Q_dot_evcnd_actual=Q_dot_evcnd_odd_actual+Q_dot_evcnd_even_actual
Q_dot_evcnd_odd_actual=m_dot_comp_odd*(h_1-h_13)
Q_dot_evcnd_even_actual=m_dot_comp_even*(h_2-h_14)

Fraction_fan_on=Q_dot_evcnd_actual/Q_dot_evcnd_max
```

```
"System Performance"
COP_odd=Q_dot_evap_odd/(Power_odd_total*convert(kw,btu/hr))
COP_even=Q_dot_evap_even/(Power_even_total*convert(kw,btu/hr))

Power_odd_total=(Power_comp_odd+Power_fan/2+Power_evcnd_pump/2+Pow
er_glycol_pumps/2)
Power_even_total=(Power_comp_even+Power_fan/2+Power_evcnd_pump/2+P
ower_glycol_pumps/2)

Power_fan=5.7*Fraction_fan_on          "kW"
Power_evcnd_pump=3        "kW"
```

```
Power_glycol_pumps=Power_10hp*Pump_10hp_running+Power_7.5hp*Pump_
7.5hp_running+Power_5hp*Pump_5hp_running+Power_2hp*Pump_2hp_runnin
g
Power_10hp=8.7          "kW"
Power_7.5hp=5.6         "kW"
Power_5hp=5.4           "kW"
Power_2hp=1.5           "kW"

"Cost Calculations"
Cost_total=Cost_odd+Cost_even
Cost_odd=Power_odd_total*Cost_kwhr*N_hours
Cost_even=Power_even_total*Cost_kwhr*N_hours
```

```
"Enthalpy Calculations"
h_1=h_3+Power_comp_odd/m_dot_comp_odd*convert(kw-hr,btu)
h_2=h_4+Power_comp_even/m_dot_comp_even*convert(kw-hr,btu)
h_3=enthalpy(r22,T=T_3,P=P_3)
h_3_max=enthalpy(r22,T=T_7,P=P_3)
h_4=enthalpy(r22,T=T_4,P=P_4)
h_4_max=enthalpy(r22,T=T_8,P=P_4)
h_5=enthalpy(r22,T=T_5,P=P_5)
h_6=enthalpy(r22,T=T_6,P=P_6)
h_7=enthalpy(r22,T=T_7,P=P_7)
h_8=enthalpy(r22,T=T_8,P=P_8)
h_9=enthalpy(r22,T=T_9,P=P_9)
h_10=enthalpy(r22,T=T_10,P=P_10)
h_13=enthalpy(r22,P=P_13,x=x_13)
h_14=enthalpy(r22,P=P_14,x=x_14)

"Pressure Calculations"
P_9=pressure(r22,T=T_sat_evap_odd,x=1)
P_10=pressure(r22,T=T_sat_evap_even,x=1)

"Temperature Calculations"
SST_odd=temperature(r22,P=P_3,x=1)
SST_even=temperature(r22,P=P_4,x=1)
SCT_odd=temperature(r22,P=P_1a,x=1)
SCT_even=temperature(r22,P=P_2a,x=1)
T_9=T_sat_evap_odd+evap_superheat
T_10=T_sat_evap_even+evap_superheat
T_13=temperature(r22,P=P_13,x=x_13)
T_14=temperature(r22,P=P_14,x=x_14)
```

```
"Piping configuration Constants"
Z_1=18;Z_1a=3;Z_2=18;Z_2a=3;Z_5=4;Z_6=4;Z_7=0;Z_7a=0;Z_8=0;Z_8a=0;Z
_9=5;Z_9a=0;Z_10=5;Z_10a=0;Z_13=12;Z_14=12
L_pipe_1a1=30;L_pipe_2a2=30;L_pipe_148=23;L_pipe_137=23
L_pipe_8a6=10;L_pipe_7a5=10;L_pipe_1010a=8;L_pipe_99a=8
N_elbow_section_1a1=5;N_elbow_section_2a2=5;N_elbow_section_148=4;N_el
bow_section_137=4
N_elbow_section_8a6=4;N_elbow_section_7a5=4;
N_elbow_section_1010a=4;N_elbow_section_99a=4
x_1a1=1;x_2a2=1;x_148=0;x_137=0;x_8a6=0;x_7a5=0;x_1010a=1;x_99a=1
d_pipe_3.125=2.945;d_pipe_2.125=1.985;d_pipe_1.625=1.505
epsilon\D_3.125=.000019
epsilon\D_2.125=.000029
epsilon\D_1.625=.00004

"Pressure Drop Calculations"
"Point 1a to 1"
Call
DeltaP(P_1a,Z_1a,Z_1,L_pipe_1a1,D_pipe_2.125,m_dot_comp_odd,epsilon\D_
2.125,N_elbow_section_1a1,x_1a1:P_1)
{P_1a-P_1=1}
"Point 2a to 2"
Call
DeltaP(P_2a,Z_2a,Z_2,L_pipe_2a2,D_pipe_2.125,m_dot_comp_even,epsilon\D
_2.125,N_elbow_section_2a2,x_2a2:P_2)
{P_2a-P_2=1}
"Point 1 to 13"
P_13=P_1-DELTA_P_evcnd
"Point 2 to 14"
P_14=P_2-DELTA_P_evcnd
"Point 13 to 7"
Call
DeltaP(P_13,Z_13,Z_7,L_pipe_137,D_pipe_1.625,m_dot_comp_odd,epsilon\D_
1.625,N_elbow_section_137,x_137:P_7)
{P_13-P_7=-2}
"Point 14 to 8"
Call
DeltaP(P_14,Z_14,Z_8,L_pipe_148,D_pipe_1.625,m_dot_comp_even,epsilon\D
_1.625,N_elbow_section_148,x_148:P_8)
{P_14-P_8=-2}
"Point 7 to 7a"
P_7a=P_7-DELTA_P_suct_hx_liq
"Point 8 to 8a"
P_8a=P_8-DELTA_P_suct_hx_liq
"Point 7a to 5"
```

```
Call
DeltaP(P_7a,Z_7a,Z_5,L_pipe_7a5,D_pipe_1.625,m_dot_comp_odd,epsilon\D_
1.625,N_elbow_section_7a5,x_7a5:P_5)
{P_7a-P_5=.5}
"Point 8a to 6"
Call
DeltaP(P_8a,Z_8a,Z_6,L_pipe_8a6,D_pipe_1.625,m_dot_comp_even,epsilon\D
_1.625,N_elbow_section_8a6,x_8a6:P_6)
{P_8a-P_6=.5}
"Point 9 to 9a"
Call
DeltaP(P_9,Z_9,Z_9a,L_pipe_99a,D_pipe_3.125,m_dot_comp_odd,epsilon\D_3.
125,N_elbow_section_99a,x_99a:P_9a)
{P_9-P_9a=.5}
"Point 10 to 10a"
Call
DeltaP(P_10,Z_10,Z_10a,L_pipe_1010a,D_pipe_3.125,m_dot_comp_even,epsil
on\D_3.125,N_elbow_section_1010a,x_1010a:P_10a)
{P_10-P_10a=.5}
"Point 9a to 3"
P_3=P_9a-(DELTA_P_suct_hx_vap+DELTA_P_suct_filter_odd)
"Point 10a to 4"
P_4=P_10a-(DELTA_P_suct_hx_vap+DELTA_P_suct_filter_even)

"Component estimated pressure drops"
DELTA_P_evcnd=10
DELTA_P_suct_hx_liq=2
DELTA_P_suct_hx_vap=2
DELTA_P_suct_filter_odd=.1788+.000197*m_dot_comp_odd
DELTA_P_suct_filter_even=.1788+.000197*m_dot_comp_even
```

```
"Expansion Valve Calculations"
C_valve=.043                    "Calculated using MFR Data"
m_dot_comp_odd=43200*VALVE_OPEN_odd*C_valve*A_inlet*sqrt(2*g_c*DEL
TA_P_expansion_valve_odd*rho_5)
m_dot_comp_even=43200*VALVE_OPEN_even*C_valve*A_inlet*sqrt(2*g_c*DE
LTA_P_expansion_valve_even*rho_6)
DELTA_P_expansion_valve_even=P_6-P_10
DELTA_P_expansion_valve_odd=P_5-P_9
A_inlet=pi*r_inlet^2/144          "Ft2"
r_inlet=1.025/2                 "Based on 1-1/8 OD type L copper tubing"
g_c=32.2

rho_5=Density(r22,P=P_5,h=h_5)
```

```
rho_6=Density(r22,P=P_6,h=h_6)
```

Appendix A-9

Mechanical Subcooling Program

```
module
deltaP(P_in,Z_in,Z_out,L_pipe,D_pipe,m_dot,epsilon\D_pipe,N_elbow_section,x
:P_out)

{P_in=the pressure at the inlet of the section evaluated (lb/in2)
Z_in=the elevation above the system baseline at the inlet of the section
evaluated (ft)
Z_out=the elevation above the system baseline at the outlet of the section
evaluated (ft)
L_pipe=the length of pipe being evaluated (ft)
m_dot=the mass flow of r22 through the section of pipe being evaluated (lb/hr)
epsilon\D_pipe=relative roughness of the section being evaluated
N_elbow_section=number of 90 degree elbows in the section being evaluated
x=quality of the fluid in the section being evaluated (zero for liquids, 1 for
vapors)}


"Basic Calcs"
A_pipe=pi*(d_pipe/2)^(2)

"Inputs for piping between sections "

rho_avg=density(r22,P=P_in,x=x)
mu_avg=viscosity(r22,P=P_in,T=T_in)
T_in_sat=temperature(r22,P=P_in,x=1)
T_in=T_in_sat+x*5-2
"Bernoulli's Equation"

Z_in-Z_out+144/rho_avg*(P_in-P_out)=h_L_section

"Solve for head loss"

h_L_section=(.00259*K_T_section*(m_dot/rho_avg*convert(ft3/hr,gal/min))^2)/d
_pipe^4

"Calculate Resistance Coefficient"

K_T_section=K_elbow_section*N_elbow_section+K_pipe_section
K_elbow_section=30*f_section
K_pipe_section=f_section*(L_pipe*12/d_pipe)
```

```
"Calculate Friction Factor and Reynolds Number"

1/sqrt(f_section)=-2*ln(epsilon\D_pipe/3.7+2.51/(Re_section*sqrt(f_section)))
        "Colebrook equation for Turbulent flow"
Re_section=rho_avg*V_section*d_pipe/(mu_avg*12)
m_dot=rho_avg*A_pipe*V_section*convert(in2,ft2)
end
```

```
"General Inputs"

{P_discharge_setting_odd=235
P_discharge_setting_even=235}
"The following two equations are needed for runs 1 through 20"
P_discharge_setting_even=P_discharge_setting_odd
Fraction_fan_on=1
"The following two equations are needed for runs 21 and 22 and should be
commented out at all other times"
{Valve_open_odd=1
Valve_open_even=1}

T_brine_in=17
Load_evaporator=53      "Tons"
P_air=14.7              "psia"
MF_glycol=.48
evap_superheat=7        "F"
Cost_kwhr=.047          "$/kw-hr"
V_dot_air=11000
{N_hours=2000
T_wb_outside_air=64     "F"
T_db_outside_air=70}


{enter one to simulate the pump operating or zero to simulate the pump in a
shutdown condition}
Pump_10hp_running=1     "487 GPM"
Pump_7.5hp_running=1    "257 GPM"
Pump_5hp_running=0      "327 GPM"
Pump_2hp_running=0      "120 GPM"

"Flow Rate Calculation"
GPM_glycol=flow_10hp*Pump_10hp_running+flow_7.5hp*Pump_7.5hp_running
+flow_5hp*Pump_5hp_running+flow_2hp*Pump_2hp_running
flow_10hp=487
flow_7.5hp=257
```

```
flow_5hp=327
flow_2hp=120
"Experimentally determined effectiveness values"
epsilon_evaporator_even=.17
epsilon_evaporator_odd=.248
epsilon_suct_heat_exch_even=.03
epsilon_suct_heat_exch_odd=.03
evcnd_offset=1

"Correlations and functions"
epsilon_evcnd_odd=evcnd_offset*(0.9102917-4.4703E-03*SCT_odd)
epsilon_evcnd_even=evcnd_offset*(0.9102917-4.4703E-03*SCT_even)
m_dot_comp_even=mflowR22EM199(SCT_even,SST_even,T_4)*N_comp_eve
n
m_dot_comp_odd=mflowR22EM199(SCT_odd,SST_odd,T_3)*N_comp_odd
Power_comp_even=PowerR22EM199(SCT_even,SST_even)*N_comp_even
Power_comp_odd=PowerR22EM199(SCT_odd,SST_odd)*N_comp_odd
C_p_glycol=CPEG(T_glycol_avg,MF_glycol)
Rho_glycol=RHOEG(T_glycol_avg,MF_glycol)

"Assumptions"
x_13=0
x_14=0
P_1a=P_discharge_setting_odd
P_2a=P_discharge_setting_even
h_13=h_7
h_14=h_8
```

```
"Energy Balances"

"Evaporator"
Q_dot_evap_odd=Load_evaporator/2*12000
Q_dot_evap_even=Load_evaporator/2*12000
m_dot_glycol=GPM_glycol*convert(gal/min,ft3/hr)*Rho_glycol
m_dot_glycol_odd=m_dot_glycol/2
m_dot_glycol_even=m_dot_glycol/2
T_glycol_avg=(T_brine_in+T_brine_out)/2
Load_evaporator*12000=m_dot_glycol*C_p_glycol*(T_brine_in-T_brine_out)

Q_dot_evap_odd=m_dot_glycol_odd*epsilon_evaporator_odd*C_p_glycol*(T_bri
ne_in-T_sat_evap_odd)
Q_dot_evap_even=m_dot_glycol_even*epsilon_evaporator_even*C_p_glycol*(T
_brine_in-T_sat_evap_even)

Q_dot_evap_odd=Q_dot_refrig_odd
```

```
Q_dot_evap_even=Q_dot_refrig_even
Q_dot_refrig_odd=m_dot_comp_odd*(h_9-h_5)
Q_dot_refrig_even=m_dot_comp_even*(h_10-h_6)

"Suction Line Heat Exchangers"

epsilon_suct_heat_exch_odd*(h_3_max-h_9)=h_3-h_9
epsilon_suct_heat_exch_even*(h_4_max-h_10)=h_4-h_10
h_3-h_9=h_7-h_7a
h_4-h_10=h_8-h_8a
```

```
"Subcooler"

{h_7a=h_5
h_8a=h_6}
T_sub=47
UA_sub_odd=50
SCT_sub=(SCT_odd+SCT_even)/2
T_16=T_sub+evap_superheat
Q_dot_sub=m_dot_ref_sub*(h_16-h_15)
P_sub=pressure(r22, T=T_sub,x=1)
h_16=enthalpy(r22,P=P_sub,T=T_16)
h_15=enthalpy(r22,T=SCT_sub,x=0)
m_dot_ref_sub=mflowr22dm808(SCT_sub,T_sub,T_16)*N_comp_sub
Power_sub=PowerR22dm808(SCT_sub,T_sub)*N_comp_sub
Power_sub_condenser=(Power_fan+Power_evcnd_pump)*(Q_dot_sub+Power_
sub*convert(kw,btu/hr))/(Q_dot_evap_odd+Q_dot_evap_even+(power_comp_ev
en+power_comp_odd)*convert(kw,btu/hr))


Q_dot_sub_odd=Q_dot_sub/2
Q_dot_sub_even=Q_dot_sub/2

Q_dot_sub_even=m_dot_comp_even*(h_7a-h_5)
Q_dot_sub_odd=m_dot_comp_odd*(h_8a-h_6)

T_7a=temperature(r22,P=P_7,h=h_7a)
T_8a=temperature(r22,P=P_8,h=h_8a)
LMTD_sub_odd=(T_7a-T_5)/ln((T_7a-T_sub)/(T_5-T_sub))
LMTD_sub_even=(T_8a-T_6)/ln((T_8a-T_sub)/(T_6-T_sub))

Q_dot_sub_odd=UA_sub_odd*(LMTD_sub_odd)
Q_dot_sub_even=UA_sub_even*(LMTD_sub_even)
```

```
COP_overall=(Q_dot_evap_odd+Q_dot_evap_even)/((Power_odd_total+Power_
even_total+Power_sub+Power_sub_condenser)*convert(kw,btu/hr))

"Cost Calculations"

Cost_total=Cost_odd+Cost_even+Cost_sub
Cost_odd=Power_odd_total*Cost_kwhr*N_hours
Cost_even=Power_even_total*Cost_kwhr*N_hours
Cost_sub=(Power_sub+Power_sub_condenser)*Cost_kwhr*N_hours



COP_odd=Q_dot_evap_odd/(Power_odd_total*convert(kw,btu/hr))
COP_even=Q_dot_evap_even/(Power_even_total*convert(kw,btu/hr))
COP_main=(Q_dot_evap_odd+Q_dot_evap_even)/((Power_odd_total+Power_e
ven_total)*convert(kw,btu/hr))
```

```
"Evaporative Condenser"
Q_dot_evcnd_max=Q_dot_evcnd_odd_max+Q_dot_evcnd_even_max
Q_dot_evcnd_even_max=m_dot_air*epsilon_evcnd_even*(h_air_sat_even-
h_air_in)
Q_dot_evcnd_odd_max=m_dot_air*epsilon_evcnd_odd*(h_air_sat_odd-
h_air_in)
v_air_in=volume(airh2o,T=T_db_outside_air,P=P_air,R=Humidity_outside_air/10
0)
Humidity_outside_air=RELHUM(AirH2O,T=T_db_outside_air,P=P_air,B=T_wb_
outside_air)*100
h_air_sat_even=enthalpy(airh2o,T=T_14,P=P_air,R=1)
h_air_sat_odd=enthalpy(airh2o,T=T_13,P=P_air,R=1)
h_air_in=enthalpy(airh2o,T=T_db_outside_air,P=P_air,R=Humidity_outside_air/
100)
m_dot_air=V_dot_air/v_air_in*60
Q_dot_evcnd_actual=Q_dot_evcnd_odd_actual+Q_dot_evcnd_even_actual
Q_dot_evcnd_odd_actual=m_dot_comp_odd*(h_1-h_13)
Q_dot_evcnd_even_actual=m_dot_comp_even*(h_2-h_14)

Fraction_fan_on=Q_dot_evcnd_actual/Q_dot_evcnd_max
```

```
"System Performance"

Power_odd_total=(Power_comp_odd+Power_fan/2+Power_evcnd_pump/2+Pow
er_glycol_pumps/2)
```

```
Power_even_total=(Power_comp_even+Power_fan/2+Power_evcnd_pump/2+P
ower_glycol_pumps/2)

Power_fan=5.7*Fraction_fan_on          "kW"
Power_evcnd_pump=3        "kW"
Power_glycol_pumps=Power_10hp*Pump_10hp_running+Power_7.5hp*Pump_
7.5hp_running+Power_5hp*Pump_5hp_running+Power_2hp*Pump_2hp_runnin
g
Power_10hp=8.7          "kW"
Power_7.5hp=5.6         "kW"
Power_5hp=5.4           "kW"
Power_2hp=1.5           "kW"
```

```
"Enthalpy Calculations"
h_1=h_3+Power_comp_odd/m_dot_comp_odd*convert(kw-hr,btu)
h_2=h_4+Power_comp_even/m_dot_comp_even*convert(kw-hr,btu)
h_3=enthalpy(r22,T=T_3,P=P_3)
h_3_max=enthalpy(r22,T=T_7,P=P_3)
h_4=enthalpy(r22,T=T_4,P=P_4)
h_4_max=enthalpy(r22,T=T_8,P=P_4)
h_5=enthalpy(r22,T=T_5,P=P_5)
h_6=enthalpy(r22,T=T_6,P=P_6)
h_7=enthalpy(r22,T=T_7,P=P_7)
h_8=enthalpy(r22,T=T_8,P=P_8)
h_9=enthalpy(r22,T=T_9,P=P_9)
h_10=enthalpy(r22,T=T_10,P=P_10)
h_13=enthalpy(r22,P=P_13,x=x_13)
h_14=enthalpy(r22,P=P_14,x=x_14)

"Pressure Calculations"
P_9=pressure(r22,T=T_sat_evap_odd,x=1)
P_10=pressure(r22,T=T_sat_evap_even,x=1)

"Temperature Calculations"
SST_odd=temperature(r22,P=P_3,x=1)
SST_even=temperature(r22,P=P_4,x=1)
SCT_odd=temperature(r22,P=P_1a,x=1)
SCT_even=temperature(r22,P=P_2a,x=1)
T_9=T_sat_evap_odd+evap_superheat
T_10=T_sat_evap_even+evap_superheat
T_13=temperature(r22,P=P_13,x=x_13)
T_14=temperature(r22,P=P_14,x=x_14)
```

```
"Piping configuration Constants"
Z_1=18;Z_1a=3;Z_2=18;Z_2a=3;Z_5=4;Z_6=4;Z_7=0;Z_7a=0;Z_8=0;Z_8a=0;Z
_9=5;Z_9a=0;Z_10=5;Z_10a=0;Z_13=12;Z_14=12
L_pipe_1a1=30;L_pipe_2a2=30;L_pipe_148=23;L_pipe_137=23
L_pipe_8a6=10;L_pipe_7a5=10;L_pipe_1010a=8;L_pipe_99a=8
N_elbow_section_1a1=5;N_elbow_section_2a2=5;N_elbow_section_148=4;N_el
bow_section_137=4
N_elbow_section_8a6=4;N_elbow_section_7a5=4;
N_elbow_section_1010a=4;N_elbow_section_99a=4
x_1a1=1;x_2a2=1;x_148=0;x_137=0;x_8a6=0;x_7a5=0;x_1010a=1;x_99a=1
d_pipe_3.125=2.945;d_pipe_2.125=1.985;d_pipe_1.625=1.505
epsilon\D_3.125=.000019
epsilon\D_2.125=.000029
epsilon\D_1.625=.00004

"Pressure Drop Calculations"
"Point 1a to 1"
Call
DeltaP(P_1a,Z_1a,Z_1,L_pipe_1a1,D_pipe_2.125,m_dot_comp_odd,epsilon\D_
2.125,N_elbow_section_1a1,x_1a1:P_1)
{P_1a-P_1=1}
"Point 2a to 2"
Call
DeltaP(P_2a,Z_2a,Z_2,L_pipe_2a2,D_pipe_2.125,m_dot_comp_even,epsilon\D
_2.125,N_elbow_section_2a2,x_2a2:P_2)
{P_2a-P_2=1}
"Point 1 to 13"
P_13=P_1-DELTA_P_evcnd
"Point 2 to 14"
P_14=P_2-DELTA_P_evcnd
"Point 13 to 7"
Call
DeltaP(P_13,Z_13,Z_7,L_pipe_137,D_pipe_1.625,m_dot_comp_odd,epsilon\D_
1.625,N_elbow_section_137,x_137:P_7)
{P_13-P_7=-2}
"Point 14 to 8"
Call
DeltaP(P_14,Z_14,Z_8,L_pipe_148,D_pipe_1.625,m_dot_comp_even,epsilon\D
_1.625,N_elbow_section_148,x_148:P_8)
{P_14-P_8=-2}
"Point 7 to 7a"
P_7a=P_7-DELTA_P_suct_hx_liq
"Point 8 to 8a"
P_8a=P_8-DELTA_P_suct_hx_liq
"Point 7a to 5"
```

```
Call
DeltaP(P_7a,Z_7a,Z_5,L_pipe_7a5,D_pipe_1.625,m_dot_comp_odd,epsilon\D_
1.625,N_elbow_section_7a5,x_7a5:P_5)
{P_7a-P_5=.5}
"Point 8a to 6"
Call
DeltaP(P_8a,Z_8a,Z_6,L_pipe_8a6,D_pipe_1.625,m_dot_comp_even,epsilon\D
_1.625,N_elbow_section_8a6,x_8a6:P_6)
{P_8a-P_6=.5}
"Point 9 to 9a"
Call
DeltaP(P_9,Z_9,Z_9a,L_pipe_99a,D_pipe_3.125,m_dot_comp_odd,epsilon\D_3.
125,N_elbow_section_99a,x_99a:P_9a)
{P_9-P_9a=.5}
"Point 10 to 10a"
Call
DeltaP(P_10,Z_10,Z_10a,L_pipe_1010a,D_pipe_3.125,m_dot_comp_even,epsil
on\D_3.125,N_elbow_section_1010a,x_1010a:P_10a)
{P_10-P_10a=.5}
"Point 9a to 3"
P_3=P_9a-(DELTA_P_suct_hx_vap+DELTA_P_suct_filter_odd)
"Point 10a to 4"
P_4=P_10a-(DELTA_P_suct_hx_vap+DELTA_P_suct_filter_even)

"Component estimated pressure drops"
DELTA_P_evcnd=10
DELTA_P_suct_hx_liq=2
DELTA_P_suct_hx_vap=2
DELTA_P_suct_filter_odd=.1788+.000197*m_dot_comp_odd
DELTA_P_suct_filter_even=.1788+.000197*m_dot_comp_even
```

```
"Expansion Valve Calculations"
C_valve=.043                    "Calculated using MFR Data"
m_dot_comp_odd=43200*VALVE_OPEN_odd*C_valve*A_inlet*sqrt(2*g_c*DEL
TA_P_expansion_valve_odd*rho_5)
m_dot_comp_even=43200*VALVE_OPEN_even*C_valve*A_inlet*sqrt(2*g_c*DE
LTA_P_expansion_valve_even*rho_6)
DELTA_P_expansion_valve_even=P_6-P_10
DELTA_P_expansion_valve_odd=P_5-P_9
A_inlet=pi*r_inlet^2/144          "Ft2"
r_inlet=1.025/2                 "Based on 1-1/8 OD type L copper tubing"
g_c=32.2

rho_5=Density(r22,P=P_5,h=h_5)
```

```
rho_6=Density(r22,P=P_6,h=h_6)
```

APPENDIX B

Data Logger Program

```
;{21X}
;
*Table 1 Program
  01: 2         Execution Interval (seconds)

1:  Internal Temperature (P17)
 1: 1         Loc [ Ref_Temp  ]


2:  Volt (Diff) (P2)
 1: 1         Reps
 2: 15        5000 mV Fast Range
 3: 1         DIFF Channel
 4: 3         Loc [ RH        ]
 5: .02866    Mult
 6: -25       Offset

3:  Volt (Diff) (P2)
 1: 1         Reps
 2: 5         5000 mV Slow Range
 3: 2         DIFF Channel
 4: 4         Loc [ OATEMP    ]
 5: .05151    Mult
 6: -13       Offset

4:  Volt (Diff) (P2)
 1: 1         Reps
 2: 5         5000 mV Slow Range
 3: 3         DIFF Channel
 4: 5         Loc [ P1        ]
 5: .06       Mult
 6: -30.64    Offset

5:  Volt (Diff) (P2)
 1: 1         Reps
 2: 5         5000 mV Slow Range
 3: 4         DIFF Channel
 4: 6         Loc [ P2        ]
 5: .06       Mult
 6: -30.22    Offset

6:  Volt (Diff) (P2)
 1: 1         Reps
 2: 5         5000 mV Slow Range
 3: 5         DIFF Channel
 4: 7         Loc [ P3        ]
 5: .012      Mult
 6: -5.908    Offset

7:  Volt (Diff) (P2)
```

```
 1: 1         Reps
 2: 5         5000 mV Slow Range
 3: 6         DIFF Channel
 4: 8         Loc [ P4         ]
 5: .0231     Mult
 6: -26.75    Offset

8:  Volt (Diff) (P2)
 1: 1         Reps
 2: 5         5000 mV Slow Range
 3: 7         DIFF Channel
 4: 2         Loc [ Delta_T    ]
 5: .02071    Mult
 6: 0         Offset

9:  Pulse (P3)
 1: 1         Reps
 2: 1         Pulse Input Channel
 3: 20        High Frequency, Output Hz
 4: 10        Loc [ W1         ]
 5: 115.2     Mult
 6: 0.0000    Offset

10:  Pulse (P3)
 1: 1         Reps
 2: 2         Pulse Input Channel
 3: 2         Switch Closure, All Counts
 4: 9         Loc [ FL1        ]
 5: 5.7636    Mult
 6: 0.0       Offset

11:  Batt Voltage (P10)
 1: 25        Loc [ Battery    ]


12:  Do (P86)
 1: 42        Set Port 2 High

13:  Full Bridge (P6)
 1: 1         Reps
 2: 1         5 mV Slow Range
 3: 8         DIFF Channel
 4: 1         Excite all reps w/Exchan 1
 5: 250       mV Excitation
 6: 26        Loc [ dummy      ]
 7: -.001     Mult
 8: .09707    Offset

14:  BR Transform Rf[X/(1-X)] (P59)
 1: 1         Reps
 2: 26        Loc [ dummy      ]
 3: 10.025    Mult (Rf)

15:  Temperature RTD (P16)
 1: 1         Reps
 2: 26        R/R0 Loc [ dummy      ]
 3: 26        Loc [ dummy      ]
 4: 1         Mult
```

```
 5: 0         Offset

16:  Beginning of Loop (P87)
 1: 0         Delay
 2: 15        Loop Count

17:  Do (P86)
 1: 41        Set Port 1 High

18:  Do (P86)
 1: 51        Set Port 1 Low

19:  Do (P86)
 1: 41        Set Port 1 High

20:  Do (P86)
 1: 51        Set Port 1 Low

21:  Thermocouple Temp (DIFF) (P14)
 1: 1         Reps
 2: 1         5 mV Slow Range
 3: 8         DIFF Channel
 4: 1         Type T (Copper-Constantan)
 5: 1         Ref Temp Loc [ Ref_Temp  ]
 6: 11     -- Loc [ T_1        ]
 7: 1.8       Mult
 8: 32        Offset

22:  End (P95)

23:  Do (P86)
 1: 52        Set Port 2 Low

24:  If time is (P92)
 1: 1         Minutes into a
 2: 2         Minute Interval
 3: 10        Set Output Flag High

25:  Set Active Storage Area (P80)
 1: 1         Final Storage
 2: 103       Array ID

26:  Real Time (P77)
 1: 1111      Year,Day,Hour/Minute,Seconds (midnight = 0000)

27:  Sample (P70)
 1: 14        Reps
 2: 11        Loc [ T_1        ]

28:  Sample (P70)
 1: 9         Reps
 2: 3         Loc [ RH         ]

29:  If time is (P92)
 1: 0         Minutes into a
 2: 15        Minute Interval
 3: 10        Set Output Flag High
```

```
30:  Set Active Storage Area (P80)
 1: 1        Final Storage
 2: 101      Array ID

31:  Real Time (P77)
 1: 110      Day,Hour/Minute (midnight = 0000)

32:  Average (P71)
 1: 14       Reps
 2: 11       Loc [ T_1       ]

33:  Average (P71)
 1: 9        Reps
 2: 3        Loc [ RH        ]

34:  Minimize (P74)
 1: 1        Reps
 2: 0        Value Only
 3: 25       Loc [ Battery   ]

35:  If Flag/Port (P91)
 1: 11       Do if Flag 1 is High
 2: 10       Set Output Flag High

36:  Set Active Storage Area (P80)
 1: 1        Final Storage
 2: 102      Array ID

37:  Real Time (P77)
 1: 0111     Day,Hour/Minute,Seconds (midnight = 0000)

38:  Sample (P70)
 1: 14       Reps
 2: 11       Loc [ T_1       ]

39:  Sample (P70)
 1: 9        Reps
 2: 3        Loc [ RH        ]


*Table 2 Program
  01: 0.0000    Execution Interval (seconds)

*Table 3 Subroutines

End Program

-Input Locations-
1 Ref_Temp  1 1 1
2 Delta_T   1 0 1
3 RH        1 3 1
4 OATEMP    1 3 1
5 P1        1 3 1
6 P2        1 3 1
7 P3        1 3 1
8 P4        1 3 1
9 FL1       1 3 1
```

```
10 W1          1 3 1
11 T_1         1 6 1
12 T_2         1 3 0
13 T_3         1 3 0
14 T_4         1 3 0
15 T_5         1 3 0
16 T_6         1 3 0
17 T_7         1 3 0
18 T_8         1 3 0
19 T_9         1 3 0
20 T_10        1 3 0
21 T_11        1 3 0
22 T_12        1 3 0
23 T_13        1 3 0
24 T_14        1 3 0
25 Battery     1 1 1
26 dummy       1 2 3
27 __________  0 0 0
28 __________  0 0 0
```

Appendix C

Data Logger Wiring Diagram

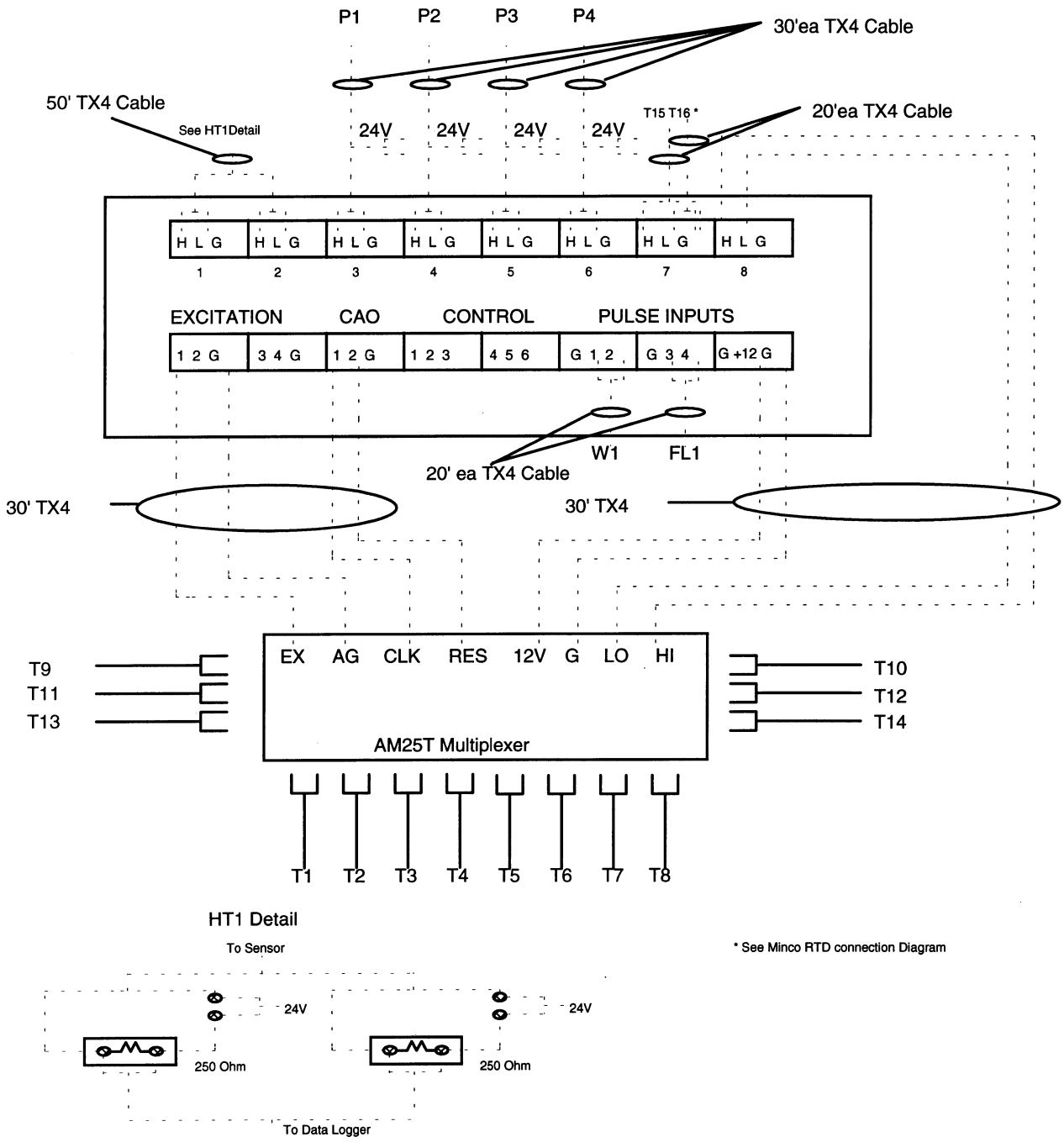

Appendix D

Brine and Refrigerant Side Heat Transfer Error Analysis

Refrigerant Side Heat Transfer error Analysis

$\dot{Q}_{refrig,hx} = \dot{m}_{refrig}\left(h_{evap,in} - h_{evap,out}\right)$ Energy Equation for analysis

The Errors in measurement for the refrigerant side are as shown in the following table.

Sensor	Error
Thermocouples	±1°F
Pressure Transducers	±.5 psia
RTD's (Matched Pair)	±.1°F
Flow Meter	±5%
Manufacturer's data	±5%

Table 1

The percentage of error for heat transfer is calculated using the following governing equation:

$$\dot{Q}_{error,\%} = \sqrt{\left(\dot{m}_{error,\%}\right)^2 + \frac{\left(h_{in,error}\right)^2 + \left(h_{out,error}\right)^2}{Äh^2}}$$

The following equations are used to calculate the error in mass flow calculations.

$$\dot{m}_{error,\%} = \frac{\dot{m}_{error}}{\dot{m}_{refrig}} 100$$

$$\dot{m}_{error} = \sqrt{\left(\dot{m}_{refrig}\,\delta\dot{m}_{mfr}\right)^2 + \left(\frac{\partial\dot{m}}{\partial SST}äSST\right)^2 + \left(\frac{\partial\dot{m}}{\partial SCT}äSCT\right)^2 + \left(\frac{\partial\dot{m}}{\partial ST}äST\right)^2}$$

$$\delta \dot{m}_{mfr} = .05$$

$$\partial SST = \left(\frac{v_{P,suction}}{R} \right) P$$

$$\partial SCT = \left(\frac{v_{P,discharge}}{R} \right) P$$

$$\partial ST = \left(\frac{v_{P,suction}}{R} \right) P$$

$$\delta P = .5$$

The correlation used to calculate mass flow from manufacturer's data is shown below as well as the partial derivatives depicting the effect of temperature and pressure reading errors.

$$\dot{m}_{refrig} = \frac{v_{65}}{v_{act}} \left(3211 + 73.03SST + .9389SST^2 - 2.852SCT - .04574SCT^2 - .06866SCTSST \right)$$

$$\frac{\partial \dot{m}}{\partial SST} = \frac{v_{65}}{v_{act}} \left(73.03 + (2).9389SCT - .06866SCT \right)$$

$$\frac{\partial \dot{m}}{\partial SCT} = \frac{v_{65}}{v_{act}} \left(-2.852 - (2).04574SCT - .06866SST \right)$$

$$\frac{\partial \dot{m}}{\partial ST} = -\frac{v_{65} P_{suction}}{R * ST^2} \left(3211 + 73.03SST + .9389SST^2 - 2.852SCT - .04574SCT^2 - .06866SCTSST \right)$$

The equations for solving the error in enthalpy calculations are shown below.

$$h_{in,error} = \sqrt{\left(\frac{\partial h_{in}}{\partial hT_{in}}\delta T_{in}\right)^2 + \left(\frac{\partial h_{in}}{\partial hP_{in}}\delta P_{in}\right)^2}$$

$$\delta T_{in} = 1$$

$$\delta P_{in} = .5$$

$$\frac{\partial h_{in}}{\partial hT_{in}} = Cp_{in}$$

$$\frac{\partial h_{in}}{\partial hP_{in}} = v_{in} - T_{in}\frac{\partial v_{in}}{\partial hT_{in}} = v_{in} - \frac{RT_{in}}{P_{in}}$$

$$h_{out,error} = \sqrt{\left(\frac{\partial h_{out}}{\partial hT_{out}}\delta T_{out}\right)^2 + \left(\frac{\partial h_{out}}{\partial hP_{out}}\delta P_{out}\right)^2}$$

$$\delta T_{out} = 1$$

$$\delta P_{out} = .5$$

$$\frac{\partial h_{out}}{\partial hT_{out}} = Cp_{out}$$

$$\frac{\partial h_{out}}{\partial hP_{out}} = v_{out} - T_{out}\frac{\partial v_{out}}{\partial hT_{out}} = v_{out} - \frac{RT_{out}}{P_{out}}$$

Brine Side Heat Transfer error analysis.

$$\dot{Q}_{brine} = \dot{m}_{brine} Cp_{btine} (\Delta T_{brine})$$

$$\dot{Q}_{brine,error,\%} = \sqrt{(\dot{m}_{brine,error,\%})^2 + (\Delta T_{brine,error,\%})^2 + Cp_{brine,error,\%}{}^2}$$

$$\dot{m}_{brine,error,\%} = 5$$

$$Cp_{brine,error,\%} = f(MF)$$

$$T_{brine,error,\%} = \frac{\Delta T_{error}}{\Delta T_{brine}} 100$$

$$\Delta T_{error} = .1$$

References

American Society of Heating, Refrigeration, and Air Conditioning Engineers (ASHRAE) Handbook, Refrigeration Volume, American Society of Heating, Refrigerating, and Air Conditioning Engineers, Atlanta, GA, 1990.

American Society of Heating, Refrigeration, and Air Conditioning Engineers (ASHRAE) Handbook, Fundamentals Volume, American Society of Heating, Refrigerating, and Air Conditioning Engineers, Atlanta, GA, 1993.

API Heat Transfer, API Ketema, Bulletin DXT 202B, Grand Prairie, TX, 1989.

Avallone, Eugene A (editor), Baumeister III, Theodore (editor), Marks' Standard Handbook For Mechanical Engineers, Tenth Edition, McGraw-Hill, New York, NY, 1996.

Baltimore Aircoil Company, Bulletin S119/1-0FA, Baltimore, MD, 1978.

Bundy, Engineer, Sporlan Valve Company, Washington, MO, private communication, 1997.

Carlyle Compressors, Lit. No. 574-036, Syracuse, NY, 1995.

Cox, Daryl, Rink Tec International, Little Canada, MN, private communication, 1998.

Crane Co., "Flow of Fluids Through Valves, Fittings, and Pipe," Technical Paper No. 410, Joliet, IL, 1988.

Domanski, P.A. and Didion, D.A., "Evaluation of suction-line/liquid-line heat exchange in the refrigeration cycle," International Journal of Refrigeration, Volume 17, Number 7, 1992.

"Engineering Weather Data", Manual AFM 88-29, U.S. Government Printing Office, Washington, D.C., 1978.

Gildehaus, Engineer, Sporlan Valve Company, Washington, MO, private communication, 1997.

Incropera, Frank P., DeWitt, David P., Introduction to Heat Transfer, Third Edition, John Wiley & Sons, New York, NY, 1996.

Klein, S.A., Alvarado, F.L. "EES – Engineering Equation Solver," F-Chart Software, Middleton, WI, 1998.

Mitchell, John W. and Braun, James E., Design Analysis, and Control of Space Conditioning Equipment and Systems, University of Wisconsin-Madison, 1997.

Refrigeration Research, General Catalog, Brighton, MI, 1997.

Sporlan Valve Company, Bulletin 80-10, Washington, MO, 1993.

Sporlan Valve Company, Bulletin 10-10, Washington, MO, 1995.

Stoecker, W.F., Industrial Refrigeration, Business News Publishing Company, Troy, MI, 1988.

Threlkeld, J.L., Thermal Environmental Engineering, Prentice-Hall, Inc., Englewood Cliffs, N.J., 1962.

Thornton, J.W., Klein, S.A., and Mitchell, J.W., "Dedicated Mechanical Subcooling Design Strategies for Supermarket Applications," International Journal of Refrigeration, Volume 17, Number 8, 1994.

Vinnicombe, G.A. and Ibrahim, G.A., "The Performance of Refrigeration Expansion Devices," Electricity Association Technology Ltd., London, UK, 1991.